Beobachtung, Quantifizierung und Anwendung von kontaktabhängiger Wachstumsinhibition zur Kontrolle von Zellwachstum und Musterbildung

Observations, quantitation and application of contact-dependent growth inhibition for controlling cell growth and patterning

# Master-Thesis

zur Erlangung des akademischen Grades

**Master of Science**

Studiengang Biochemie

Fakultät Chemie

Technische Universität München

vorgelegt von

**Beatrice Ramm**

aus

Gräfelfing

angefertigt in der Arbeitsgruppe

Proteinchemie

unter Anleitung von

Aymelt Itzen

in Kooperation mit Drew Endy, Department of Bioengineering, Stanford University

München, März 2015

## Zusammenfassung

Kontaktabhängige Wachstumsinhibition (CDI) ist ein natürliches System in *E. coli* und anderen Proteobakterien, bei dem durch physische Interaktion ein auf der Zelloberfläche präsentiertes Toxin von einer Zelle in eine Nachbarzelle übertragen wird. Die polymorphe und modulare CDI ist vermutlich in bakterieller Kommunikation und Konkurrenz involviert. Im Rahmen dieser Arbeit wurde die Rolle der CDI während bakteriellen Wachstums auf Oberflächen mittels Zeitraffermikroskopie untersucht. Das Aufeinandertreffen von Inhibitorzellkolonien mit resistenten und empfindlichen Zielzellkolonien wurde beobeachtet. Der Vergleich der Videoaufnahmen zeigte, dass CDI die Zellteilung von empfindlichen Zielzellen inhibiert. Dadurch begradigt sich die Kontaktfläche der beiden Kolonien. CDI wurde für die dynamische Kontrolle von Zellwachstum, als Kontrollsignal für ein logisches Puffergatter und für einen neuen Selektionsmarker verwendet. Vier unterschiedliche Toxin-Antitoxin-Paare wurden auf ihre Fähigkeit getestet die Wachstumsrate von *E. coli* reversibel zu verändern. Das als ECL bezeichnete Toxin-Antitoxin-Paar variierte das Zellwachstum auf Populations- und vermutlich auch auf Einzelzellebene. ECL wurde in ein System zur Markierung der Zellabstammung integriert um einfache Muster in *E. coli* Kolonien zu generieren. Ein logisches Puffergatter basierend auf einer veränderten Tryptophan Attenuatorsequenz wurde entworfen. Dieses Gatter wird durch ein CDI Toxin mit Alanin tRNase Aktivität reguliert. Die Tryptophan Attenuatorsequenz wurde mit Hilfe eines Programmes zur RNA Sekundärstrukturvorhersage so verändert, dass sie Attenuation als Antwort auf eine verringerte Alanin tRNA Konzentration zeigt. Erste Tests des logischen Puffergatters zeigten keinerlei Funktionalität. Um einen neuen Selektionsmarker zu entwerfen, wurden die Gene für das ECL Toxin-Antitoxin-Paar separiert. Das Toxingen wurde in das bakterielle Genom unter der Kontrolle eines induzierbaren Promoters integriert, während das Antitoxin konstitutiv als translationale mRFP1 Fusion von dem zu selektierenden Plasmid exprimiert wurde. Durch Vergleich von fluoreszierenden und nicht fluoreszierenden Kolonien konnte die Selektionseffizienz quantifiziert werden. Die Mutationshäufigkeit von ungefähr $10^{-5}$ lag im Bereich von auxotrophen *E. coli* Stämmen.

## Abstract

Contact-dependent growth inhibition (CDI) is a natural system in *E.coli* and other proteobacteria, in which a surface displayed toxin is transferred from one cell to its neighbor upon physical interaction. The polymorphic and modular CDI supposedly functions in bacterial communication and competition. This thesis investigates the involvement of CDI in growth on surfaces and also its potential as a new tool for synthetic biology. Time-lapse microscopy of colliding microcolonies was used to explore the significance of CDI during surface growth. Comparison of time-lapse movies obtained by collision of inhibitor cells with susceptible and immune target cells revealed that CDI leads to target cell filamentation and smoothes the colony interface. CDI was employed for tunable growth rate control, as control signal for a logic buffer gate and for a novel selection marker system. Four different toxin/antitoxin pairs were tested for their ability to reversibly change growth rate upon inducible expression in cells. The toxin/antitoxin pair called ECL was able to regulate cell growth on a population and presumably single cell level. This pair was subcloned into a cell-lineage marking system to generate simple patterns in *E.coli* colonies. A logic buffer gate based on a modified tryptophan attenuation module responding to a CDI toxin with Ala tRNase activity was devised. The tryptophan leader sequence was modified using RNA folding software to show attenuation based on the level of alanine tRNA, which in turn can be controlled by the amount of toxin. The logic buffer gate showed no functionality during initial tests. A toxin/antitoxin pair was separated to generate a novel selection system. The toxin was integrated into the chromosome under control of an inducible promoter, whereas the antitoxin was constitutively expressed as a translational mRFP1 fusion from the plasmid to be selected. Selection performance was quantified by comparing fluorescent with non-fluorescent colonies. Escape frequency was similar as in auxotroph *E.coli* strains.

## Acknowledgements

I would like to thank Drew Endy for the opportunity to perform my master thesis in his lab. Furthermore I am thankful for the fruitful and exciting scientific discussion and his advice.

My special thanks goes to Aymelt Itzen for the supervision and his support.

In addition I would like to thank Pakpoom Subsoontorn for getting me started in the lab and his feedback on design of experiments. I would also like to thank Paul Jaschke for being a huge source of knowledge on every lab problem I could encounter. I thank Atri Choksi and Eric Wei for tackling the time-lapse microscopy setup with me.

I would also like to thank the whole Endy Lab/NIST group that creates a wonderful environment to work in.

Finally I would like to thank my parents. Without their support I would not have come so far.

# 1 Inhalt

**Zusammenfassung** ..... **ii**

**Abstract** ..... **iii**

**Acknowledgements** ..... **iv**

**1 Bacterial contact-dependent growth inhibition** ..... **1**

*1.1 A new form of bacterial communication: Contact-dependent growth inhibition* ..... *1*

*1.2 CDI is a diverse and modular system* ..... *3*

*1.3 What is CDI's biological role?* ..... *4*

**2 Research Goal** ..... **5**

**3 Materials and Methods** ..... **6**

*3.1 Materials* ..... *6*

3.1.1 General instrumentation ..... 6

3.1.2 Software ..... 6

3.1.3 Antibiotic stocks ..... 6

3.1.4 Media ..... 7

3.1.5 *E.coli* Strains ..... 7

3.1.6 Plasmids ..... 8

3.1.7 Oligonucleotides and synthetized genes ..... 9

*3.2 Molecular Cloning* ..... *9*

3.2.1 PCR amplification ..... 9

3.2.2 Assembly of DNA parts ..... 10

3.2.3 Colony PCR ..... 12

3.2.4 Gel electrophoresis ..... 12

3.2.5 Plasmid isolation ..... 13

3.2.6 Preparation of chemical competent cells ..... 13

3.2.7 Transformation of chemical competent cells ..... 13

3.2.8 Sequencing ..... 13

3.2.9 Glycerol stocks ..... 13

3.2.10 Chromosomal integration of genetic devices ..... 13

*3.3 Time-Lapse microscopy* ..... *14*

3.3.1 Strains used for time-lapse microscopy ..... 14

3.3.2 Microscope setup ..... 15

3.3.3 Preparation of agarose pads ..... 15
3.3.4 Preparation of imaging samples ..... 16
3.3.5 Image acquisition ..... 16
3.3.6 Image processing ..... 16
*3.4 Growth experiments in liquid culture ..... 16*
3.4.1 Standard growth experiment ..... 16
3.4.2 Test for reversible growth rate change ..... 17
3.4.3 Determination of growth rate μ ..... 17
*3.5 Plate-based selection assay ..... 18*
3.5.1 Procedure of the plate-based selection assay ..... 18
3.5.2 Estimation of escape frequency ..... 18
*3.6 Growth competition in liquid media ..... 18*
**4 Control of cell growth by CdiA-CT$^{ECL}$/CdiI$^{ECL}$ expression for pattern formation ..... 19**
*4.1 Differential growth as a hallmark of pattern formation in nature ..... 19*
*4.2 Results ..... 19*
4.2.1 Assessing the suitability of CdiA-CT variants for growth rate control ..... 19
4.2.2 Growth rate change by ECL is reversible ..... 23
4.2.3 CdiA-CT$^{ECL}$ can control cell growth when homogenously induced ..... 24
4.2.4 Using CdiA-CT$^{ECL}$ expression to control colony morphology ..... 27
*4.3 Discussion ..... 31*
4.3.1 CdiA-CT$^{ECL}$ is a better candidate for growth regulation than other CDI rRNases ..... 31
4.3.2 The ECL expression module can be employed for efficient growth regulation ..... 31
4.3.3 Growth suppression by cdiA-CT$^{ECL}$ expression is reversible ..... 32
4.3.4 Improved experimental setup is necessary for CDI pattern formation ..... 33
**5 Observation of CDI during surface growth on single-cell level ..... 34**
*5.1 Time-lapse microscopy is suitable to investigate CDI during surface growth ..... 34*
*5.2 Results ..... 34*
5.2.1 Time-lapse microscopy of colliding microcolonies with constitutive CDI inhibitors ..... 34
5.2.2 Time-lapse microscopy of colliding microcolonies with inducible CDI inhibitors ..... 41
5.2.3 CdiI$^{EC869\ o11}$ overexpression causes excessive filamentation of *E.coli* ..... 48
*5.3 Discussion ..... 51*
5.3.1 Collision with CDI$^{EC93\text{-}EC869\ o11}$ inhibitors causes target cell filamentation ..... 51
5.3.2 Colony interface of inhibitor/target colonies is smoothened by target cell filamentation ..... 51
5.3.3 CDI$^{EC93\text{-}EC869\ o11}$ is far less potent during surface growth than in liquid media ..... 52

5.3.4 Biological implications of the observed “weak” CDI during surface growth ..... 54
5.3.5 CdiI$^{EC869\ o11}$ overexpression presumably induces the SOS response ..... 54

**6 A CDI/attenuation based buffer gate ..... 56**

*6.1 Design of an attenuation-based genetic buffer gate ..... 56*

*6.2 Results ..... 60*

6.2.1 RNA secondary structure guided design of the CdiA-CT$^{Bp1026b}$ attenuation-based buffer gate ..... 60

*6.3 Discussion ..... 64*

**7 A novel CDI based selection marker ..... 66**

*7.1 Current selection marker systems ..... 66*

*7.2 Results ..... 67*

7.2.1 Design of a novel selection system based on CDI ..... 67
7.2.2 Selection based on cdiA-CT/cdiI ..... 70

*7.3 Discussion ..... 77*

**8 Conclusion and Outlook ..... 79**

**9 List of abbreviations ..... 82**

**10 Bibliography ..... 83**

**11 Appendix ..... 89**

*11.1 Additional Figures ..... 89*

*11.2 Schematic construct diagrams ..... 91*

*11.3 Additional tables ..... 93*

# 1 Bacterial contact-dependent growth inhibition

## 1.1 A new form of bacterial communication: Contact-dependent growth inhibition

Interaction is an essential, defining part of every society (Lasswell, 1948), which is also true for bacterial communities (Bassler and Losick, 2006). Much is known already about the long-range form of communication via diffusible signaling molecules termed quorum sensing (Ng and Bassler, 2009; LaSarre and Federle, 2013). However, there are other short-range forms of communication depending on direct cell contact, for example the C signaling in *Myxococcus xanthu* (Lobedanz and Søgaard-Andersen, 2003). Another more widespread short range communication form is contact-dependent growth inhibition (CDI). CDI was first discovered in the *Escherichia coli* isolate EC93 in 2005 (Aoki et al., 2005). These cells, extracted from rat feces, strongly suppressed the growth of *E.coli* K12 when cocultured in liquid culture. Using two different sizes of a porous membrane, one allowing cells to pass through one not, they could demonstrate that cells needed to be in direct contact for growth inhibition to take place (Aoki et al., 2005). Furthermore, $CDI^+$ cells showed autoaggregation and binding to target cells.

Growth inhibitory activity is conferred by the *cdiBAI* gene cluster (see Fig. 1A). CdiB and CdiA constitute a two-partner secretion system, where CdiB supposedly an outermembrane protein, secretes and displays the CdiA protein. CdiA is a huge, filamentous hemagglutinin protein (~300 kDa) and can be imagined as a stick protruding probably several hundred angstrom from the surface of the cell (Ruhe, Low, et al., 2013). The far C-terminal end of CdiA, termed CdiA-CT (~25 kDa) constitutes the actual toxin domain. The third gene *cdiI* encodes an antitoxin, protecting the cell itself from the harmful effect of the CdiA-CT domain.

The conserved outer-membrane protein BamA (β-barrel assembly machine gene A, also called yaeT) has been identified as the CDI receptor. Upon contact with another *E.coli* cell the displayed CdiA presumably binds to BamA (Aoki et al., 2008). CdiA-CT is proposed to undergo proteolytic cleavage and to be transferred into the cytoplasm of the target cell (see Figure 1B) (Hayes et al., 2014).

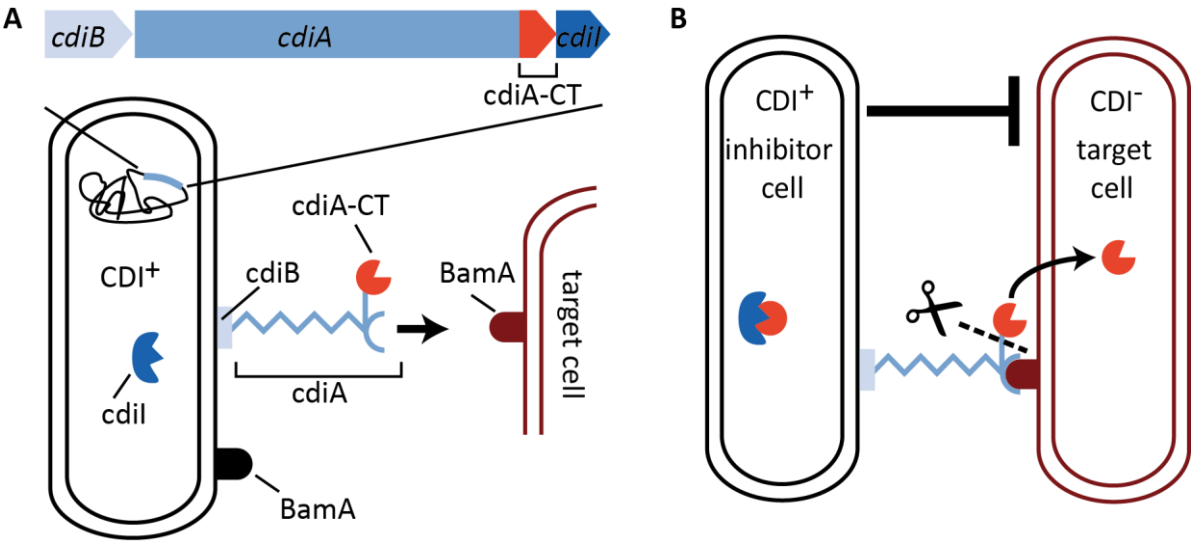


**Figure 1: CDI depends on the *cdiBAI* gene cluster located on the chromosome. CdiB is an outer membrane protein responsible for delivery and display of the CdiA protein. CdiA can be imagined as a long stick which binds to BamA on other cells. Its far C-terminal part is the actual toxin domain, CdiA-CT. CdiI protects the cell itself from the toxin activity of CdiA-CT. (B) Upon binding of CdiA to BamA on neighboring cells the CdiA-CT domain is cleaved off and transferred into the cytoplasm of the neighboring cells.**

As BamA is an essential outer membrane protein of *E.coli*, toxins are not only transferred into target cells ($CDI^-$) whose growth they inhibit (Figure 2A), but also to cells of the exact same inhibitor species ($CDI^+$) (Figure 2B). Compared to the interaction of $CDI^-$ cells (Figure 2C), $CDI^+$ inhibitor cells adhere to each other and transfer the toxin. The interaction between $CDI^+$ cells might have additional benefits, e.g. facilitated horizontal gene transfer or might play a role in biofilm formation. $CDI^+$ *E.coli* inhibit other $CDI^-$ *E.coli* strains, but cannot inhibit or bind other enterobacteria, like *Salmonella enterica* or *Proteus mirabilis*. Although BamA is a conserved and essential outer membrane protein, the *E.coli* CdiA cannot bind to BamA of other species, due to a polymorphism of the three extracellular loops (Ruhe, Low, et al., 2013; Ruhe, Wallace, et al., 2013) (Figure 2D).

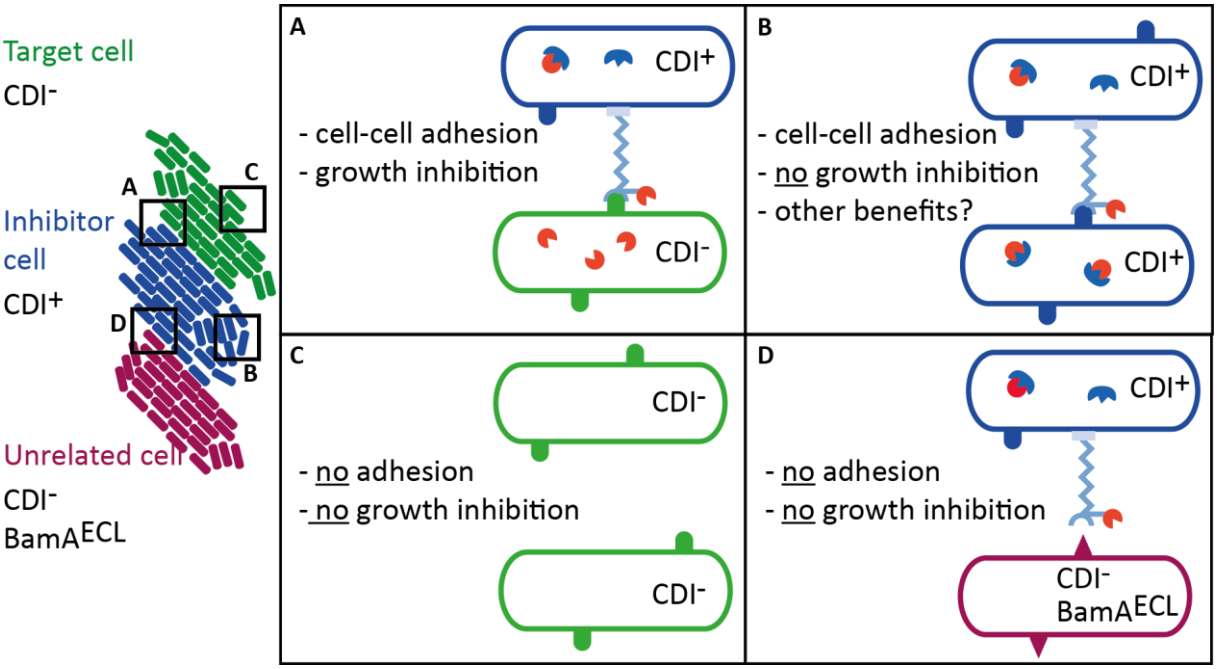


**Figure 2: Possible interactions between CDI+ and CDI- cells. (A) CDI$^+$ cells bind to CDI$^-$ and inhibit their growth. (B) CDI$^+$ cells bind to each other and transfer the toxin among themselves. (C) CDI- cells do not adhere to each other. (D) CDI$^+$ *E.coli* cells cannot bind and inhibit other enterobacteria, for example *Enterobacter clocae* (ECL), due to BamA polymorphism.**

## 1.2 CDI is a diverse and modular system

CDI systems have been found in various α-, β-, and γ-proteobacteria including in plant pathogens (*Dickeya* spp. and *Erwinia pyrifoliae)*, animal pathogens (*Moraxella catarrhalis)*, and in the human pathogens *Klebsiella pneumonia, Yersinia pestis* and uropathogenic *E.coli* (Aoki et al., 2011).

CDI is not only widely distributed in several bacterial species but also polymorph within one species. More than 1/6$^{th}$ of the sequenced *E.coli* genomes (576) contain a *cdi* gene cluster with at least 17 different *cdiA-CT* sequence types (Ruhe, Low, et al., 2013). The sequence of the N-terminal part of CdiA is highly conserved, whereas the CdiA-CT sequences considerably vary after a common start peptide motif VENN (Ruhe, Low, et al., 2013). To date toxin activities range from DNases (EC869 o11), ionophores (EC93), generic tRNases (UPEC536), specific tRNases (Bp 1026b and EC869 o5) to 16S rRNases (ECL) (Aoki et al., 2009, 2010; Morse et al., 2012; Webb et al., 2013; Ruhe et al., 2014) (see Figure 3).

The sequence conservation of CdiA-NT and the divergence after the VENN peptide motif to diverse toxin sequences suggests the modularity of CDI. Indeed chimeras where CdiA-CT domains are fused to the N-terminal part of CdiA originating from the first discovered toxin EC93 are fully functional (Aoki et al., 2010).

Remarkably CdiA-CT divergence seems to be coupled to CdiI divergence resulting in non-crossreacting toxin immunity pairs (Ruhe, Low, et al., 2013; Hayes et al., 2014).

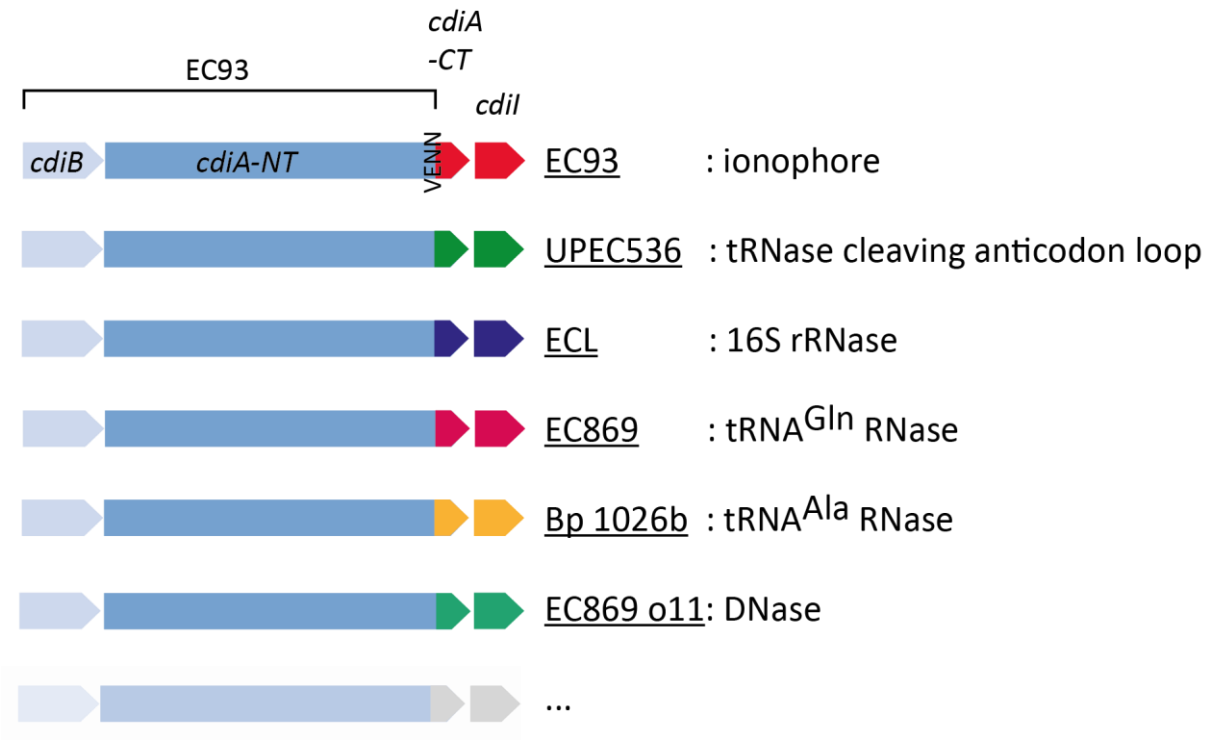


**Figure 3: CDI is a modular system. Chimeras consisting of the N-terminal CdiA domain from EC93 and various CdiA-CT toxins are fully functional.**

## 1.3 What is CDI's biological role?

It has clearly been shown that CDI is important in intraspecies competition. (Aoki et al., 2010; Nikolakakis et al., 2012; Koskiniemi et al., 2013). Different strains of the same species, e.g. different *E.coli* isolates compete by CDI, whereas CDI$^+$ *E.coli* can neither bind nor inhibit other species like Enterobacter clocae, due to the abovementioned BamA polymorphism.

As CDI is based on BamA present on all cells of the same species, CDI$^+$ cells also transfer the toxin constantly into cells originating from the exact same clone. In the light of the huge metabolic load for producing the toxin (cdiA is more than 3000 amino acids long) the continuous toxin transfer seems futile. Hence, it is likely that CDI has other beneficial effects for inhibitor cells.

The UPEC536 toxin, a generic tRNase, needs a cell permissive factor to be active within target cells. It is only able to degrade tRNase, thus inhibit target cell growth, when it is bound to CysK, an enzyme involved in cysteine metabolism. As CysK is not an essential enzyme target cells could easily escape the effect of the toxin. It has been proposed that toxin transfer in this case might not primarily be for intrastrain competition but might represent a communication channel between CDI$^+$ cells. Toxin transfer could have an influence on cysteine metabolism in a bacterial community (Diner et al., 2012).

A study on the CDI in *Burkholderia pseudomallei* during biofilm formation showed that cells expressing different CDI types mutually excluded each other from pillar structures. Thus CDI might allow bacteria to distinguish between self and non-self, enriching self cells in a given environment (Anderson et al., 2014).

CDI as a form of kin discrimination possibly constitutes an example of a so-called “green-beard” gene (West and Gardner, 2010; Strassmann et al., 2011). Carrier of a green-beard allele are able to identify other carriers of this allele and help those, whereas they harm cells that do not carry this allele. $CDI^+$ cells aggregate excluding cells from other strains (BamA polymorphism), thereby enumerating “self” cells in a community. Actions of microbes within this community, for example secretion of substances, benefit $CDI^+$ cells, (other green-beards). $CDI^-$ cells (no green-beards) of a different species are excluded from the community as their receptor cannot be recognized and bound , whereas other $CDI^-$ of the same strain (no green-beard) are even harmed by transfer of the toxin into their cytoplasm (West and Gardner, 2010; Strassmann et al., 2011; Ruhe, Wallace, et al., 2013).

# 2 Research Goal

The broad toxin diversity combined with non-crossreacting toxin/antitoxin pairs and the modularity of CDI make it a compelling choice of study, not only from a scientific but as well from an engineering perspective. This thesis investigates the role of CDI during surface growth and evaluates its potential as a new tool for synthetic biology.

Time-lapse microscopy of colliding microcolonies shall be employed to observe CDI during surface growth on a single cell level.

After characterization of several CDI toxin/antitoxin pairs, the gained insight shall be used for synthetic biology applications. CDI shall be employed to dynamically control growth of *E.coli* for pattern formation, for control of a logic buffer gate and as a novel selection marker system.

# 3 Materials and Methods

## 3.1 Materials

### 3.1.1 General instrumentation

The instruments used for experiments are listed in Table 1.

**Table 1: Overview of the general laboratory equipment used**

| Instrument | Instrument name | Manufacturer |
|---|---|---|
| Centrifuges | Avanti J-E | Beckman Coulter |
| | Microcentrifuge 5415 D | Eppendorf (Hamburg, D) |
| Shaker | Forma Orbital Shaker | Thermo Scientific (Waltham, MA) |
| | LT-X (Lab-Therm) | Kuhner Shaker (Birsfelden, CH) |
| Thermal Cyclers | S1000 Thermal Cycler | Bio-Rad (Hercules, CA) |
| | DNA Engine PTC-200 Peltier Thermal Cycler | Bio-Rad (Hercules, CA) |
| Plate Reader | SpectraMax i3 Multi-Mode Detection Platform | Molecular Devices (Sunnyvale, CA) |
| Gel Imaging Station | GBox XT4 | Syngene (Cambridge, UK) |
| Gel Electrophoresis | Owl EasyCast Gel Electrophoresis | Thermo Scientific (Waltham, MA) |
| Spectrophotometers | Nanorop 2000C | Thermo Scientific (Waltham, MA) |
| | WPA biowave CO8000 cell density meter | Biochrom (Cambridge, UK) |

### 3.1.2 Software

An Overview over the software used can be found in Table 2.

**Table 2: Overview over the used software**

| Software | Application | Distributor |
|---|---|---|
| R | Analysis of plate reader data | (R Core Team, 2014) |
| ImageJ | Image processing of microscopy images | Wayne Rasband |
| ApE version 2.0.47 | Display and manipulation of DNA sequences | M. Wayne Davis |
| Adobe Illustrator CS5 | Graphics design | Adobe (San Jose, CA) |
| RNAstructure (version 5.6) | RNA secondary structure prediction | Mathews Laboratory, University of Rochester (Reuter and Mathews, 2010) |
| VARNA (version 3-91) | Visualization of RNA secondary structure | (Blin et al., 2009) |
| µManager (version 1.3.43) | Control of the microscope | (Edelstein et al., 2010) |

### 3.1.3 Antibiotic stocks

Antibiotic stocks with the respective concentrations listed in Table 3 were prepared as 1000x stocks and stored ad -20°C. Antibiotic stocks were diluted 1:1000 unless otherwise noted.

**Table 3: List of antibiotic stock concentrations**

| Antibiotic | Stock concentration |
|---|---|
| carbenicillin | 100 mg/ml in $H_2O$ |
| chloramphenicol | 25 mg/ml in 100 % ethanol |
| tetracycline | 5 mg/ml in 70 % ethanol |
| kanamycin | 50 mg/ml in $H_2O$ |

### 3.1.4 Media

LB media and LB Agar were autoclaved after preparation. All individual solutions for supplemented M9 media were either filter-sterilized (pore size 0.2 µm) (thiamine hydrochloride) or autoclaved and stored (see Table 4). All solutions were combined using sterile techniques to prepare supplemented M9 media. Thiamine hydrochloride was added directly before use.

**Table 4: Composition of LB and supplemented M9 media**

| LB media | supplemented M9 media |
|---|---|
| 10 g Tryptone | 200 ml 5x M9 salts (56.4 g/l M9 salts) |
| 10 g yeast extract | 20 ml 10% casamino acids (0.1g/ml casamino acids) |
| 10 g NaCl | 10 ml 40% glycerol |
| 1 ml 1N NaOH | 2 ml 1M $MgSO_4$ |
| | 100 µl 1M $CaCl_2$ |
| | 733.9 ml $H_2O$ |
| | 34 mL thiamine hydrochloride (10 mg/ml) |

### 3.1.5 *E.coli* Strains

DH5αZ1 was used for molecular cloning and construct tests. MC4100 was used for time-lapse microscopy due to its fast growth rate. BW27786 was used for homogenous expression of the pBAD promoter (Khlebnikov et al., 2001). The genotypes of the strains can be found in Table 5.

**Table 5: Overview over the used *E.coli* strains**

| Strain | Genotype | Obtained from |
|---|---|---|
| DH5αZ1 | Δ(argF-lac)169, ϕ80dlacZ58(M15), ΔphoA8, glnX44(AS), λ-, deoR481, rfbC1, gyrA96(NalR), recA1, endA1, thiE1, hsdR17, $laci^q$, PN25-tetR, $Sp^R$ | Endy Laboratory, Stanford University, CA |
| BW27786 (Khlebnikov et al., 2001) | Δ(araD-araB)567, ΔlacZ4787(::rrnB-3), λ-, Δ(araH-araF)570(::FRT), ΔaraEp-532::FRT, ϕPcp13araE534, Δ(rhaD-rhaB)568, hsdR514 | CGSC, Yale University, CT |
| MC4100 | [araD139]B/r, Δ(argF-lac)169, λ-, e14-, flhD5301, Δ(fruK-yeiR)725(fruA25), relA1, rpsL150(strR), rbsR22, Δ(fimB-fimE)632(::IS1), deoC1 | Hayes Laboratory, UCSB, CA |

### 3.1.6 Plasmids

Plasmids used were either property of the Endy Laboratory (Stanford University, CA), of the Hayes Laboratory (UC Santa Barbara, CA) or of Fernan Federici (Universidad Católica de Chile, Chile). Construct diagrams can be found in the appendix 11.2.

**Table 6: List of assembled constructs**

| Construct | Purpose | Assembly type | PCR | Primer | Template |
|---|---|---|---|---|---|
| pBR1 | pBAD cdiA-CT$^{UPEC536}$, pTet cdiI$^{UPEC536}$ | Golden Gate | 1 | BR1 + BR2 | pCH10540 |
| | | | 2 | BR3 + BR4 | pCH10540 |
| | | | 3 | TS349 + TS460 | pTS1465 |
| | | | 4 | TS433 + TS455 | pTS1305 |
| pBR4 | Ctrl for pBR1/6/7/8 | Cut with XbaI and SpeI | | | pBR1 |
| pBR6 | pBAD cdiA-CT$^{ECL}$, pTet cdiI$^{ECL}$ | Golden Gate | 8 | BR15 + BR16 | pCH10445 |
| | | | 9 | BR17 + BR18 | pCH10445 |
| | | | 3 | TS349 + TS460 | TS1465 |
| | | | 4 | TS433 + TS455 | pBR1 |
| pBR7 | pBAD cdiA-CT$^{EC869}$, pTet cdiI$^{EC869}$ | Golden Gate | 10 | BR19 + BR20 | pCH10525 |
| | | | 11 | BR21 + BR22 | pCH10525 |
| | | | 3 | TS349 + TS460 | pTS1465 |
| | | | 4 | TS433 + TS455 | pBR1 |
| pBR8 | pBAD cdiA-CT$^{1026b}$, pTet cdiI$^{1026b}$ | Golden Gate | 12 | BR23 + BR24 | pCH10415 |
| | | | 13 | BR25 + BR26 | pCH10415 |
| | | | 3 | TS349 + TS460 | TS1465 |
| | | | 4 | TS433 + TS455 | pBR1 |
| pBR24 = pAT | pAT J23100 cdiI$^{ECL}$ mKate2 Selection plasmid | Gibson Assembly | 37 | BR44 + BR54 | p67 |
| | | | 38 | BR41 + BR55 | pBR6 |
| pBR25 | pBAD cdiA-CT$^{ECL}$, pTet cdiI$^{ECL}$ in pKTR | Gibson Assembly | 68 | BR56 + BR57 | pKTR |
| | | | 66 | BR58 + BR59 | pBR6 |
| pBR26 | pTet cdiI$^{ECL}$ in pKAG | Gibson Assembly | 69 | BR88 + BR89 | pKAG |
| | | | 67 | BR59 + BR60 | pBR6 |
| pBR33 | Integration yields ara_cdiA-CT strain | Gibson Assembly | 55 | BR80 + BR81 | pIT4KH |
| | | | 56 | BR82 + BR83 | pBR6 |
| pBR33_GFP | Integration yields ara_Ctrl strain | Gibson Assembly | 55 | BR80 + BR81 | pIT4KH |
| | | | 57 | BR82 + BR83 | pTS1465 |
| pBR34 | | Gibson Assembly | 82 | BR104 + BR105 | pCH10445 |
| | | | 58 | BR 82 +BR65 | pBR6 |
| | | | 59 | BR83 + BR64 | pBR6 |
| pBR29 | Bp 1026b attenuation based buffer gate with YFP reporter | Gibson Assembly | 49 | BR71 + BR72 | pSB4C5 |
| | | | 50 | BR73 + BR74 | Geneblock1 |
| | | | 51 | BR75 + BR76 | pTS1067 |
| pBR44 | Bp 1026b attenuation based buffer gate with GFP reporter | Gibson Assembly | 74 | BR71 + BR72 | pTS1242 |
| | | | 75 | BR92 + BR93 | pTS1129 |
| | | | 76 | BR73 + BR91 | pBR29 |

### 3.1.7 Oligonucleotides and synthetized genes

All oligonucleotides and synthesized genes were ordered from Integrated DNA Technologies (Coralville, Iowa). A list with all oligonucleotide and synthesized gene sequences can be found in the appendix (Table 16).

## 3.2 Molecular Cloning

### 3.2.1 PCR amplification

For amplification of desired parts the *PfuUltra II Hotstart DNA Polymerase master mix* (Agilent Technologies, Santa Clara, CA) was used. Reaction mixture and PCR program were used according to Table 7.

**Table 7: Reaction mixture for PCRs using Pfu Ultra II 2x master mix**

| **Reagent mixture** | | **PCR program** | | | |
|---|---|---|---|---|---|
| **Reagent** | **Volume [µl]** | **step** | **T [°C]** | **Time [s]** | **Cycles** |
| Pfu Ultra II 2x master mix | 20 | initial denaturation | 94 | 300 | |
| DNA template (20-100ng/µl) | 0.4 | denaturation | 94 | 60 | |
| Primer 1 (20 mM) | 0.4 | annealing | 55 | 30 | 36x |
| Primer 2 (20mM) | 0.4 | elongation | 72 | 30 per kb | |
| $H_2O$ | 20 | final elongation | 68 | 600 | |
| | | storage | 4 | ∞ | |

If DNA parts could not be amplified successfully using Pfu polymerase, the *Phusion High-Fidelity PCR Master Mix with HF Buffer* (Fisher, Waltham, MA) was employed. A gradient PCR was run (see Table 8) to determine the optimal annealing temperature.

**Table 8: Reaction mixture for PCRs using *Phusion High-Fidelity PCR Master Mix***

| **Reaction mixture** | | **PCR program** | | | |
|---|---|---|---|---|---|
| **Reagent** | **Volume [µl]** | **step** | **T [°C]** | **Time [s]** | **Cycles** |
| Pfu Ultra II 2x master mix | 12.5 | initial denaturation | 98 | 30 | |
| DNA template (0.5-5ng/µl) | 1 | denaturation | 98 | 5 | |
| Primer 1 (20 mM) | 0.375 | annealing | 60-68 | 10 | 35x |
| Primer 2 (20mM) | 0.375 | elongation | 72 | 15 per kb | |
| $H_2O$ | 11 | final elongation | 72 | 300 | |
| | | storage | 4 | ∞ | |

If both Pfu and Phusion polymerase failed in amplification of the target sequence *Platinum PCR Supermix* (Invitrogen, Carlsbad, CA) was used (see Table 9).

The plasmid DNA used as template for PCR reactions can result in significant background in subsequent assembly steps. To reduce background plasmid DNA was digested using the enzyme DpnI (NEB), which

cuts methylated DNA. After PCR reaction 1 µl of DpnI was added directly to the mixture. Incubation for 1.5 h at 37 °C was followed by the inactivation of the enzyme for 20 min at 80°C.

Subsequently PCR products were purified using the *QIAquick PCR purification kit* (Venlo, Netherlands). DNA was eluted in 50 µl distilled $H_2O$ and stored at -20°C until further use.

**Table 9: Reaction mixture for PCRs using *Platinum PCR Supermix***

| **Reaction mixture** | | **PCR program** | | | |
|---|---|---|---|---|---|
| **Reagent** | **Volume [µl]** | **step** | **T [°C]** | **Time [s]** | **Cycles** |
| Platinum PCR Supermix | 24 | initial denaturation | 94 | 60 | |
| DNA template (5 – 10 ng/µl) | 0.5 | denaturation | 94 | 15 | |
| Primer 1 (20 mM) | 0.25 | annealing | 55 | 16 | 35x |
| Primer 2 (20mM) | 0.25 | elongation | 72 | 60 per kb | |
| | | storage | 4 | ∞ | |

## 3.2.2 Assembly of DNA parts

Constructs were either assembled by Golden Gate Assembly (Engler et al., 2008, 2009) or Gibson Assembly (Gibson et al., 2009). Both methods are PCR-based, scarless, i.e. sequence independent, and multi-part assembly methods. Golden Gate Assembly was preferred over Gibson Assembly in case the ends of the parts to be assembled were likely to form secondary structures or for small parts (<200 bp). In both cases Gibson Assembly relying on the annealing of overlapping regions cannot perform well. Gibson Assembly was chosen when parts or vector backbones contained internal BsaI cut sites.

### *3.2.2.1 Golden Gate Assembly*

Golden Gate Assembly is based on type IIs restriction enzymes. Type IIs restriction enzymes cleave outside their recognition site generating sticky ends consisting of any desired nucleotide sequence (see Figure 4). Examples of these enzymes are BbsI, BsmBI and BsaI-HF (NEB, Ipswich, MA) the enzyme used here. PCR amplification with overhang primers was used to add the BsaI recognition sites. Primers were designed such that BsaI recognition sites were facing outwards relatively to their cut site. Concentration of individual PCR products was adjusted such that equimolar amounts of all parts were present. Reaction mixture and the thermocycler program performed are listed in Table 10. 10 µl of the reaction mixture were used for the transformation of chemical competent cells.

**Table 10: Reaction mixtures for assembly of DNA fragments via Golden Gate Assembly**

| **Reaction mixture** | | **program** | | |
|---|---|---|---|---|
| **Reagent** | **Volume [µl]** | **Temperature [°C]** | **Time [s]** | **Cycles** |
| T4 ligase buffer | 1 | 37 | 120 | 25x |
| n PCR products (20-100 ng/µl) | 0.5 each | 16 | 300 | |
| T4 ligase | 0.5 | 37 | 600 | |
| BsaI-HF | 0.5 | 80 | 600 | |
| $H_2O$ | 8 – n*0.5 | 4 | ∞ | |
| Total volume | 10 | | | |

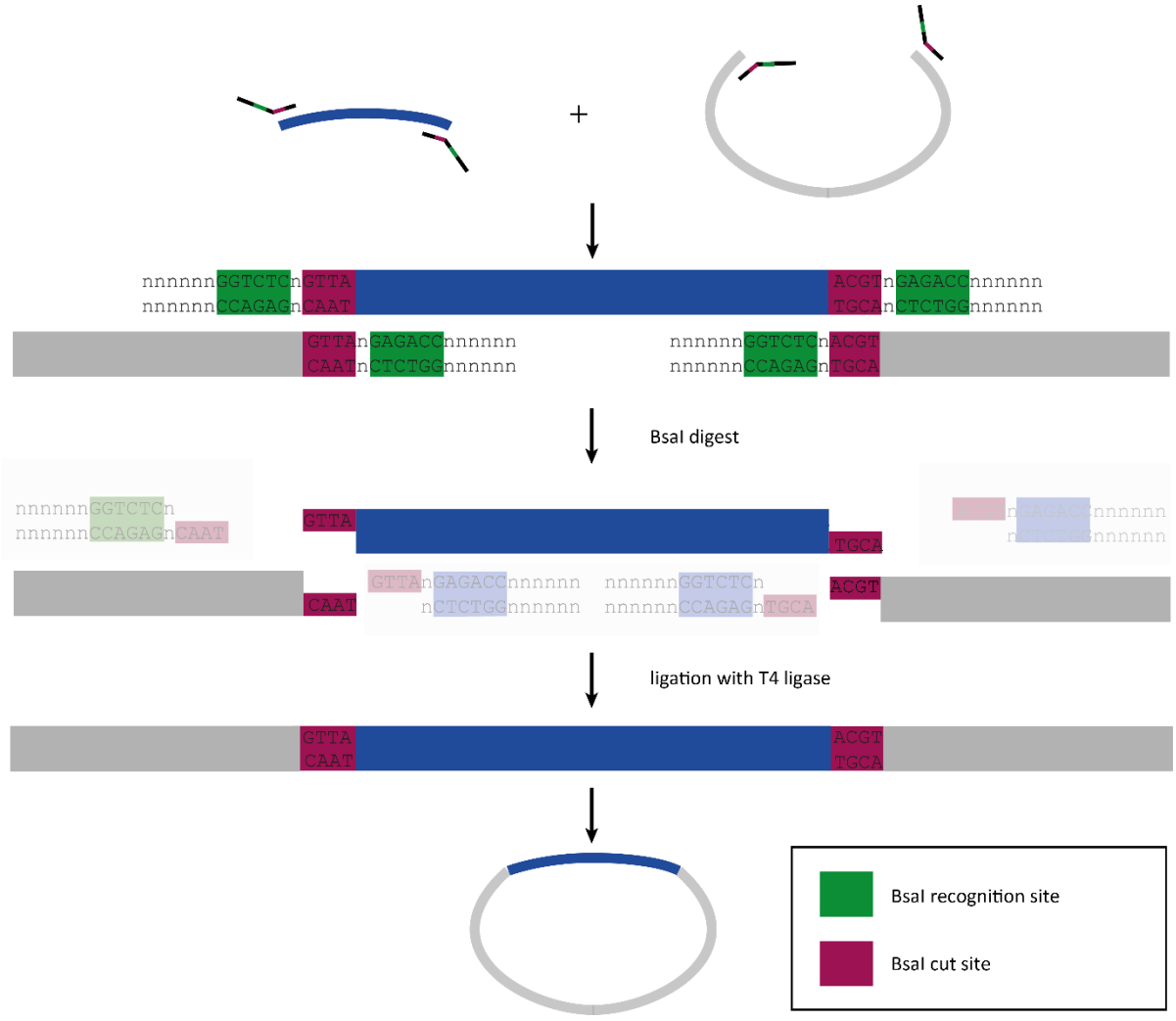


**Figure 4: Schematic representation of the Golden Gate Assembly method. DNA fragments are equipped with flanking BsaI recognition sites by PCR with suitable primers. After digestion with BsaI the fragments are ligated by T4 ligase yielding the circular construct.**

#### *3.2.2.2 Gibson Assembly*

Gibson assembly is an isothermal method to assemble several overlapping DNA fragments (Gibson et al., 2009). The Gibson assembly master mix was prepared according to Table 11 and stored in 15 µl aliquots at -20°C. Linearized fragments with complimentary overlaps (>25 bp) to adjacent fragments were generated by PCR amplification with specific primers. 100 ng of the linearized vector backbone and equimolar concentration of the other fragments to be assembled were added to 15 µl Gibson Assembly master mix (see Table 11). The final volume of the mixture was adjusted to 20 µl and incubated at 50°C for 1 h. 5 µl of the mixture was used for transformation of 50 µl chemical competent cells.

**Table 11: Composition of 1.2 ml Gibson Master Mix**

| Reagent | Volume [µl] | composition |
|---|---|---|
| 5x ISO buffer | 320 | 0.5 M Tris-HCl at pH 7.5, 0.05 M $MgCl_2$, 250 µM dGTP, 250 µM dATP, 250 µM dCTP, 250 µM dTTP, 0.05 M DTT, 5mM NAD, 0.25 g/ml PEG-8000 |
| T5 exonuclease [10 U/µl] | 0.64 | |
| Phusion polymerase [2 U/µl] | 20 | |
| Taq ligase [40 U/µl] | 160 | |
| $dH_20$ | 699.4 | |

### 3.2.3 Colony PCR

Colony PCR was used for screening of positive clones after assembly. Individual colonies were picked and resuspendend in 50 µl of distilled $H_2O$. 1 µl of this suspension and the respective primers were added to the *Kapa Hifi Hotstart DNA Polymerase Readymix* (see Table 12). After completion of the PCR program, length of generated PCR products was verified by gel electrophoresis.

**Table 12: Reaction mixture and PCR program colony PCR**

| Reaction mixture | | PCR program | | | |
|---|---|---|---|---|---|
| **Reagent** | **Volume [µl]** | **step** | **T [°C]** | **Time [s]** | **Cycles** |
| Kapa Hifi Hotstart Readymix | 5 | initial denaturation | 94 | 300 | |
| Colony in 50 µl $H_2O$ | 1 | denaturation | 94 | 60 | 36x |
| Primer 1 (20 mM) | 0.25 | annealing | 55 | 30 | |
| Primer 2 (20mM) | 0.25 | elongation | 72 | 15 per kb | |
| $H_2O$ | 3.5 | final elongation | 68 | 600 | |
| | | storage | 4 | ∞ | |

### 3.2.4 Gel electrophoresis

Gel electrophoresis was conducted to analyze the length of generated PCR fragments. Samples were loaded on 1% (w/v) agarose gels supplemented with ethidium bromide (1 µg/ml) and run at 110 V in

TBE buffer for about 40 min. A 2 log DNA ladder (NEB, Ipswich, MA) was used as a molecular weight standard.

### 3.2.5 Plasmid isolation

For plasmid isolation with the *QIAprep Spin Miniprep kit* (Venlo, Netherlands), 3 ml of a stationary overnight culture were used and plasmids were isolated according to manufacturer's instructions.

### 3.2.6 Preparation of chemical competent cells

For the preparation of chemical competent cells a stationary overnight culture was diluted 1:100 in fresh LB media (50-500 ml). After cells were grown to logarithmic phase ($OD_{600}$ 0.3-0.5) at 37° C (30° C) they were harvested by centrifugation for 10 min at 3000 rpm at 4° C. Pellets were resuspended in chilled TSS buffer (12.5 mM M PEG-8000, 29.5. mM $MgCl_2 \bullet 6H_2O$, 55 mM DMSO in LB media) (10 % volume of the original culture). 50 µl of the solution was aliquoted in tubes and frozen in liquid nitrogen. Aliquots were stored at -80°C until further use.

### 3.2.7 Transformation of chemical competent cells

Chemical transformation was performed to introduce the assembled DNA constructs or plasmids into *E.coli*. 0.5 µl of plasmid-DNA (~100 ng) was used for the transformation of 50 µl chemical-competent *E. coli* cells. The mixture was incubated on ice for 30 min. After heat-shock for 45 s at 42 °C, the mixture was kept on ice for another 2 min. The bacteria culture was then diluted with LB-Media (1:10) and incubated for 1 h at 37 °C and 600 rpm to allow for recovery and expression of resistance genes. Eventually cells were plated on LB plates supplemented with the respective antibiotics and incubated at 37 °C overnight.

### 3.2.8 Sequencing

All newly obtained or built plasmids were sequenced by Elim Biopharmaceuticals Inc. (Hayward, CA). Samples were prepared as a premix of plasmid DNA (about 500 ng) and the respective sequencing primer (2 µM).

### 3.2.9 Glycerol stocks

Glycerol stocks with 20% glycerol were generated for long-term storage of plasmids and strains at -80°C.

### 3.2.10 Chromosomal integration of genetic devices

Chromosomal integration was performed to stably insert genetic devices into the genome of an *E.coli* strain. The integration vectors as well as helper vectors were kindly provided by Francois St-Pierre (Endy Lab, Stanford University). The integration vectors (pIT4 vectors) are enhanced versions of the

original CRIM vectors developed by Haldimann and Wanner (Haldimann and Wanner, 2001). The integration vectors contain a specific phage attachment site (attP) which is recognized by the corresponding phage integrase encoded on the helper vectors. The complete integration vector is integrated at the respective attB site on the *E.coli* genome. Helper vectors contain a temperature-sensitive replicon thus are only propagated when cells are grown at 30° C. They express the phage integrase under control of the temperature sensitive factor lambda CIts (42°C). Upon induction of the phage integrase at 42°C the integration vector is integrated into the genome at the respective attB site.

The desired *E.coli* strain was transformed with the respective helper plasmid (HK22 integrase) and chemical competent cells were prepared. The genetic device to be integrated and the backbone of the pIT4KH vector were amplified via PCR. Gibson Assembly was performed to yield a pIT4KH vector containing the genetic device. 5 µl of the Gibson Assembly was used for the transformation of 50 µl helper vector containing competent cells. Cells were incubated on ice for 30 min, subsequently heat shocked for 45 s at 42° C and incubated for another 2 min on ice. 400 µl LB was added and cells were incubated at 30° C for 1 h to avoid loss of helper plasmid. After recovery cells were heat shocked at 42 °C for 30 min to allow for integrase expression. Cells were then plated on antibiotic plates (1/5 of concentration listed in Table 3) and incubated overnight at 37° C. Success of integration was tested by colony PCR (see 3.2.3) with verification primers P1, P2, P3 and P4 (see Table 16). Positive clones were tested for functional activity.

## **3.3** Time-Lapse microscopy

The procedure for time-lapse microscopy roughly followed the protocol of Young (Young et al., 2012). All bacterial cultures used for time-lapse microscopy were grown in supplemented M9 media to minimise autofluorescence.

### 3.3.1 Strains used for time-lapse microscopy

Time-lapse microscopy of colliding microcolonies at lower cell density was performed using the constitutive $CDI^{EC93\text{-}EC869\ o11}$ inhibitor strain CH2718 (target strains CH2578 and CH2579). Time-lapse microscopy of colliding microcolonies at higher cell density was performed with the IPTG inducible $CDI^{EC93\text{-}EC869\ o11}$ inhibitor strain CH2699 (target strains CH9404 and CH2578).

**Table 13: Strains used for collision experiments monitored by time-lapse microscopy**

| Name | description | Genotype | Obtained from |
|---|---|---|---|
| CH2578 | Susceptible target strain | MC4100 rif[1] mKate2::cat with pTrc99a | Hayes Laboratory, UCSB, CA |
| CH2579 | Immune target strain expressing cdiI$^{EC869\ o11}$ | MC4100 rif[1] mKate2::cat with pTrc99a::EC869 o11 cdiI | Hayes Laboratory, UCSB, CA |
| CH2718 | Constitutive CDI$^{EC93\text{-}EC869\ o11}$ inhibitor strain | MC4100 rif[1] GFP::kan with pDAL879::EC93-o11 CT/I | Hayes Laboratory, UCSB, CA |
| CH9404 | Immune target strain | MC4100 rif[1] *ΔyciB* mKate2::cat with pTrc99a | Hayes Laboratory, UCSB, CA |
| CH2699 | IPTG-inducible CDI$^{EC93\text{-}EC869\ o11}$ inhibitor strain | MC4100 rif[1] GFP::kan with pCH12502 (IPTG inducible cosmid) | Hayes Laboratory, UCSB, CA |

[1] spontaneous rifampicin resistance

### 3.3.2 Microscope setup

All images were taken using a Nikon (Tokyo, Japan) Eclipse TE2000-E inverted microscope equipped with Perfect Focus. The microscope was positioned on an antivibration table to avoid loss of focus during image acquisition. Phase contrast illumination was supplied by a halogen bulb. Lambda-XL (Sutter Instruments, Novato, CA) connected via a liquid light guide to the microscope served as epifluorescence lightsource. The open-source software μmanager (version 1.3.43) (Edelstein et al., 2010) was used to control camera, the MS 2000 motorized stage (ASI instruments, Warren, MI) and shutters. All images were acquired using a CoolSnap HQ2 CCD camera (Photometric, Tucson, AZ) and a 60x Plan Apo oil immersion objective (NA 1.4). During image acquisition temperature of the samples was constantly kept at 37°C by using an environmental chamber with heat control (World Precision Instruments, Sarasota, FL). The 89006 filter set from Chroma Technology Corp (Bellow Falls, VT) was used.

### 3.3.3 Preparation of agarose pads

22mm$^2$ cover slips (VWR, Radnor, PA) were cleaned with 70% ethanol and dried with air to remove dust. For preparation of agarose pads supplemented M9 media (see Table 4) with 1.5 % (w/v) UltraPure™ Low Melting Point Agarose (Life Technologies, Carlsbad, CA) was heated in the microwave and then allowed to cool before addition of thiamine hydrochloride and the appropriate antibiotics. 800 µl of the liquid agarose mixture was pipetted onto a 22mm$^2$ cover slip positioned on a dime. Another cover-slip was immediately placed on top yielding an evenly thick agarose cover-slip sandwich. Pads were covered and left to solidify at room temperature for 60 min. The top cover slip was removed and the pad was cut into 16 evenly sized, squared pads with a razor blade.

### 3.3.4 Preparation of imaging samples

Overnight cultures (LB media) were inoculated from glycerol stocks and incubated at 37° and 270 rpm. After 12 – 16 h ($OD_{600}$ 5.0 -6.0) cells were diluted to an $OD_{600}$ of 0.01 in fresh supplemented M9 media. After growing to mid-log phase (0.3-0.5) cells were diluted in fresh M9 media. For time-lapse imaging with constitutive inhibitor cells cells were individually diluted to an $OD_{600}$ of 0.015. 0.5 µl of the diluted inhibitor was spotted on the agar pad, subsequently 0.5 µl of the respective target strain dilution was spotted right on top of the inhibitor drop. For time-lapse imaging using IPTG-inducible inhibitor cells, strains were individually diluted to an $OD_{600}$ of 0.1. Inhibitor strains and target strains were mixed directly before 1 µl of the mixture was applied onto the agar pad.

After spotting of cells the pads were left to dry for 30 - 45 min. Afterwards the agarose pads were flipped onto the glass bottom dish (WillCo Wells, Amsterdam, Netherlands), such that the seeded side was in contact with the glass. The glass bottom dish was lidded and transferred into the temperature-controlled enclosure for acclimatization before sealing with parafilm. Non-fluorescent control cells (MC4100) were imaged for every separate experiment to correct for autofluorescence of cells.

### 3.3.5 Image acquisition

Maximal 2 different imaging positions on the same agarose pad were chosen to reduce photobleaching. X, Y and focus position for cells selected were saved in a position list. Perfect Focus offset was adjusted. Fluorescence exposure time was adjusted to allow for high intensity but at the time same to limit photobleaching (usually 250 ms for GFP and 400 ms for mKate2 fluorescence).

### 3.3.6 Image processing

ImageJ (Wayne Rasband) was used for processing of images. Image series from one position were imported into ImageJ and brightness of images as a whole was adjusted such that non-fluorescent cells imaged on a separate pad did not show on the images. All images from the same day and same imaging channel were set to the same display range. False color images were generated by merging the fluorescent channels and the phase-contrast images.

## 3.4 Growth experiments in liquid culture

### 3.4.1 Standard growth experiment

Growth experiments in liquid culture were performed to assess the impact of toxin expression on cell growth. Overnight cultures of the respective strains were inoculated and grown for 12- 16 h at 37°C and 270 rpm. The $OD_{600}$ of the stationary overnight cultures was measured in duplicates with the Spectramax i3 (Molecular Devices, Sunnyvale, CA). Cells were then diluted to an $OD_{600}$ of 0.01 in 6 ml fresh LB media supplemented with the appropriate antibiotics. Using an automatic pipette 200 µl of the dilution was aliquoted into the wells of a clear-bottom 96 well plate (Greiner Bio-One,

Kremsmünster, Austria). New serial dilutions starting from the stock solutions of anhydrotetracycline (atc) (2 mg/ml) and arabinose (10% w/v) were generated for each experiment. 2 µl of the respective serial dilution solution (see Table 14) were added where appropriate. Each condition was tested in triplicate. The starting $OD_{600}$ was recorded using the Spectramax i3. Afterwards plates were sealed with the gas permeable Aereseal sealing film (Excel Scientific, Victorville, CA) to avoid contamination and evaporation of liquid. Plates were incubated at 37 °C, 80 % humidity and 460 rpm in the LT-X plate shaker. Samples were taken out hourly for $OD_{600}$ measurements in the Spectramax i3.

**Table 14: Inducer concentrations for growth experiments**

| inducer | Dilution concentration | Final concentration |
|---|---|---|
| anhydrotetracycline | 20 µg/ml | 200 ng/ml |
| arabinose | 10 % (w/v) | 0.1 % |
| | 1 % (w/v) | 0.01 % |
| | 0.1 % (w/v) | 0.001% |
| | 0.5 % (w/v) | 0.005 % |
| | 0.01 % (w/v) | $5 \cdot 10^{-4}$ % |
| | 0.05 % (w/v) | $1 \cdot 10^{-4}$ % |
| | 0.005 % (w/v) | $5 \cdot 10^{-5}$ % |
| | 0.0075 % (w/v) | $7.5 \cdot 10^{-5}$ % |
| | 0.001 % (w/v) | $1 \cdot 10^{-5}$ % |
| | $1 \cdot 10^{-4}$ % (w/v) | $1 \cdot 10^{-6}$ % |

### 3.4.2 Test for reversible growth rate change

To test reversibility of growth rate change a standard growth experiment according to 3.4.1 using the final arabinose concentrations 0 % and 0.001 % (w/v) was performed. When cells supplemented with 0 % arabinose reached stationary phase, the liquid was removed from each well and transferred to 1.5 ml tubes. Tubes were centrifuged for 3 min at 3000 rpm and resuspended in fresh LB without inducer. After three of these washing steps the $OD_{600}$ of each sample was measured using the Spectramax i3. Cells were diluted to an $OD_{600}$ of 0.01 in a final volume of 200 µl of fresh LB media and supplemented with the respective inducer concentrations. After another growth cycle cells were washed three times as described above, rediluted in fresh LB to an $OD_{600}$ of 0.01 and the respective inducer was added.

### 3.4.3 Determination of growth rate µ

The mean growth curves obtained ($OD_{600}$ over time) for every inducer concentration were plotted as $\ln(OD_{600})$ over time. These curves were linearly fit during exponential growth phase (usually time points between 2 to 4 h). For an exemplary fit see Figure 41. The slope of the fits corresponds to the growth rate µ. µ was determined for two independent experiments and plotted against the arabinose concentrations used during the experiments.

## 3.5 Plate-based selection assay

### 3.5.1 Procedure of the plate-based selection assay

For the plate-based selection assay chemically competent cells of the strains were prepared (see chapter 3.2.6). The plasmids pAT and pCtrl were diluted to the same concentration (1 ng/µl; 0.25 ng/µl). 1 µl of each plasmid was used for transformation of both strains in triplicates. After 30 min incubation on ice cells were heat-shocked at 42°C for 45 s and subsequently kept on ice for 2 min. 1 ml of LB media supplemented with 0.1% L-arabinose was added to the cells that were incubated for 1 - 3 h at 37° C on a rotator. 100 µl (75µl) of each sample was plated on a LB agar plate with 0.1 % arabinose and a LB agar plate with carbenicillin (100 µg/ml). Plates were incubated for 12-16 h at 37° C. Red and white colonies on all plates were counted and pictures of the plates were taken using a Scanner (Epson Perfection V600, Epson America, Long Beach, CA).

### 3.5.2 Estimation of escape frequency

The amount of cells plated was estimated to be $1 \cdot 10^7$. Competent cells were made from cells grown to an OD of 0.3 corresponding to $2.34 \cdot 10^8$ cells/ml (Volkmer and Heinemann, 2011). Every aliquot of competent cells (50 µl) thus contains about $1.17 \cdot 10^8$ cells/ml (cells were resuspended in TSS buffer at 10% of their original volume). $1/10^{th}$ of the aliquot was spread on plates corresponding to about $1 \cdot 10^7$ cells plated per plate not accounting for cell growth occurring within the 3 h recovery time. On average 112 of these $1 \cdot 10^7$ cells were able to form colonies on arabinose plates, thus escaping the selection pressure by toxin expression. The escape frequency is therefore estimated to be less than $1 \cdot 10^{-5}$.

## 3.6 Growth competition in liquid media

For growth competition in solution overnight cultures were inoculated from permanent stocks. After 12 - 16 h overnight cultures were diluted 1:100 in 25 ml fresh LB media with carbenicillin. Inhibitor strains were grown in baffled flasks, target strain in normal flasks. When $OD_{600}$ of inhibitor cells reached mid-log phase all strains were diluted to an $OD_{600}$ of 0.1. Target and inhibitor strain were mixed at a 1:1 ratio in a total volume of 10 ml LB. When IPTG-inducible $CDI^{EC93\text{-}EC869\ o11}$ strains were used IPTG was added at a final concentration of 1.5 mM. For time point 0 samples were immediately removed from the flaks and diluted in M9 salts. Dilutions ($10^4$-$10^6$) were plated on LB chloramphenicol plates (25 µg/ml) to select for target cells and on LB kanamycin plates (10 µg/ml) to select for inhibitor cells. Cells were left to grow in competition at 37°C and 270 rpm for 3 h. After 3 h samples were removed from the flasks and $10^1$ dilutions were plated immediately, before finishing higher dilutions ($10^2$ - $10^8$). Plates were incubated for 16 - 20 h at 37°C and colonies were counted.

# 4 Control of cell growth by CdiA-CT$^{ECL}$/CdiI$^{ECL}$ expression for pattern formation

## 4.1 Differential growth as a hallmark of pattern formation in nature

The complexity of higher order organisms makes it often difficult to determine the underlying design principles of arising patterns in cell populations. A simplified system easy to manipulate and quantifiable could provide valuable information on general principles in pattern formation. *E.coli* is simple to engineer and formed patterns could be observed in detail using time-lapse microscopy (Locke and Elowitz, 2009).

Differential cell growth is one of the key processes involved in morphogenesis in higher organism (Oster and Murray, 1989; Meinhardt, 2008; Lander, 2011). To investigate how simple patterns arise from differential cell growth, growth rate of E.coli would need to be changeable on a single cell level.

To date growth rate control of E.coli is usually based on external control: differences in media composition or antibiotic treatment (Azam et al., 1999; Chang et al., 2002; Sezonov et al., 2007; Ehrenberg et al., 2013). With these external controls growth of cells is usually controlled on a population level, whereas growth of single-cells cannot be influenced.

An intrinsic growth control would be desirable to control growth of cell subpopulations and dynamically change growth rate during patterning. Contact-dependent growth inhibition offering a large variety of different toxin activities (Hayes et al., 2014) might provide means to dynamically control *E.coli* growth rate.

## 4.2 Results

### 4.2.1 Assessing the suitability of CdiA-CT variants for growth rate control

The requirements for a dynamic control of growth rate by toxin/antitoxin pairs are: tight control, i.e. no growth rate change without induction, a dynamic range of growth rate, the ability to be rescued by their respective antitoxins and reversibility of growth rate change.

In order to find toxins that meet the above mentioned criteria toxin/antitoxin pairs (CdiA-CT/CdiI) to be tested were selected on a rational basis. DNases and ionophores were excluded as their effect on the cell was judged to be irreversible. In contrast the effect of toxins with RNase activity should at least to a certain degree be reversible. As a result four toxin/antitoxin pairs with confirmed RNase activity were chosen for initial tests. CdiA-CT$^{ECL}$ which is a 16S rRNase (Beck et al., 2014), CdiA-CT$^{EC869\ o5}$ a Gln tRNAse (Ruhe et al., 2014), CdiA-CT$^{Bp\ 1026b}$ a Ala tRNase (Morse et al., 2012; Nikolakakis et al., 2012) and CdiA-CT$^{UPEC536}$ a generic tRNase (Aoki et al., 2010).

At first glance the simplest expression system would be to express the toxin under a set of constitutive promoters with different strength to achieve varying growth rate of the strain. However, cloning of vectors with constitutive toxin expression might proof very difficult. Positive clones would grow very slowly or might not even grow at all. Even when the toxin was expressed under inducible promoter, all attempts to separate the toxin from the antitoxin gene on plasmids failed.

As the dynamic range of available promoters is limited in order to meet the criteria of a range of growth rate both toxin and antitoxin should be expressed under inducible promoters. The gene for the toxin CdiA-CT was regulated by the arabinose inducible pBAD promoter, whereas antitoxin CdiI was expressed under the regulation of the anhydrotetracycline (atc) inducible pTET promoter. All four toxin/antitoxin pairs were cloned into the J64100 vector with a ColE1 origin (15-20 copies) and a chloramphenicol resistance cassette (see Figure 5).

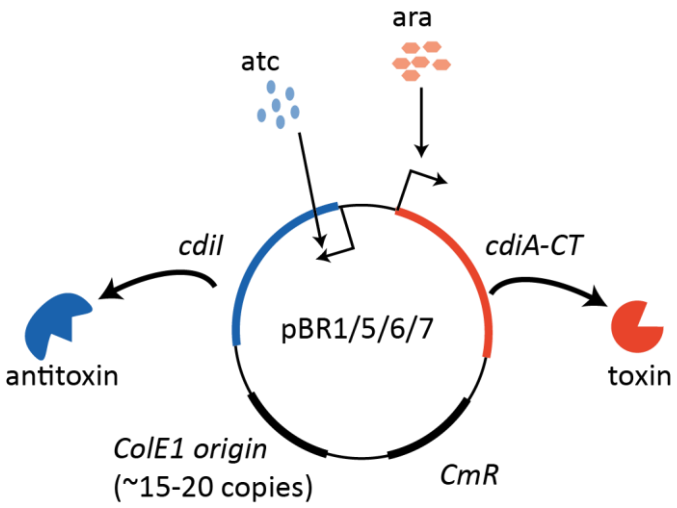


**Figure 5: Schematic showing the main features of the toxin/antitoxin expression plasmids.**

*E.coli* DH5αZ1 cells were transformed with the four successfully constructed plasmids. Cell growth of DH5αZ1 carrying the expression plasmids was monitored using a standard growth experiment. To vary the amount of toxin expressed four different arabinose concentrations were used (0 %, 0.001 %, 0.01 % and 0.1 % arabinose (w/v)). Antitoxin was either not expressed (0 ng/ml atc) or fully induced (200 ng/ml atc).

Growth of DH5αZ1 carrying the empty vector (pBR4) was similar for different arabinose concentrations in the absence or presence of atc (Figure 6A/B). Albeit cells growing at the highest arabinose concentration (0.1 % arabinose) showed a slightly decreased $OD_{600}$.

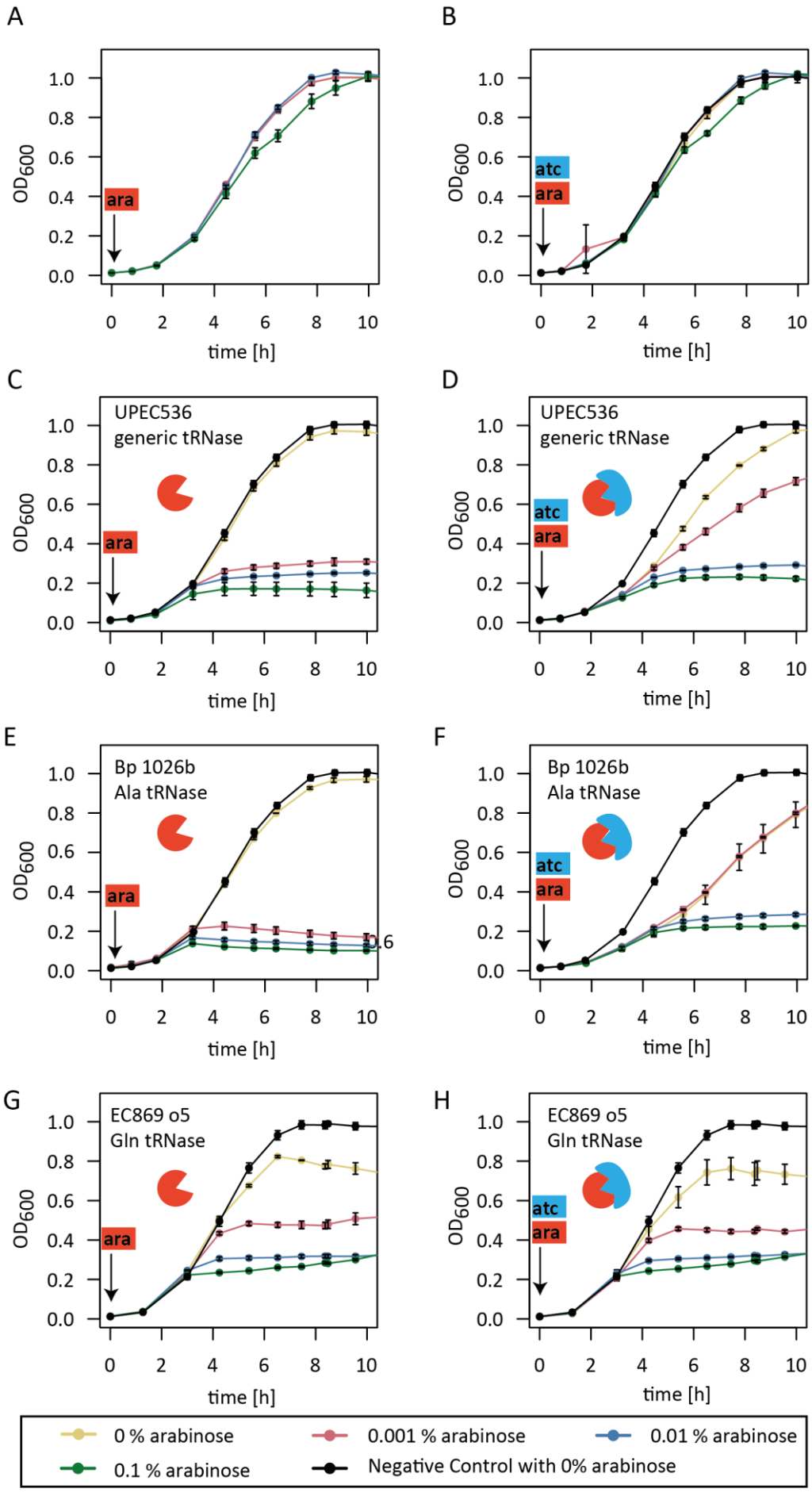
A
B
C
D
E
F
G
H
OD600
time [h]
ara
atc
UPEC536
generic tRNase
Bp 1026b
Ala tRNase
EC869 o5
Gln tRNase
0 % arabinose
0.001 % arabinose
0.01 % arabinose
0.1 % arabinose
Negative Control with 0% arabinose

**Figure 6: The toxins UPEC536, Bp1026b and EC869 o5 suppress growth when expressed within DH5αZ1. (A) DH5αZ1 growth is not influenced by addition of arabinose without (A) and with 200 ng/ml atc (B). Expression of CdiA-CT of UPEC536 (C) and of Bp 1026b (E) in DH5αZ1 suppresses growth. Expression of the cognate antitoxin is able to partially recover cell growth for the lowest toxin induction (D/F). DH5αZ1 carrying the plasmid for CdiA-CT$^{EC869\ o5}$ expression shows a growth defect in absence of induction and varying growth rate for different induction levels (G). Expression of EC869 o5 antitoxin does not seem to have any beneficial effect on growth rate of DH5αZ1. Values are the mean ± SD of three independent samples.**

Cells containing the vector with the toxin/antitoxin pair of the generic tRNase UPEC536 showed normal growth in the absence of induction (see Fig. Figure 6C, yellow line). When the toxin was expressed cells seemed to stop growing, i.e. reach stationary phase after only 4 h post induction and regardless of the expression level only reached a maximum $OD_{600}$ of about 0.3. Full induction of antitoxin expression lead to a slight growth defect even in the absence of toxin expression (see Figure 6D, yellow line) and seemed to prolong lag phase (compare colored lines with black line in Figure 6D). Antitoxin expression was able to increase cell growth for the lowest toxin induction (0.001 % arabinose, pink line Figure 6D), but could not recover cell growth for higher toxin levels (blue and green line Figure 6D).

Cells carrying the plasmid with the expression cassettes for the Ala tRNase Bp 1026b showed a similar behavior as with UPEC536. In the absence of toxin induction (see Figure 6E, yellow line) cells grow similar to the negative control, when the toxin is induced cells stop growing after about 3 h (see Figure 6E, pink, green, blue lines). After 4 h the $OD_{600}$ seems to be slightly decreasing which might be due to cell death. When the antitoxin is fully induced cell show a longer lag phase and a decreased growth rate even in the absence of toxin expression (see Figure 6F, yellow line). Antitoxin expression can alleviate growth suppression for the lowest toxin expression level (pink line) and seems to stop $OD_{600}$ decrease (cell death) in the case of higher induction levels (green, blue line Figure 6F).

Cells carrying the Gln tRNase EC869 o5 expression module DH5αZ1 shows a growth defect even without toxin induction (compare black and yellow line in Figure 6G). In contrast to cells carrying Bp 1026b and UPEC536 expression plasmids those with EC869 o5 show different growth rates for different toxin induction levels (pink, green and blue line Figure 6G). Full antitoxin expression does not seem to relieve toxin effect in any case (see Figure 6H).

All three expression modules UPEC536, Bp 1026b and EC869 o5 do not meet the criteria for tunable growth rate control. In the case of the first two growth rate cannot be tuned and toxin effect is not fully reversible by antitoxin expression. Expression of EC869 o5 cannot be tightly regulated and CdiI$^{EC869\ O5}$ expression does not reverse the toxin effect.

The fourth toxin tested, the 16S rRNase ECL, is the most promising candidate for growth rate control (see Figure 7A). Growth rate of *E.coli* DH5αZ1 carrying the expression plasmid grow at the same rate as the negative control in the absence of inducer (see Figure 7A black and yellow line). Low toxin

induction (pink line) slows cell growth, higher induction levels lead to a similar growth stop observed by overexpression of the other toxins (blue, green line). Full induction of the antitoxin does not affect cell growth in the absence of toxin induction (see Figure 7B yellow and black line). At the lowest toxin induction level antitoxin expression is able to fully recover growth (see Figure 7B pink line). At higher toxin induction level cell growth is partially recovered leading to a lowered growth rate (blue and green line).

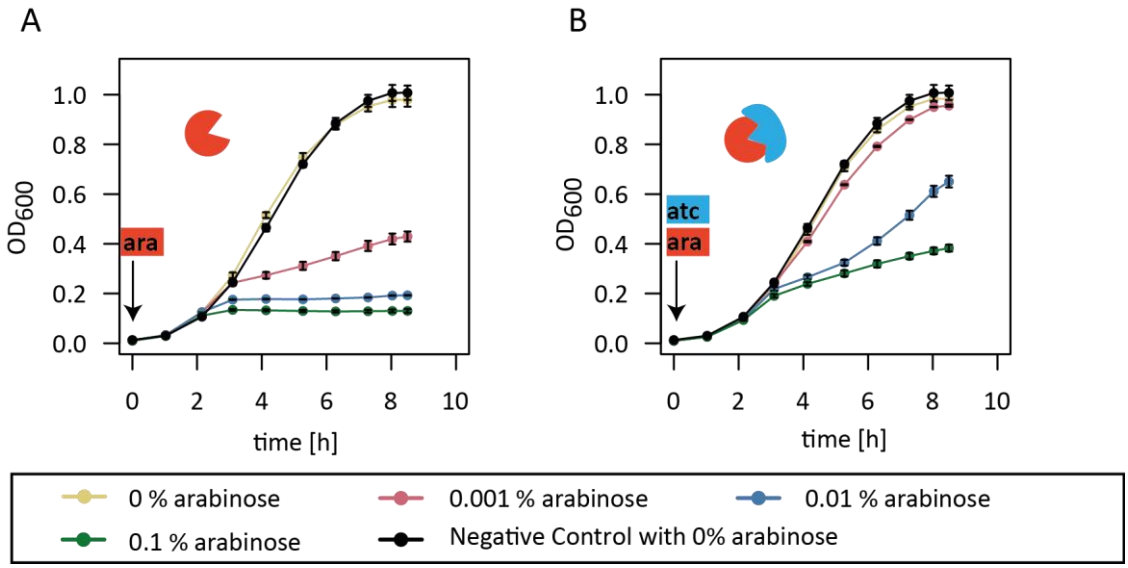


**Figure 7: Growth of DH5αZ1 carrying the ECL expression plasmid can be tightly regulated. (A) Increasing toxin induction slows cell growth. (B) Full expression of the ECL antitoxin by atc addition can rescue growth of DH5αZ1 subjected to the lowest toxin induction level and partially recover growth for higher induction levels. Values are the mean ± SD of three independent samples.**

### 4.2.2 Growth rate change by ECL is reversible

In order to determine if growth rate change caused by CdiA-CT$^{ECL}$ can be reversed a regrowth experiment was performed (see Figure 8). DH5αZ1 carrying the ECL expression plasmid (pBR6) or the backbone control (pBR4) were grown in the presence of the lowest arabinose concentration 0.001 % and in absence of arabinose. In phase I cells carrying pBR6 subjected to arabinose showed slowed growth as previously shown (compare Figure 7A with Figure 8A) and growth comparably to cells carrying the control plasmid in the absence of arabinose (compare pink line Figure 8A/B). After cells that were not treated with arabinose reached stationary phase (Figure 8A, pink line), arabinose was removed by washing and cells were rediluted to $OD_{600}$ 0.01. In phase II these cells were then either subjected to 0.01 % arabinose or did not receive inducer. Cells without inducer recovered growth reaching the same final $OD_{600}$ of 1.0 as control cells (compare pink lines, Figure 8A and B), but showed a significantly longer lag phase than control cells or cells grown without inducer in phase I. The cells which showed recovered growth in the absence of arabinose were washed, rediluted and split into cells that received arabinose and those that did not (phase III). Recovered cells in the presence of

arabinose showed growth suppression whereas cells without inducer showed growth rate comparably to growth in phase I or the negative control. The lag phase of cells was shorter again and can be compared to the lag phase of phase I or the negative control.

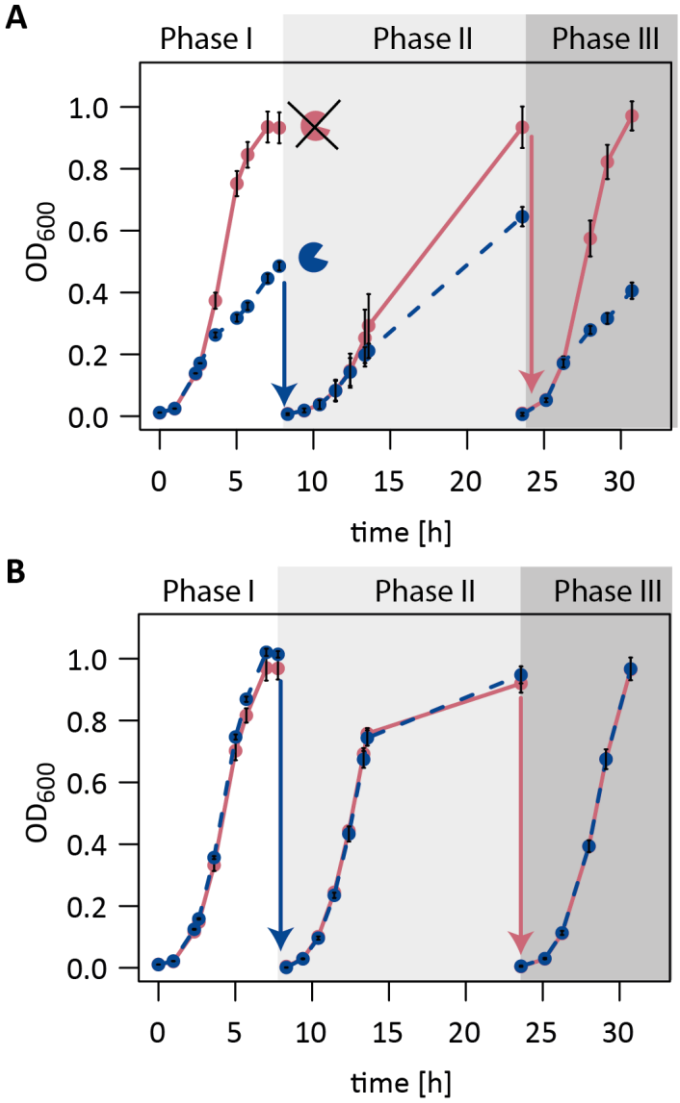


**Figure 8: Growth slowdown caused by ECL induction is fully recoverable. (A) DH5αZ1s containing the ECL expression plasmid that are subjected to 0.001 % arabinose (blue lines) show slowed growth or normal growth in absence of arabinose (pink lines) (phase I). In phase II growth of formerly ECL expressing cells can be fully recovered in absence of arabinose (pink line), but shows longer lag phase. The ECL expression module stays functional as growth can still be suppressed (blue line). Growth of recovered cells can be suppressed when again subjected to arabinose (blue line) and shows normal growth in absence of arabinose (pink line). (B) DH5αZ1 growth is not influenced by arabinose addition (blue line). Growth in all three phases is similar independent of arabinose addition. Lag phase of all cells is comparable. Values are the mean ± SD of three independent samples.**

### 4.2.3 CdiA-CT$^{ECL}$ can control cell growth when homogenously induced

Expression of the pBAD promoter in DH5αZ1 is not homogenous, but shows an all-or-none response to induction. Intermediate levels of arabinose as inducer result in an intermediate expression level.

However, this intermediate expression level is not due to all cells expressing an intermediate level of the gene of interest, but is caused by only a fraction of cells expressing the gene of interest on a high level. This behavior is caused by the autocatalytic positive feedback loop in the arabinose operon. Expression of the high- and low-affinity arabinose transporter is regulated by AraC which is induced by arabinose. A very low amount of inducer will result in the upregulation of transporter which in turn will increase intracellular arabinose concentration leading to even higher transporter concentration. Low arabinose concentrations lead to a mixed population with cells fully induced and cells not induced (Siegele and Hu, 1997).

Slowed growth of *E.coli* DH5αZ1 could only be observed for the low arabinose concentration of 0.001 %, whereas higher arabinose concentrations (0.01% and 0.1 % arabinose) seemed to stop growth. Thus the observed slowed growth for 0.001 % arabinose may in fact be a mixed population of halted cells and normally growing cells.

For most applications, amongst others pattern formation, a uniform cell growth would be desirable. The strain BW27786 was used to test if the ECL expression system can be used to slow cell growth in when the toxin is homogenously expressed. BW27786 is deficient for arabinose breakdown and the high-affinity arabinose transporter and constitutively expresses the low-affinity arabinose transporter AraE from the chromosome. It has been shown that expression from the pBAD promoter in this strain is homogenous, i.e. intermediate inducer levels lead to intermediate gene expression in all cells (Khlebnikov et al., 2001).

As BW27786 does not contain the *tetR* expression cassette on the genome needed for the regulation of pTET, cells were cotransformed with the ECL expression plasmid (pBR6) and a plasmid coding for a constitutively expressed *tetR* (pTS1127). 8 different arabinose concentrations for toxin induction were tested. Cells carrying the ECL expression plasmid (pBR6) showed normal growth comparable to growth of cells containing the control plasmid (pBR4) (see Figure 9A, black and dark blue line). Lower arabinose concentrations ($1 \cdot 10^{-6}$ % and $1 \cdot 10^{-5}$ % (w/v)) did not seem to have any effect on growth rate. Intermediate inducer concentration (($5 \cdot 10^{-5}$ %, $7.5 \cdot 10^{-5}$ % and $1 \cdot 10^{-4}$ % (w/v)) slowed cell growth considerably. Cells subjected to high levels of inducer (0.001 % and 0.01 % (w/v)) stopped growing after 2 h but seemed to resume growth after 7 h showing a steep increase in $OD_{600}$ even surpassing $OD_{600}$ of cells with intermediate inducer level.

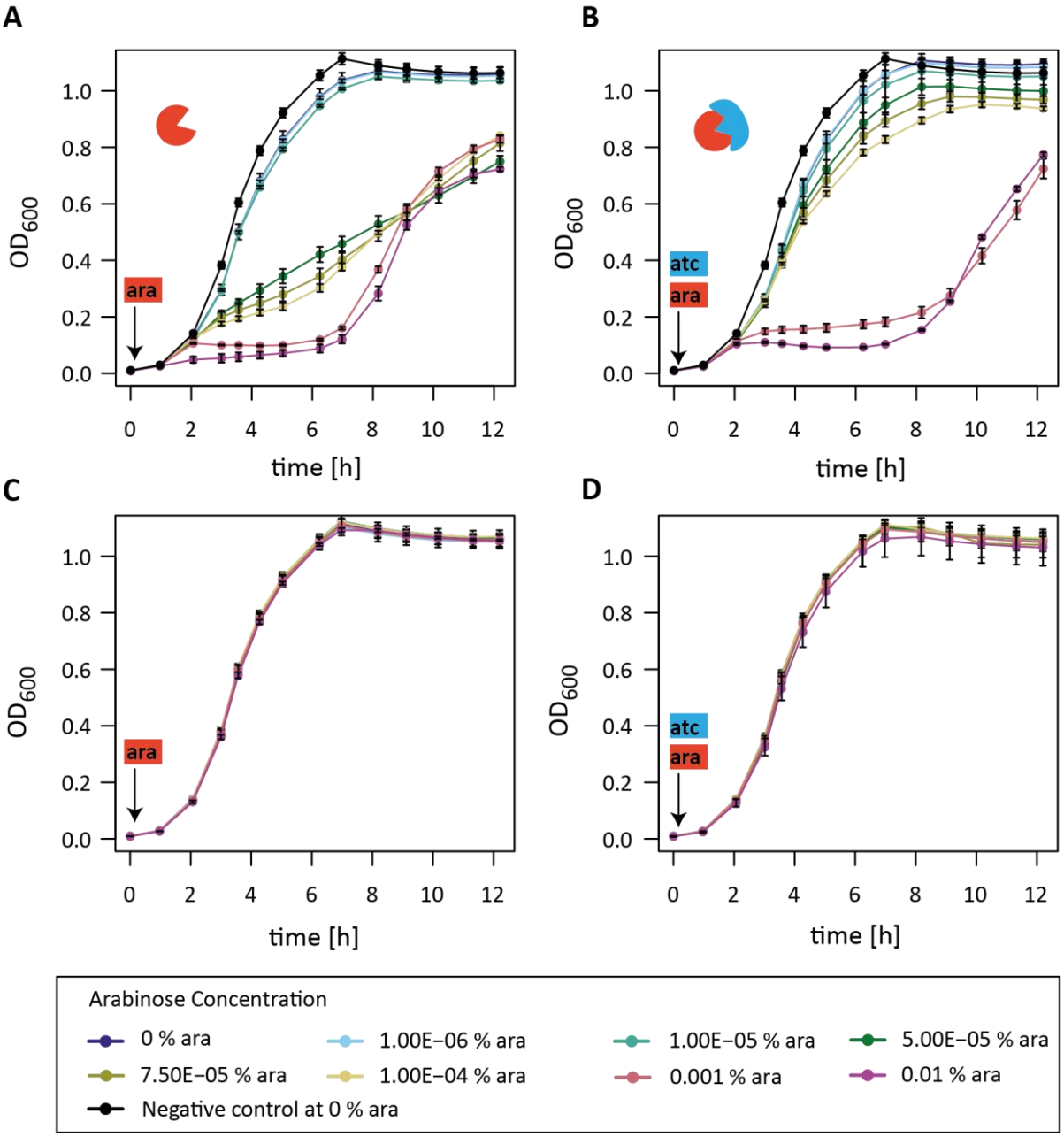


**Figure 9: Expression of ECL can slow growth when homogenously expressed in BW277786. (A) Growth of *E.coli* BW27786 carrying the ECL expression plasmid (pBR6) is increasingly slowed with increasing arabinose concentrations. Cells subjected to high arabinose concentrations (pink and purple line) seem to stop growing completely for the first 7 hours, but show a steep increase in $OD_{600}$ after 7 hours. (B) Cells express antitoxin (atc addition) and varying levels of toxin. Growth of cells expressing intermediate arabinose concentrations can be partially rescued, whereas the halted state of cells subjected to high toxin levels seems to be stabilized (pink and purple lines). Growth of BW27786 containing the control plasmid (pBR4) is not influenced by arabinose addition to the media in the absence (C) or presence of atc (D). Values are the mean ± SD of three independent samples.**

Antitoxin induction had no detrimental effect on cell growth in general and thus cells at low levels of inducer grow at a similar rate as the control cells containing pBR4. Cell growth at intermediate levels of toxin induction can be partially recovered by antitoxin expression resulting in slightly decreased growth rate (see Figure 9B). At high toxin induction levels antitoxin expression slightly increases the stationary phase $OD_{600}$ that is reached after about 3 h (see pink and purple line, Figure 9B). More

important antitoxin expression seems to shift the time when cells start to regrow from 7 to about 9 hours. Growth of cells only containing the empty backbone pBR4 is neither influenced by different arabinose concentration nor by atc addition (see Figure 9C/D).

### 4.2.4 Using CdiA-CT$^{ECL}$ expression to control colony morphology

Haseloff and coworkers recently developed a cell-lineage marking system (Rudge et al., 2013). This system comprises two low copy plasmids with an identical origin of replication and an antibiotic marker for kanamycin. In addition one plasmid contains a tetracycline resistance gene and a gene cassette for constitutively expressing mRFP1 (pKTR), whereas the other contains an ampicillin resistance gene and a constitutively expressed gene encoding superfolderGFP. Both plasmids can be maintained within one cell by selection with ampicillin and tetracycline. When cells are transferred in media containing kanamycin the plasmids are randomly segregated resulting in *E.coli* cell-lineages marked with two different fluorescent proteins. Cells growing on agarose pads generate fluorescently labeled patterns that can be observed via microscopy (Rudge et al., 2013).

A very simple pattern that could be realized using the cell-lineage marking system is shown in Figure 10. By placing the cassette for the ECL module from plasmid pBR6 onto one of the segregation plasmids the growth of one of the cell-lineages could be regulated. Addition of increasing arabinose concentrations to the media would change the colony morphology by decreasing the sector size of the cell-lineage carrying the toxin expressing plasmid.

The toxin/antitoxin expression cassette from pBR6 was subcloned into the pKTR vector provided by Fernan Federici yielding plasmid pBR25. The antitoxin module was placed onto the second segregation plasmid (pBR26) to make both plasmids more comparable and to avoid undesired selection effects.

*E.coli* BW277786 was cotransformed with the plasmids pBR25 and pBR26 and for control with pKAG and pKTR. As BW27786 lacks *tetR* and it cannot be supplemented on another plasmid as in earlier experiments, the antitoxin module will be constitutively expressed on both plasmids.

Growth of cells carrying the modified and unmodified cell-lineage marking plasmids (see Figure 11) was first assessed in liquid culture. Even in the presence of constitutively expressed antitoxin, growth of BW277786 carrying pBR25 could be decreased by increasing arabinose concentrations. When growth of cells with pBR25 is compared with cells with pBR26 the longer lag phase is notable. However, comparing growth of cells carrying the original segregation plasmids pKTR and pKAG, cells with pKTR (corresponds to pBR25) show also an extended lag phase (see Figure 11C and D). Cells containing both pBR25 and pBR26 subjected to low arabinose concentrations ($1 \cdot 10^{-5}$ %, $5 \cdot 10^{-5}$ %, $1 \cdot 10^{-4}$ %) show almost normal growth (see Figure 11E). Higher arabinose concentrations cause slowed growth of

BW277786 carrying both pBR25 and pBR26 albeit less drastic as in cells only containing pBR25 (compare Figure 11E and A). Growth of BW27786 tranformed with both pKAG and pKTR is not influenced by varying arabinose concentrations (see Figure 11F).

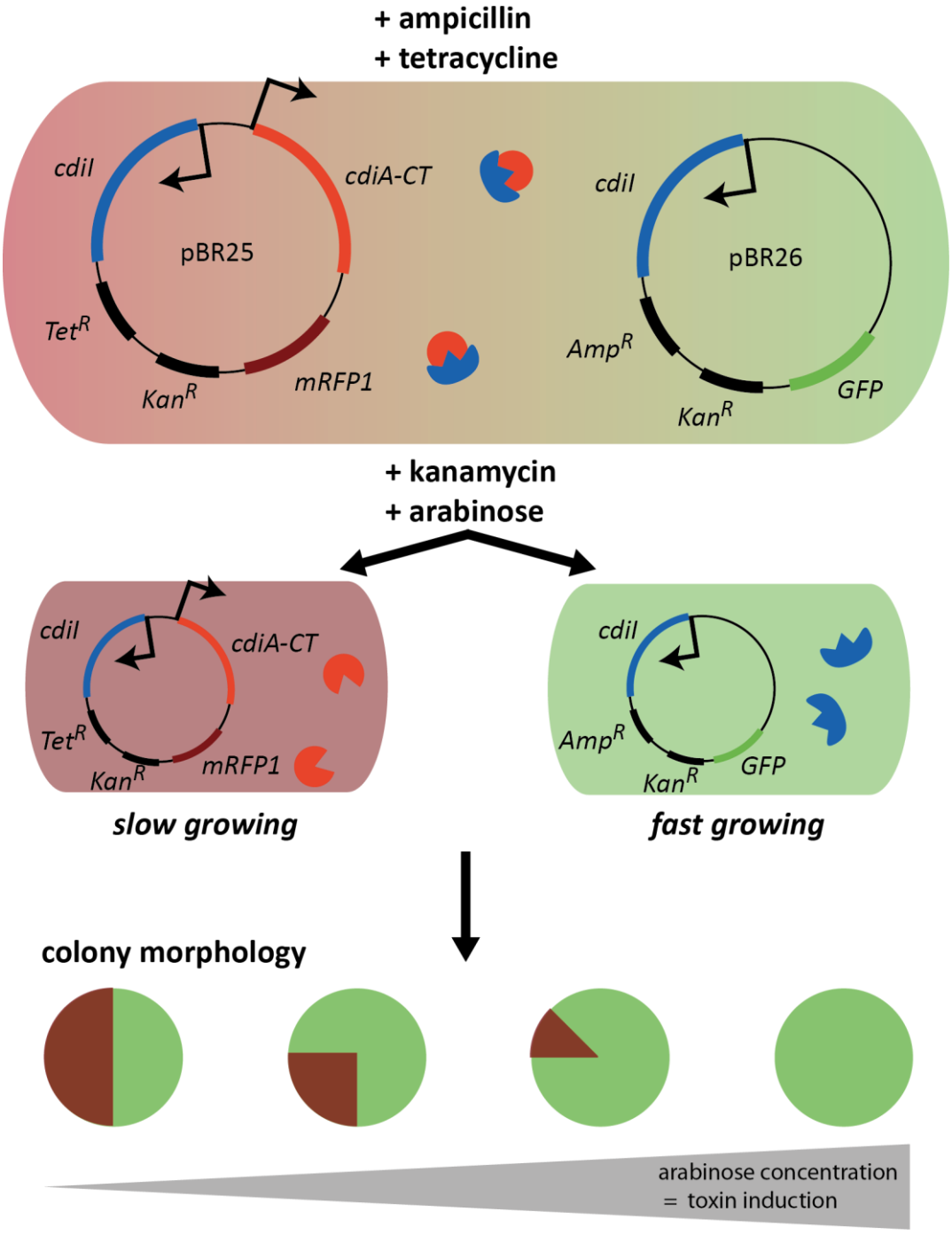


**Figure 10: Schematic explaining how the cell-lineage marking system in conjunction with toxin expression can be used to generate simple patterns in colonies.**

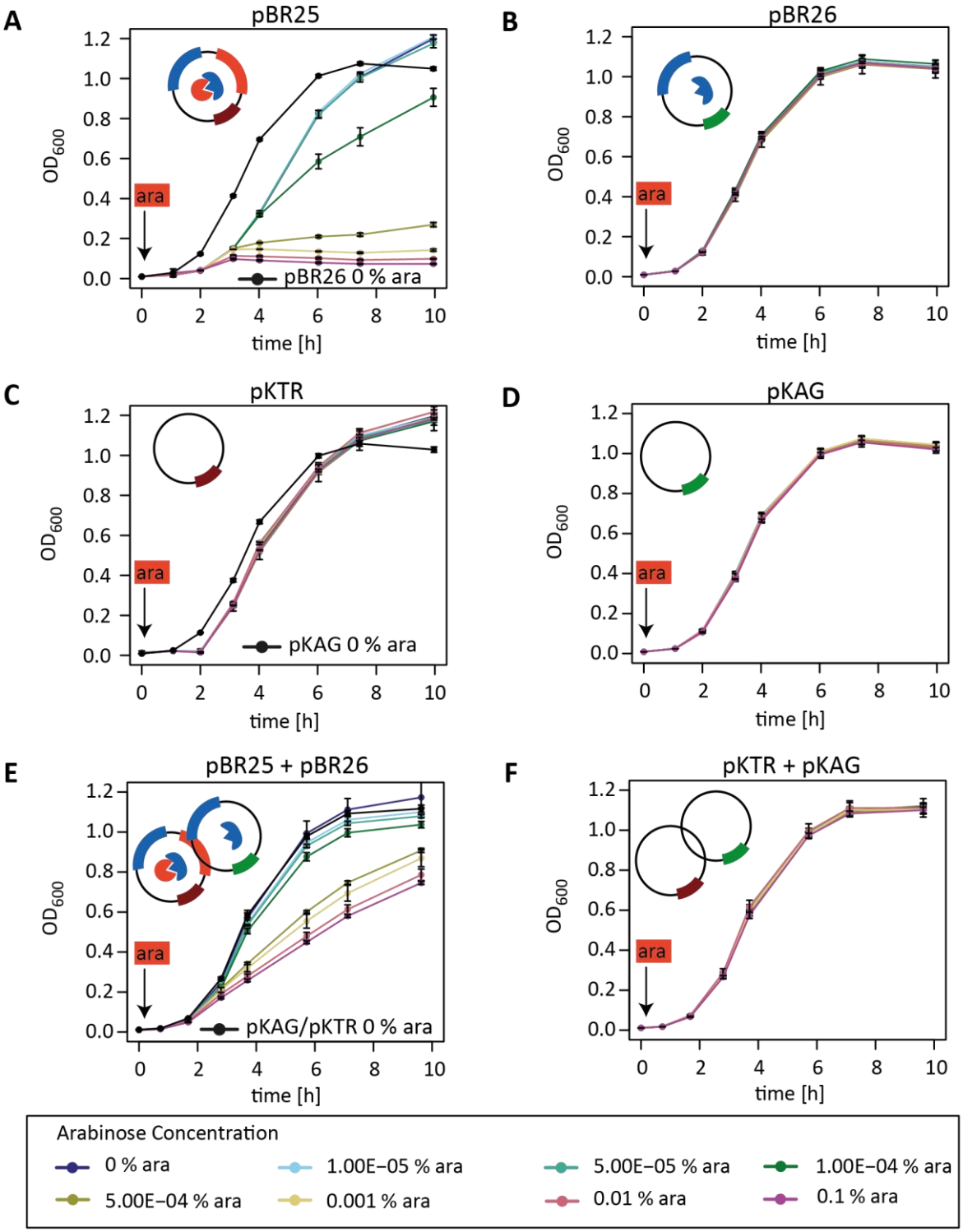


**Figure 11: The ECL expression module is functional on the segregation plasmid. (A) Growth of BW277786 carrying pBR25 can be regulated by addition of arabinose. (B) BW27786 carrying pBR26 shows similar growth for varying arabinose concentrations. BW277786 carrying the original segregation plasmids pKTR (C) and pKAG (D) show normal growth rates at varying arabinose concentrations. (E) Growth of BW27786 carrying pBR25 and pBR26 is influenced less by varying arabinose concentrations. (F) Cells carrying both original segregation plasmids are not influenced by arabinose in their growth. Values are mean ± SD for three independent samples.**

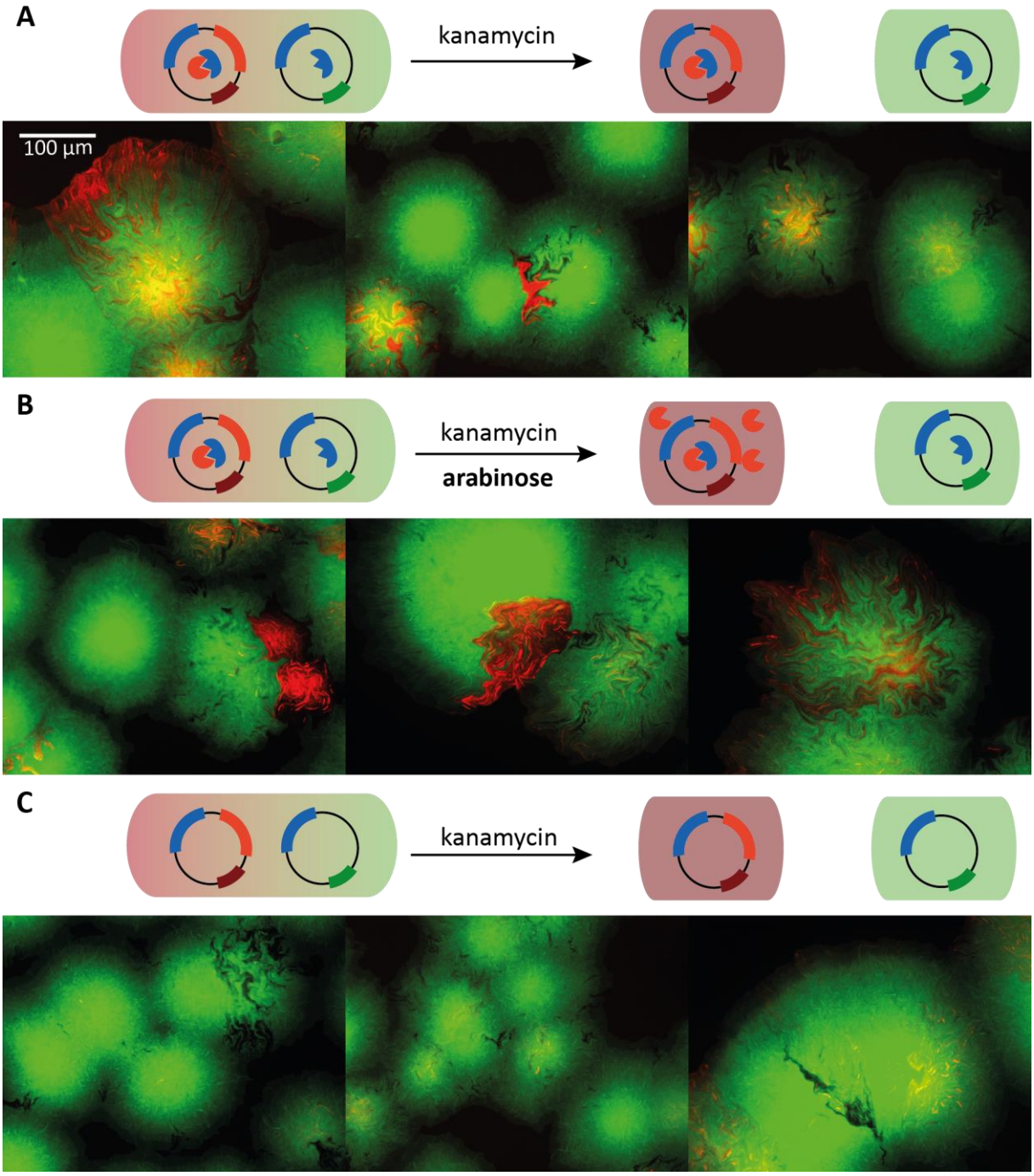


**Figure 12: BW27786 containing pBR25 or pKTR show decreased growth independent of toxin concentration. (A)Colonies formed by cells originally carrying pBR25 and pBR26 on agar pads with segregation inducing kanamycin. Green colony sectors corresponding to cells carrying pBR26 seem to be much larger than red colony sectors (pBR25 carrying cells). (B) Colonies formed by cells originally carrying pBR25 and pBR26 on agar pads with kanamycin and $1 \cdot 10^{-4}$ % arabinose to induce toxin expression. (C) Colonies formed by cells originally carrying pKAG and pKTR on agar pads containing kanamycin.**

## 4.3 Discussion

### 4.3.1 CdiA-CT$^{ECL}$ is a better candidate for growth regulation than other CDI rRNases

From all toxin/antitoxin pairs tested herein, the CdiA-CT$^{ECL}$/cdiI$^{ECL}$ pair performed best in regulating the growth of *E.coli* DH5αZ1. Low expression level of CdiA-CT$^{ECL}$ yielded intermediate growth rate, high expression levels a complete growth stop. Growth could be rescued at least partially by expression of the cognate antitoxin CdiI$^{ECL}$. That CdiA-CT$^{ECL}$, 16S rRNase, of all toxins tested performs best might have two reasons.

First, the 16S rRNase activity of ECL has a "balanced" effect on the cell. When 16S rRNase is degraded, all proteins made in the cell will be effected equally. The specific Gln tRNase CdiA-CT$^{EC869\ o5}$ in contrast, might imbalance protein production, i.e. production of proteins containing a lot of Gln will be impacted stronger than of other proteins. Indeed basal expression of the promoter, thus very small CdiA-CT$^{EC869\ o5}$ amounts is sufficient to seriously impact cell growth.

The specific Ala tRNase CdiA-CT$^{Bp\ 1026b}$ does not evoke growth defects during basal expression, but low expression levels already lead to a complete growth stop.

Considering this aspect CdiA-CT$^{UPEC536}$ as a generic tRNase should be a good choice for growth regulation as it will impact protein production homogenously. However, even low expression levels of the toxin seem to stop growth. Its effect might be more detrimental to the cell as recovery requires synthesis of all tRNAs, as opposed to only the 16S rRNA in the case of the ECL toxin.

Second, ECL 16S rRNase activity might mimic natural growth regulation in *E.coli* best. Growth rate is coupled to ribosome synthesis in *E.coli*, with the production of the rRNAs being the rate-liming step (Gourse et al., 1996).

Another reason why the ECL expression module was chosen for further experiments is its fully functional antitoxin CdiI$^{ECL}$. Only in the case of the ECL expression module was the antitoxin able to fully restore growth for the lowest toxin expression level. CdiI$^{Bp\ 1026b}$ and CdiI$^{UPEC536}$ expressed in toxin absence seemed to even negatively regulate growth and CdiI$^{EC869\ o5}$ did not seem to neutralize its toxin at all.

### 4.3.2 The ECL expression module can be employed for efficient growth regulation

Growth rate of DH5αZ1 carrying the ECL expression plasmid can be regulated by different inducer concentrations. Due to the bimodality of the pBAD promoter in DH5αZ1 (see chapter 4.2.3) regulation of growth is presumably on a population level, i.e. the growth of a fraction of cells is completely inhibited whereas the rest of the cells keep growing at a normal pace.

Using the strain BW27786, that enables homogenous expression of the pBAD promoter, it could be demonstrated that growth of presumably single-cells can be regulated by expression of ECL. Figure 13 shows the dynamic range of growth rate control. Growth rate of BW27786 can be regulated over the whole range by different levels of arabinose inducing the toxin expression in the absence or presence of full antitoxin expression.

For further fine-tuning of growth rate different antitoxin expression levels could be varied over different toxin expression levels, presumably allowing the adjustment of even more different growth rates.

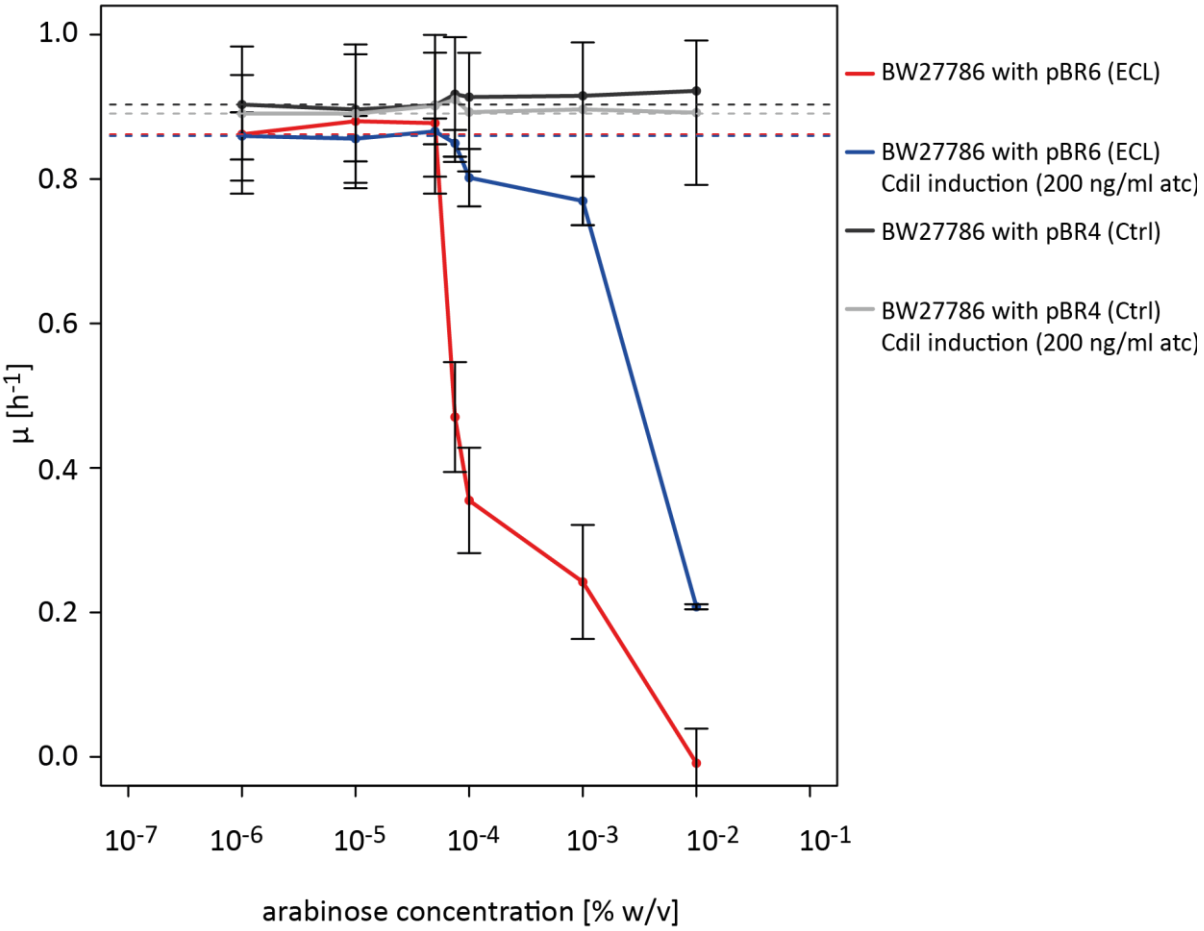


**Figure 13: Dynamic range of growth rate control using ECL expression in BW27786. Values are mean ± SD from two independent experiments. Dashed lines represent the corresponding growth rates when no arabinose is added.**

### 4.3.3 Growth suppression by cdiA-CT$^{ECL}$ expression is reversible

It could be shown that for low toxin levels growth of DH5αZ1 could fully be recovered when inducer was removed. As the growth suppression module was still functional, regrowth of cells after suppression cannot be due to previously mutated cells or contaminations.

A further hint as to that growth suppression by CdiA-CT$^{ECL}$ is transient gives the reproducible behavior of BW27786 carrying the ECL expression module (pBR6) at high arabinose concentrations. After 2 h of toxin induction cells seemed to stop growing completely. However, they resume growth at a very high growth rate at about 7 h post-induction when no antitoxin is present and at about 9 h when antitoxin is fully expressed. This behavior might be caused by a negative feedback loop. Protein synthesis of cells expressing toxin at a very high level will eventually be shut down completely, thus toxin production will stop, too. After all toxin is degraded and 16S rRNA has been reproduced by the cells, they resume growth until anew toxin production will inhibit growth again. The time until cells regrow is longer when antitoxin is expressed. Binding of the antitoxin to the toxin might stabilize the toxin, shielding it from degradation, thereby prolonging the time until all toxin is degraded.

### 4.3.4 Improved experimental setup is necessary for CDI pattern formation

Subcloning of the ECL expression module on the segregation plasmids showed that the ECL expression module can as well regulate growth of BW27786 when contained on a low-copy vector and in the presence of continuous antitoxin expression. However, employing the segregation plasmids for their actual purpose for pattern generation was not successful. As freshly seeded agar pads need about 30 to 45 min to dry cells can freely diffuse in the liquid on top and presumably keep dividing. Thus cells might already contain only one of the two segregation plasmid when they are finally dried on the pad, explaining why most of the colonies only contained one fluorescent protein.

This does not explain though why most of the colonies observed were all green and almost no all red colonies were observed. Experiments in liquid culture showed that cells carrying the pBR25 or pKTR plasmid have a longer lag phase than cells containing pBR26 or pKAG. Thus red colonies might just be overgrown by green colonies. Growth deficiency of red cells could be caused by different phototoxicity of the fluorescent proteins mRFP1 and superfolder GFP.

To further test the ability to form simple pattern using growth modulation by ECL expression the experimental setup needs to be optimized. Reducing drying time on the pad might be a critical step. Furthermore in order to be able to observe patterns at higher magnification a faster segregation by lower plasmid copy number and faster degradation of fluorescent proteins would be desirable.

# 5 Observation of CDI during surface growth on single-cell level

## 5.1 Time-lapse microscopy is suitable to investigate CDI during surface growth

To date CDI has mostly been investigated during culture in liquid media. CDI leads to cell aggregation and has been shown to enhance biofilm formation (Garcia et al., 2013; Ruhe, Wallace, et al., 2013). To get a deeper insight into CDI's biological role (see chapter 1.3) investigation of CDI during surface growth is desirable. Time-lapse microscopy (TLM) allows to investigate and quantify effects on a single-cell level (Locke and Elowitz, 2009; Young et al., 2012). TLM has been used earlier to quantify bacterial interactions like conjugative transfer (Lawley et al., 2002) or toxin transfer by type VI secretion systems (LeRoux et al., 2012).

## 5.2 Results

### 5.2.1 Time-lapse microscopy of colliding microcolonies with constitutive CDI inhibitors

To investigate the effect of CDI during surface growth a time-lapse microscopy experiment was devised. Collision of initially separated target cell colonies with inhibitor cell colonies was to be monitored by time-lapse microscopy. The chimeric EC93-EC869 o11 CDI system ($CDI^{EC93\text{-}EC869\ o11}$) was used for all experiments. CdiA-$CT^{EC869\ o11}$ exerts DNase activity (Morse et al., 2012).

$CDI^{EC93\text{-}EC869\ o11}$ inhibitor and target strains were received from Christopher S. Hayes (University of California Santa Barbara). Inhibitor cells contained a plasmid constitutively expressing $CDI^{EC93\text{-}EC869\ o11}$. Susceptible target cells contained an empty vector, whereas immune target cells expressed the corresponding antitoxin *cdiI*$^{EC869\ o11}$ from a plasmid. Inhibitor cells constitutively expressed GFP from the chromosome as visual marker, whereas target cells expressed mKate2 (see Figure 14).

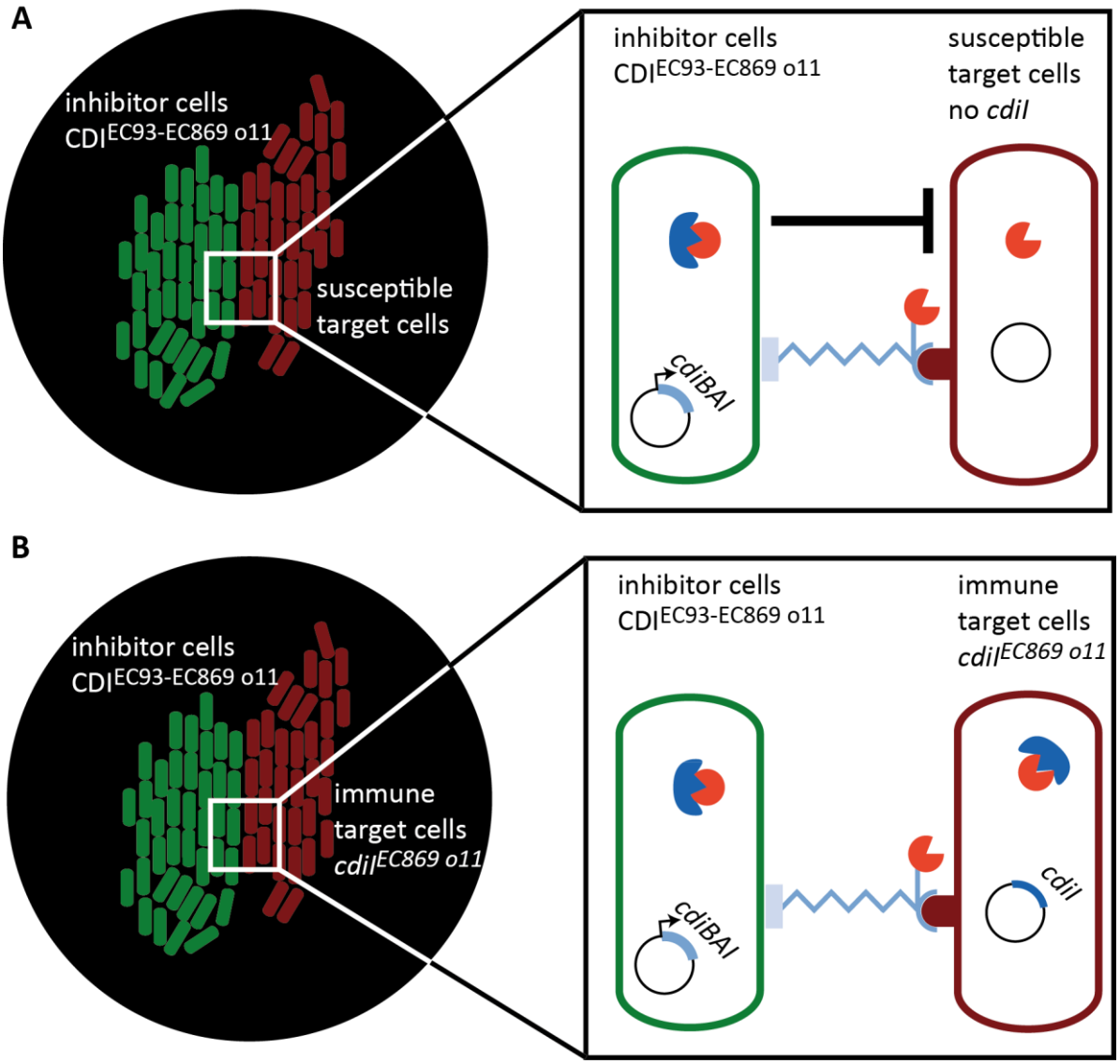


**Figure 14: Schematic explaining the time-lapse microscopy setup. (A) Time-lapse imaging of collision of GFP expressing CDI$^{EC93\text{-}EC869\ o11}$ inhibitors with susceptible targets is observed. (B) As a control collision of the same CDI$^{EC93\text{-}EC869\ o11}$ inhibitor strain with immune target cells that express cdiI$^{EC869\ o11}$ is monitored.**

Growth competitions in liquid media were performed to ascertain the functionality of the strains (see chapter 3.3.1). Susceptible target strain viability was reduced about $10^4$ when cocultured with CDI$^{EC93\text{-}EC869\ o11}$ inhibitor cells for 3 h (see Figure 15). Coculture of inhibitors with the immune target strain expressing the cognate antitoxin CdiI$^{EC869\ o11}$ results in about $10^3$ increase in cell viability for both inhibitor and target strain after 3 h of coculture. This result is consistent with the work of Morse *et al.,* demonstrating the functionality of the strains used in this work (Morse et al., 2012).

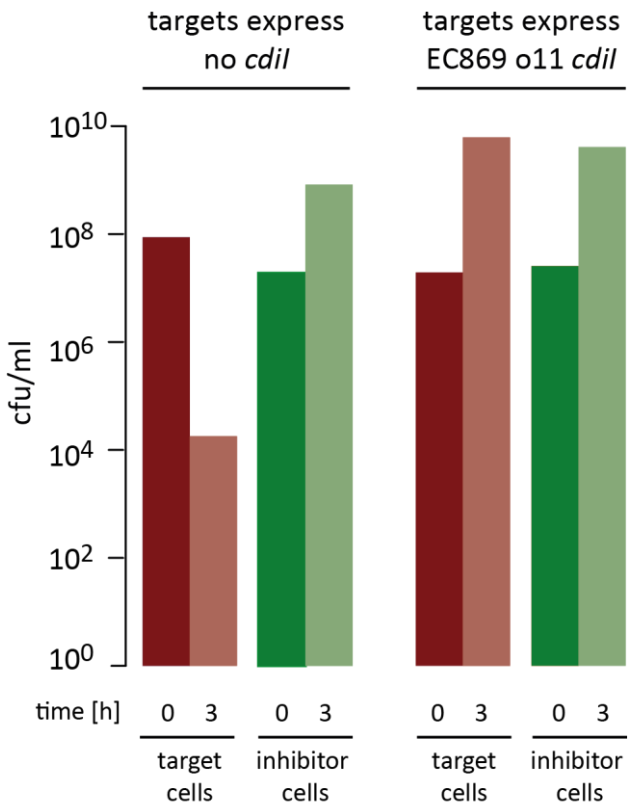


**Figure 15: Inhibitor cells constitutively expressing CDI$^{EC869\ o11}$ suppress growth of susceptible target cells, but not of target cells expressing the cognate antitoxin *cdiI*$^{EC869\ o11}$ after 3 h of coculture in liquid media.**

Subsequently time-lapse microscopy was performed. Inhibitor and target cells were applied to the same pad at a low density and positions were chosen where two different cells (inhibitor and target) were positioned close to each other. GFP expressing CDI$^{EC93\text{-}EC869\ o11}$ inhibitor cells showed slightly slower growth than mKate2 expressing target cells when growing on the agar pads. When CDI$^{EC93\text{-}EC869\ o11}$ inhibitor colonies collided with susceptible target cell colonies, target cells underwent filamentation at the interface of the two colonies (see Figure 16). Cell lysis events of these filamentous cells could very rarely be observed. Most of the times the filamentous cells at the interface remained at the colony border until time-lapse acquisition was finished (after 12 h). As cells quickly start to grow in several layers especially at the colony interfaces, it cannot be ruled out that cell lysis events were simply blocked from view. The border between the two colonies appeared to be smooth through the filamentous cells lining up in parallel to the interface.

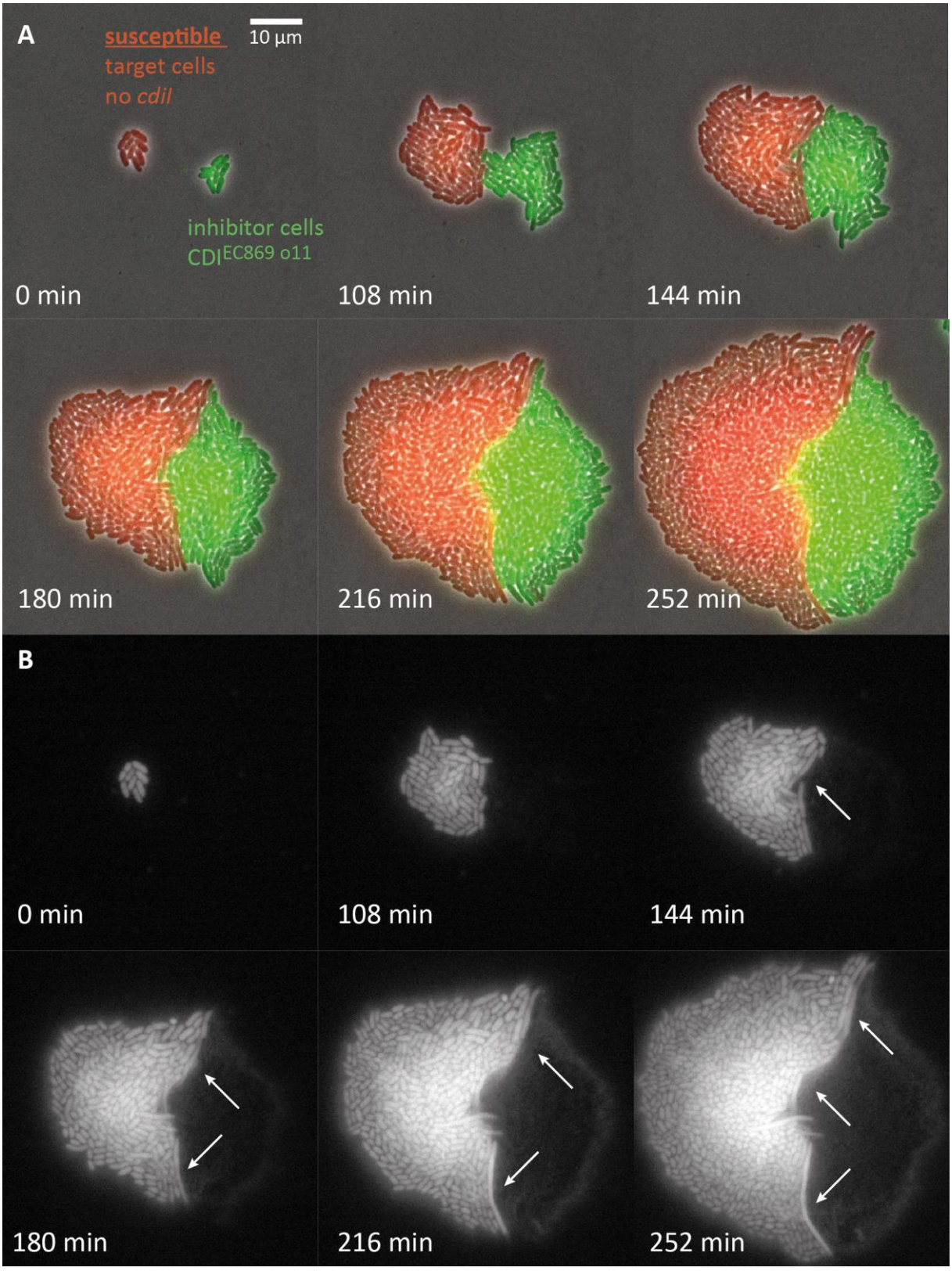


**Figure 16: Susceptible target cells show increased filamentation at the colony interface with CDI$^{EC93\text{-}EC869\ o11}$ inhibitor cells. (A) Film strip of a time-lapse movie showing collision of CDI$^{EC93\text{-}EC869\ o11}$ inhibitor colony (green) with a susceptible target strain colony (red). Phase-contrast images were merged with fluorescence images. (B) Target cell fluorescence (mKate2) in gray scales of the same time-series as shown in (A). White arrows indicate filamentous cells.**

In contrast collision of CDI$^{EC93\text{-}EC869\ o11}$ inhibitor cells with immune target cells expressing *cdiI*$^{EC869\ o11}$ did not induce any morphology change of target cells at the interface (see Figure 17). Both cell types appear to grow normally when colliding. The border of the two colonies seems to be more jagged with invaginations of both cell types into the other colony.

To be able to compare a larger number of different collisions observed by time-lapse microscopy time-points of the first contact between colonies was manually determined and images 144 min after this first contact were selected to display collision outcome (see Figure 18A and B).

Collision of inhibitor cells with susceptible target cells reliably induces filamentation of target cells smoothing the collision border (see Figure 18A). When inhibitor cells collide with immune target cells (expressing CdiI$^{EC869\ o11}$) the border of the two colonies shows invasion of cells from one type into the colony of the other type, respectively, appearing more folded than in collision with susceptible target cells (see Figure 18B).

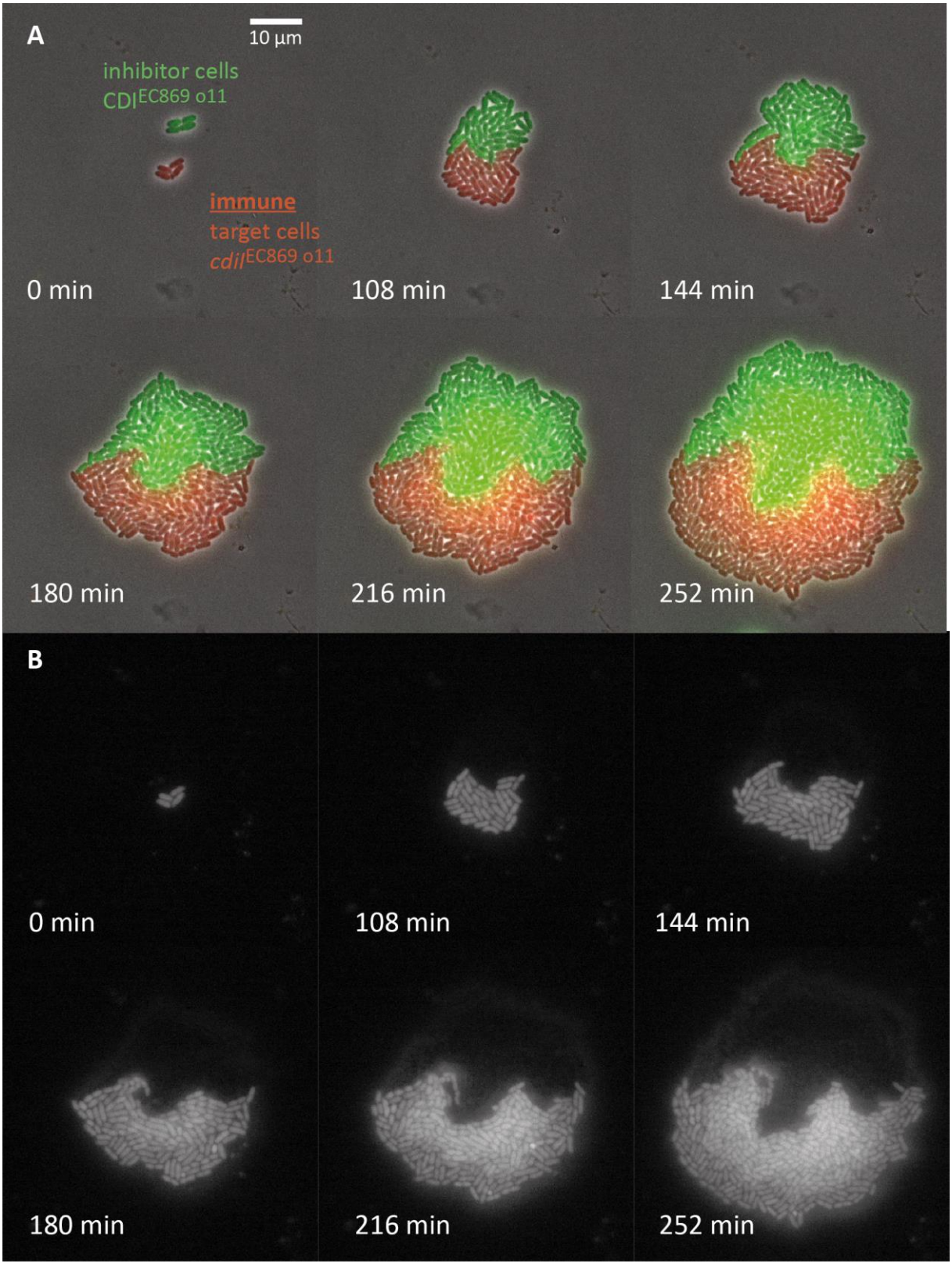


**Figure 17: Immune target cells expressing CdiI$^{EC869\ o11}$ show normal growth at the colony interface with CDI$^{EC93\text{-}EC869\ o11}$ inhibitor cells. (A) Time-lapse microscopy film strip of collision of CDI$^{EC93\text{-}EC869\ o11}$ inhibitor colony (green) with a susceptible target strain colony (red). Images were merged from phase-contrast and fluorescence images. (B) Target cell fluorescence (mKate2) in gray scales of the same time-series as in (A).**

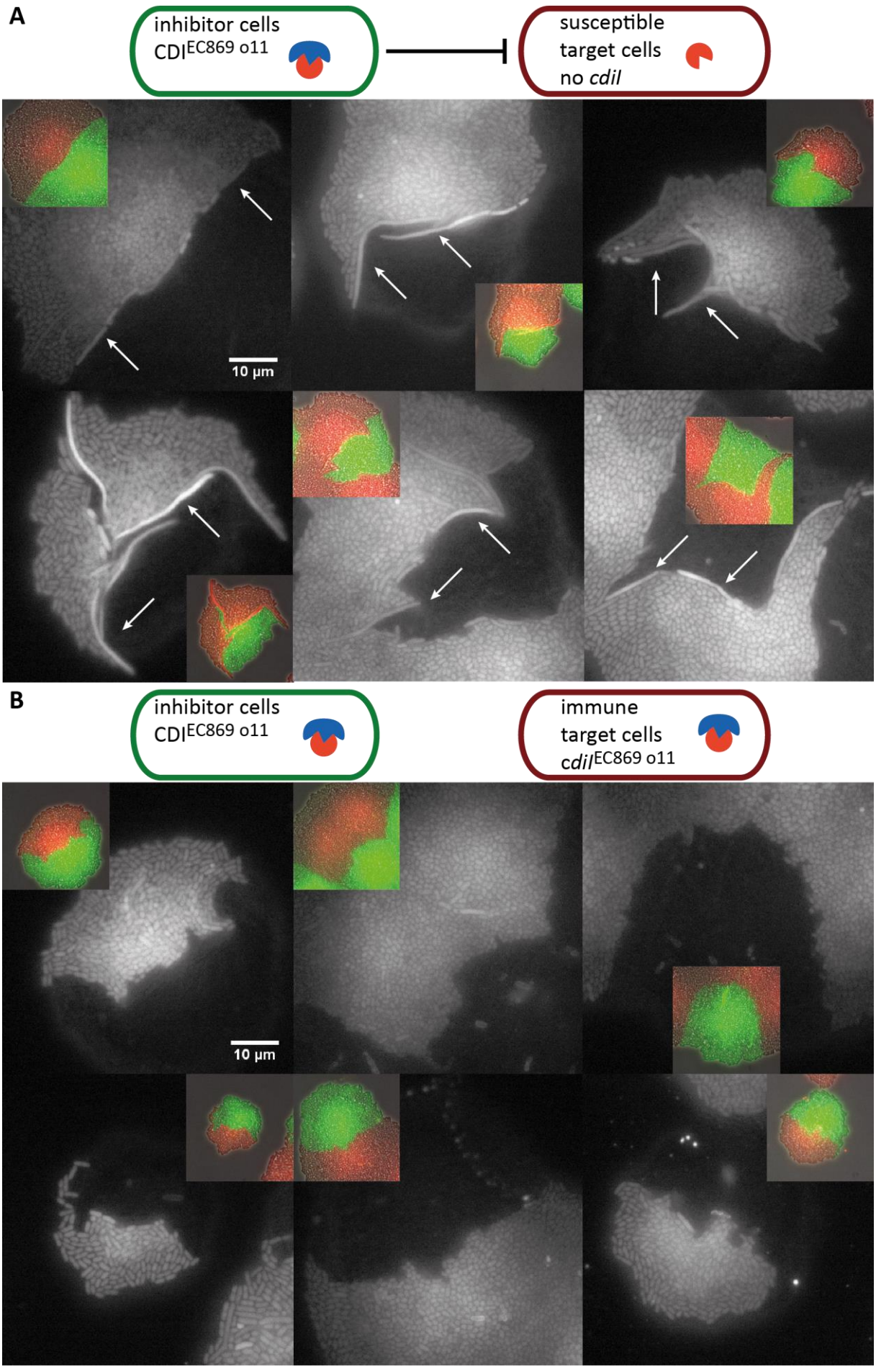
A
inhibitor cells
CDI^EC869 o11
susceptible
target cells
no cdiI
10 µm
B
inhibitor cells
CDI^EC869 o11
immune
target cells
cdiI^EC869 o11
10 µm

**Figure 18: Filamentation of susceptible target cells at the border interface smoothes the colony border. (A) Susceptible target cell fluorescence (mKate2) 144 min after first contact with CDI$^{EC93\text{-}EC869\ o11}$ inhibitor colonies. White arrows indicate filamentous target cells. Insets show the same imaging time-point as a merge of phase-contrast, mKate2 and GFP fluorescence channel. (B) Immune target cell fluorescence (mKate2) 144 min after first contact with CDI$^{EC869\ o11}$ inhibitor colonies. Insets show the same imaging time-point as a merge of phase-contrast, mKate2 and GFP fluorescence channel.**

### 5.2.2 Time-lapse microscopy of colliding microcolonies with inducible CDI inhibitors

A higher cell density on pads at the start of the experiment would be desirable for both easier position selection and higher statistics of collision events. Increasing the density using inhibitor cells constitutively expressing CDI$^{EC93\text{-}EC869\ o11}$ leads to already deformed target cells at the start of the experiment. This is corroborated by the fact that growth inhibition by CDI in liquid culture can lead to reduction of target cell viability within minutes (Aoki et al., 2005). Pads need to dry for 30 - 45 min, during this time period cells can freely diffuse in the liquid resulting in preexposure of target cells to the toxin. Thus position selection for images taken in chapter 5.2.1 was based on selecting cells with normal cellular morphology at the start of the experiment.

A new inhibitor strain containing an IPTG inducible CDI$^{EC93\text{-}EC869\ o11}$ was employed for higher density pads. By addition of IPTG to the pad CDI expression will be induced when cells are positioned on the pad. As overexpression of CdiI$^{EC869\ o11}$ in the immune target cells used for earlier time-lapse experiments seems to inhibit cell segmentation (see chapter 5.2.3) a different immune target strain was used as a control target strain (see Figure 19). This immune target strain is a *ΔyciB* mutant. yciB is an uncharacterized predicted inner membrane protein (Uniprot ID: P0A710), presumably playing a role in barrier septum assembly in *E.coli*. It has been shown that *ΔyciB E.coli* show a defect in biofilm formation and a reduced amount of outer membrane proteins (Niba et al., 2007).

Functionality of the strains was first tested in growth competitions in liquid media (see Figure 20). Similar to the experiments with constitutive inhibitors, susceptible target cell viability was reduced about $10^3$ after 3 h of coculture with the IPTG-inducible CDI$^{EC93\text{-}EC869\ o11}$ inhibitor strain. In contrast growth of the *ΔyciB* target strain was not suppressed by coculture with inhibitor cells.

Time-lapse microscopy with mixtures of IPTG-inducible CDI$^{EC93\text{-}EC869\ o11}$ inhibitor cells and target cells at a 1:1 ratio and $OD_{600}$ of 0.1 was performed using agarose pads supplemented with 1.5 mM IPTG. When competing inhibitor cells with susceptible target cells filamentation of target cells at the colony interfaces was observed (see Figure 21). Similar to the results reported in chapter 5.2.1 with constitutive inhibitors, target cells became filamentous smoothing the colony borders. Same as in earlier time-lapse experiments cell lysis events were usually not detected. Filamentous cells at the interface shielded other target cells behind the filamentous cells from contact with inhibitor cells. This

is especially well to see in Figure 21, where red cells seem to be encapsulated within a green colony. It appears that filamentation of target cells is stronger when colonies collide early during acquisition thus initial seeding is closer at the beginning. Time-lapse imaging of inhibitor cells mixed with immune *ΔyciB* cells shows no filamentation of immune target cells (see Figure 22). Taking a closer look at images taken 240 min after time-lapse start for different positions reveals the differences in cell and colony morphology between susceptible and immune target cells (compare Figure 23 and Figure 24).

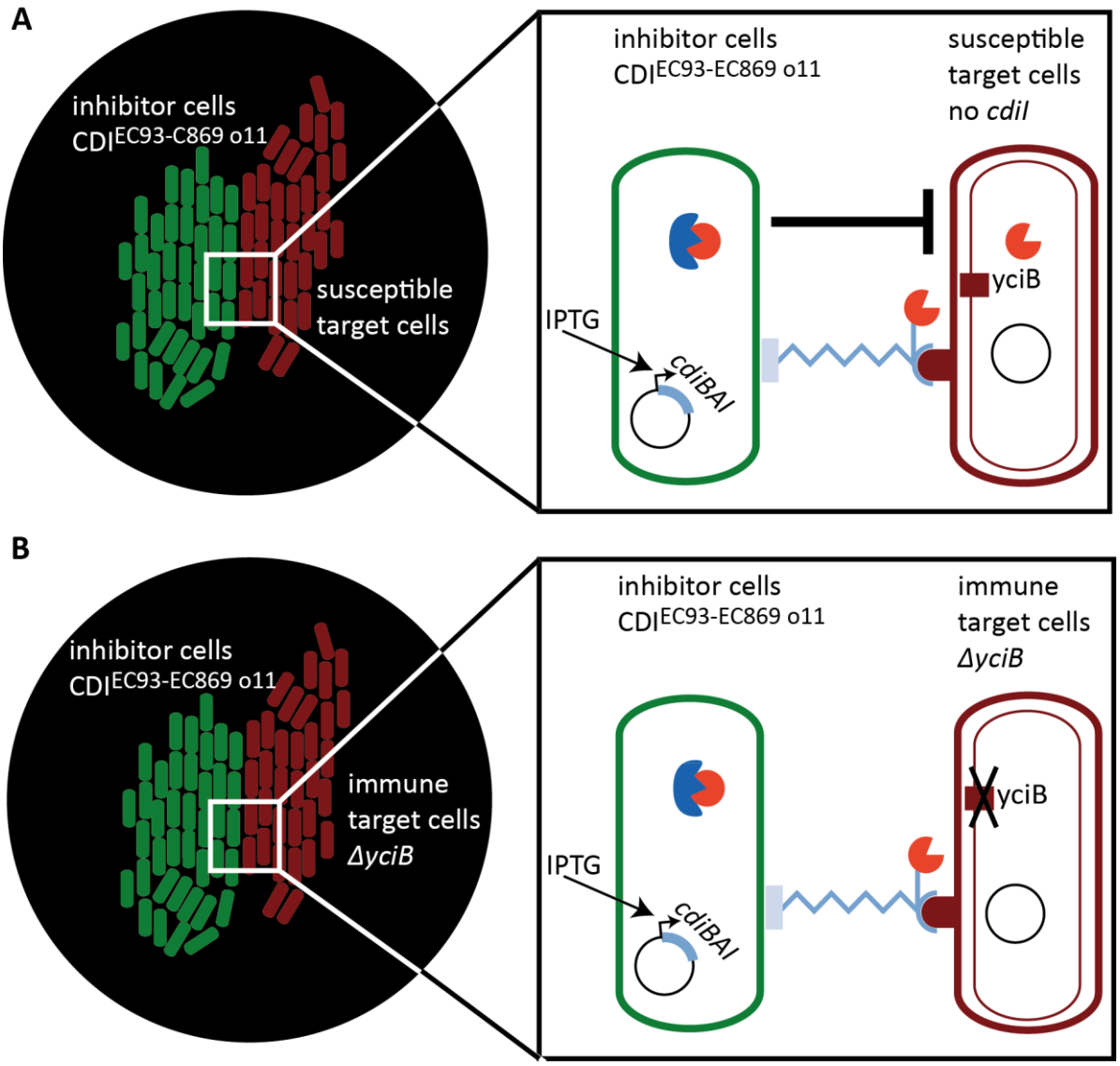


**Figure 19: Schematic explaining the setup for time-lapse microscopy with higher cell density. (A) Collision of GFP expressing CDI$^{EC93\text{-}EC869\ o11}$ inhibitor cells with susceptible mKate2 expressing target cells is observed. (B) As a control the collision of the same inhibitor cells with an immune target cell strain is observed. Immune target cells are *ΔyciB*.**

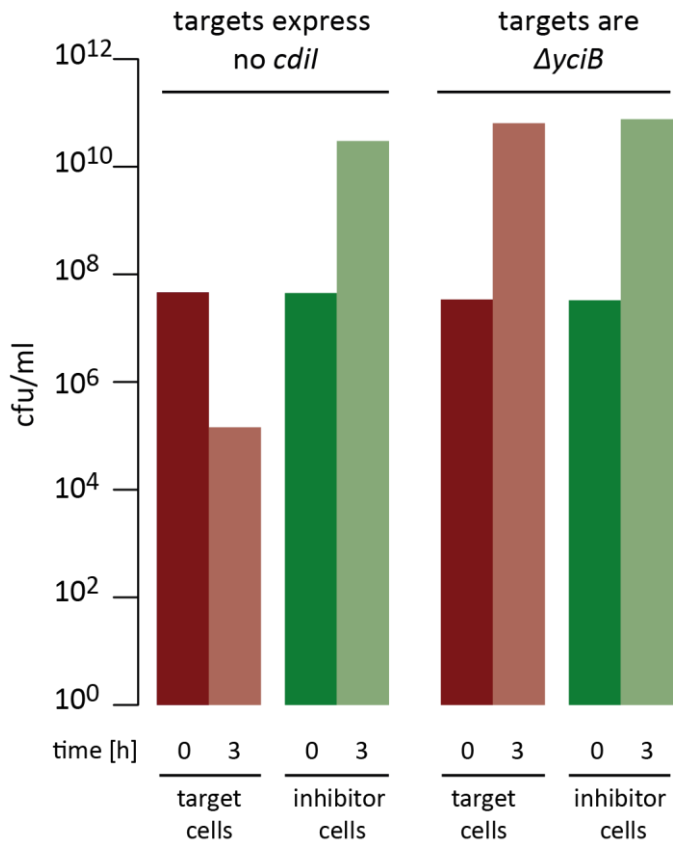


**Figure 20: Coculture of IPTG- inducible CDI$^{EC93\text{-}EC869\ o11}$ inhibitor cells with susceptible target strains in liquid culture for 3 h reduces target cell viability in the presence of IPTG. The *ΔyciB* target strain is immune to growth suppression by CDI inhibitors.**

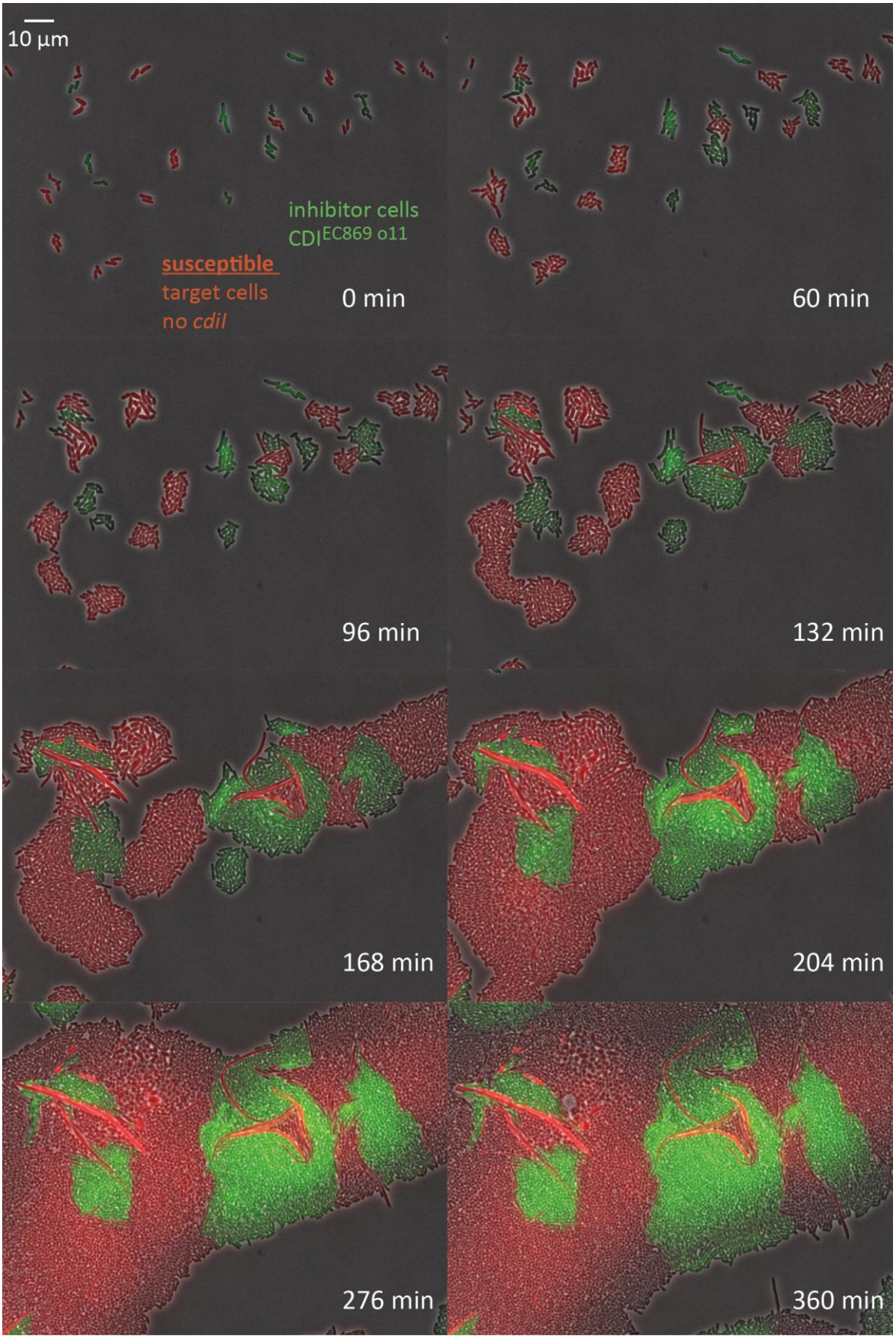


**Figure 21: Time-lapse microscopy of collisions of IPTG-inducible CDI$^{EC93\text{-}EC869\ o11}$ inhibitor cells (green) with susceptible target cells (red).**

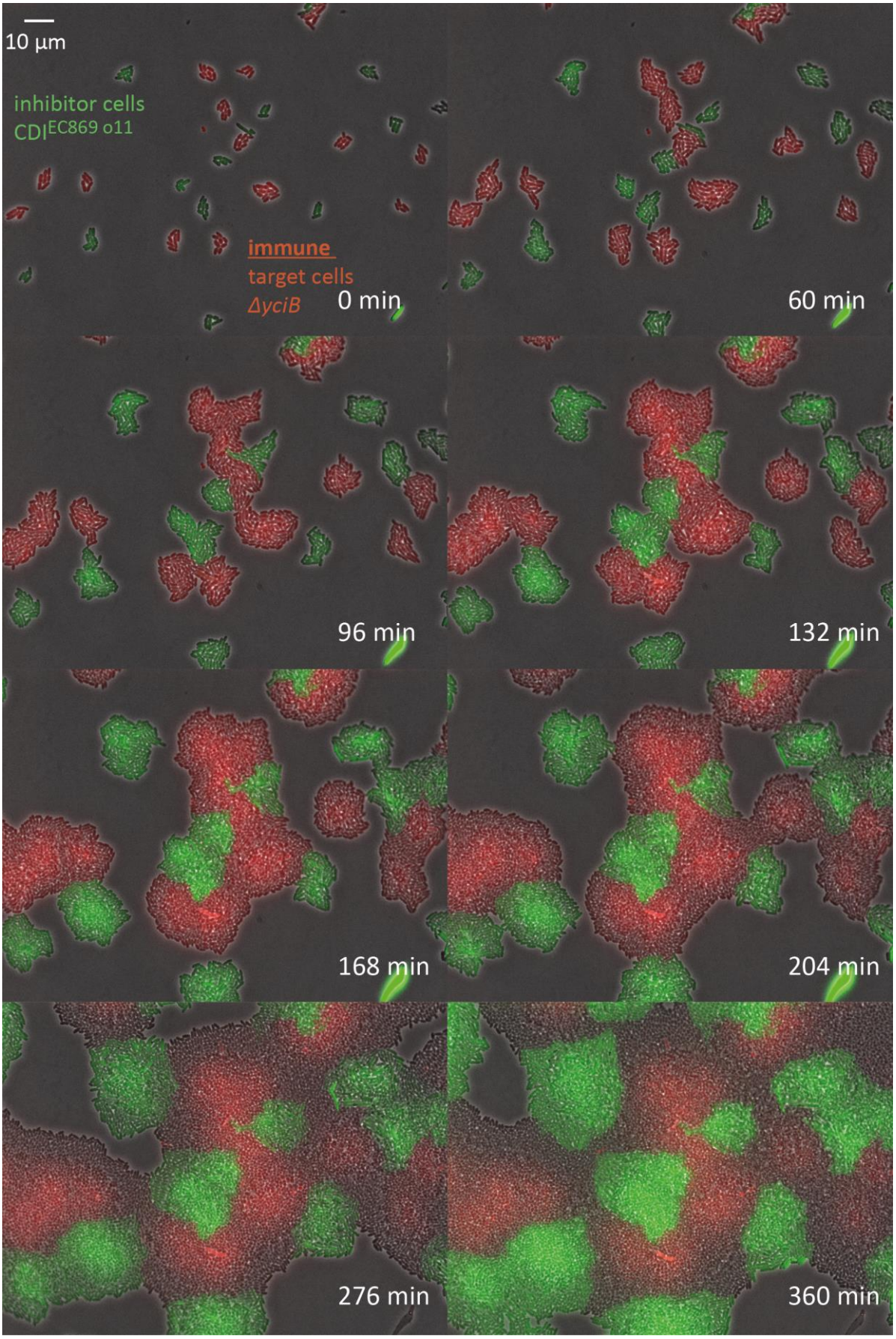


**Figure 22: Time-lapse microscopy of collisions of IPTG-inducible CDI$^{EC93\text{-}EC869\ o11}$ inhibitor cells (green) with immune *ΔyciB* target cells (red).**

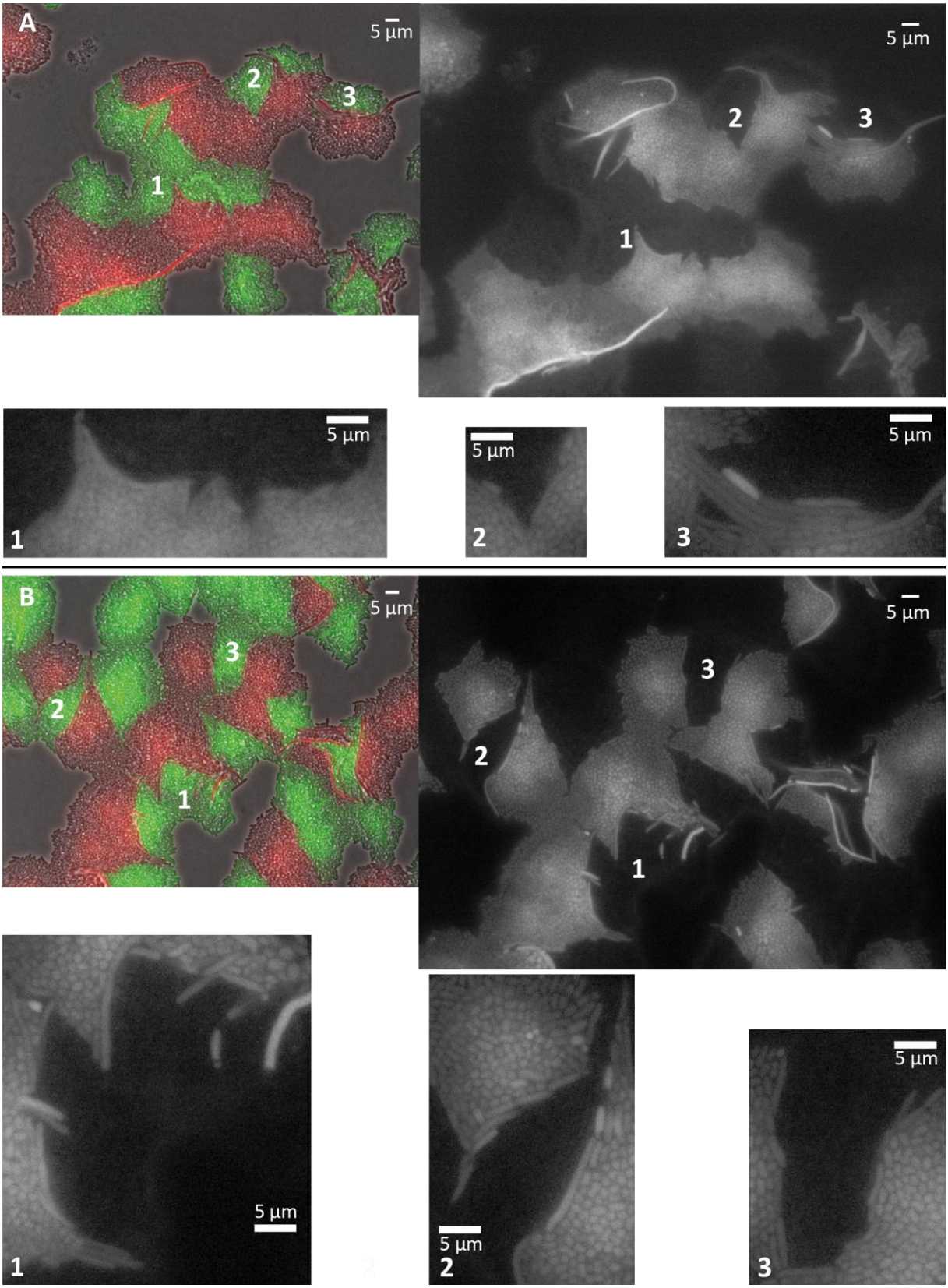


**Figure 23: Filamentation of susceptible target cells smoothes the interface between target cell and CDI$^{EC93\text{-}EC869\ o11}$ inhibitors colonies. (A) and (B) show two example images 240 min after start of time-lapse imaging, left image is a merge of phase-contrast and fluorescent images, the right image only shows target cell fluorescence. The insets 1, 2 and 3 reveal target cell morphology change.**

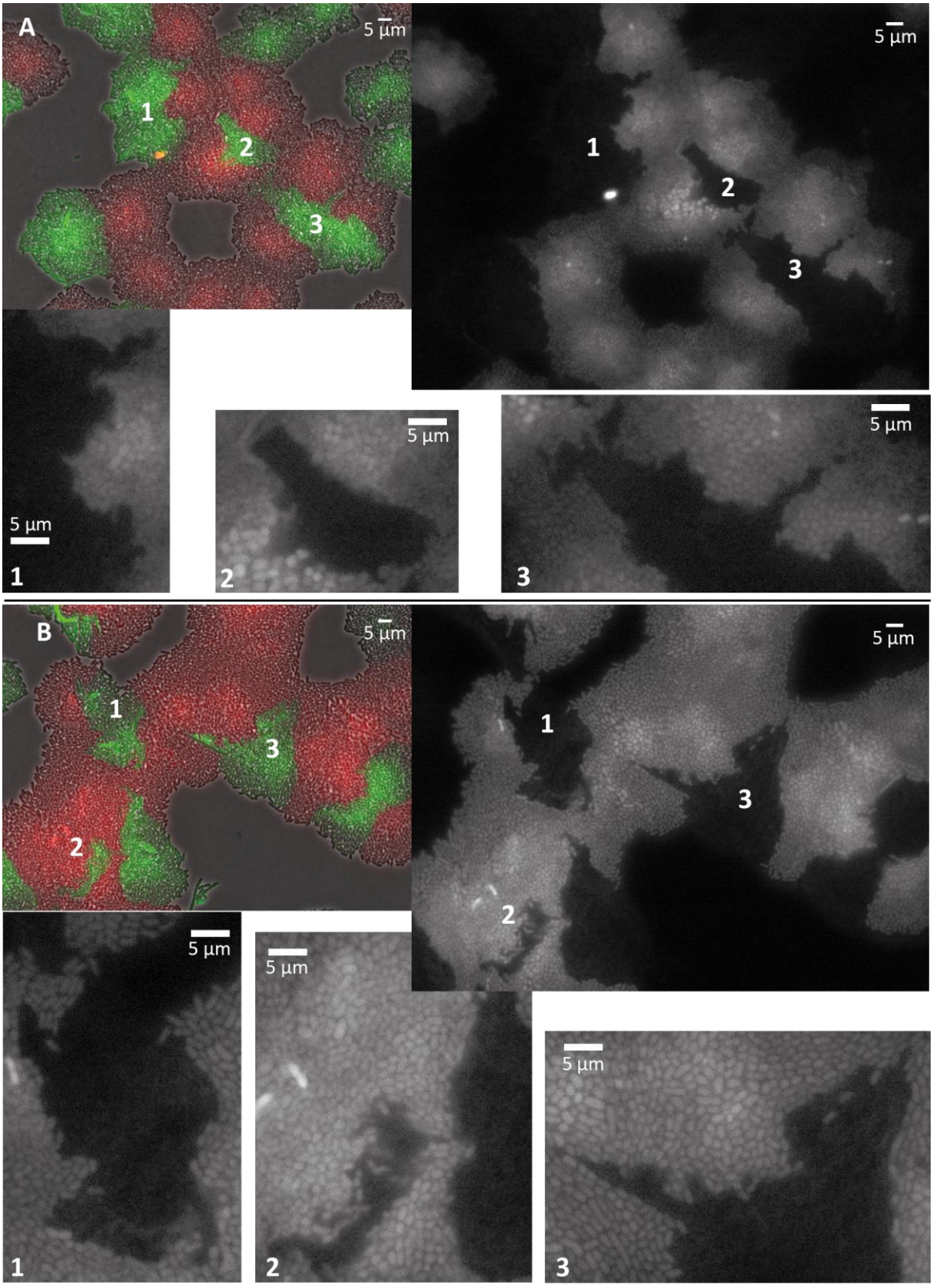


**Figure 24: The interface between immune target cells colonies and CDI$^{EC93\text{-}EC869\ o11}$ inhibitors colonies is jagged with invasions of each cell type into the opposite colony. (A) and (B) show two example images taken 240 min after imaging start. The left image is merged from phase-contrast and fluorescent images, the right image only shows target cell fluorescence. The insets 1, 2 and 3 reveal the fine structure along the colony borders.**

### 5.2.3 CdiI$^{EC869\ o11}$ overexpression causes excessive filamentation of *E.coli*

The immune target strain used in chapter 5.2.1 contains a plasmid with an IPTG-inducible *cdiI*$^{EC869\ o11}$. Immunity to inhibition by the CDI$^{EC93\text{-}EC869}$ inhibitor cells is conferred by leaky, basal expression of the antitoxin in absence of inducer. During the setup for higher density time-lapse microscopy with IPTG-inducible inhibitor cells it was discovered that overexpression of CdiI$^{EC869\ o11}$ by IPTG induction seems to suppress cell division in *E.coli*. Cells do not divide, but continue to grow resulting in very long filaments that buckle and loop (see Figure 25). Imaging of cells at 20x magnification revealed that cell length reaches up to several 100 µm (see Figure 26).

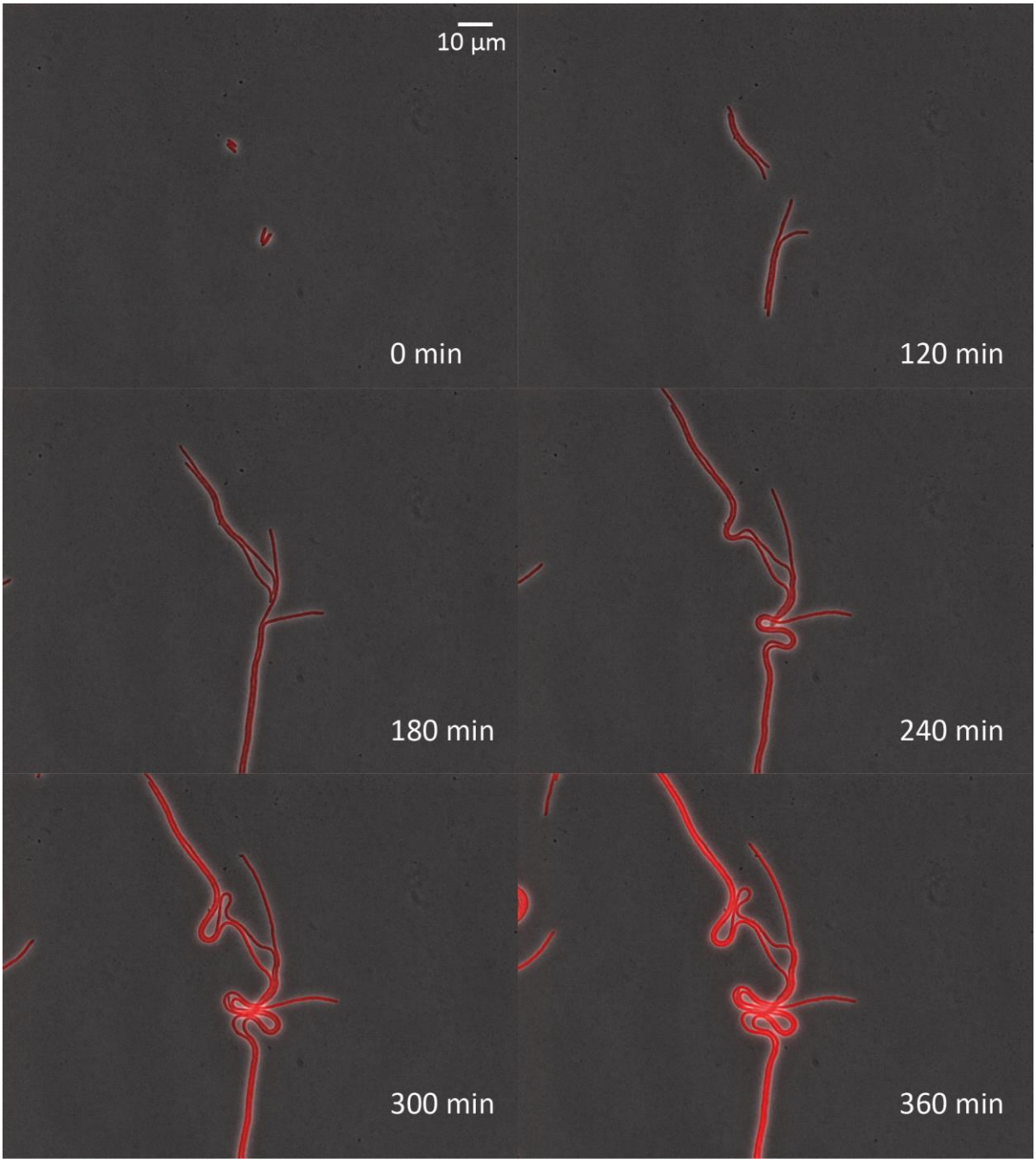


**Figure 25: Film strip showing excessive *E.coli* filamentation caused by IPTG-induced overexpression of CdiI$^{EC869}_{o11}$.**

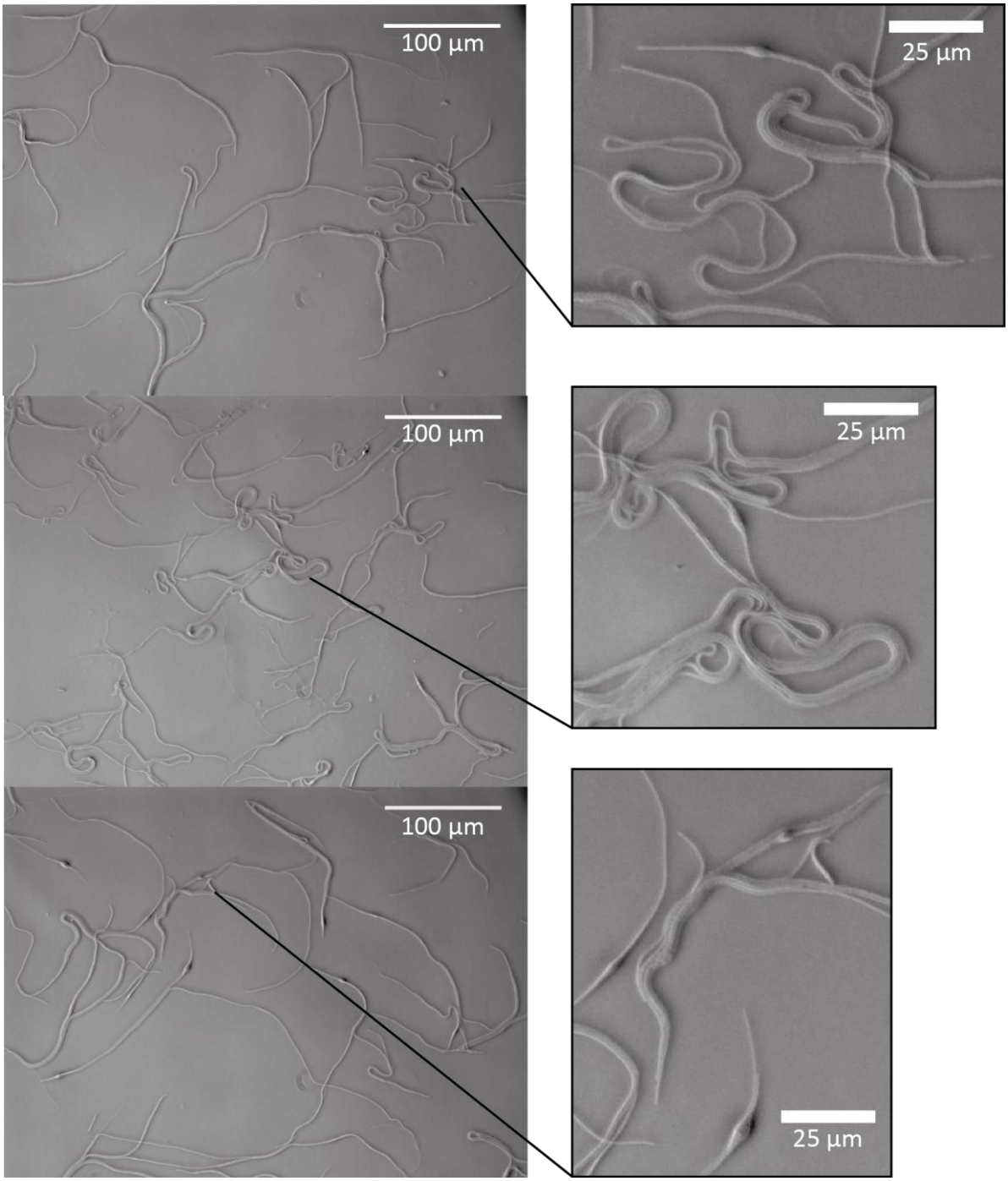


**Figure 26: Filamentous *E.coli* cells overexpressing CdiI$^{EC869\ o11}$ at 20x magnification after 16 h growth on agar pads with 1.5 mM IPTG. Individual cell length reaches up to several 100 µm.**

## 5.3 Discussion

### 5.3.1 Collision with CDI$^{EC93\text{-}EC869\ o11}$ inhibitors causes target cell filamentation

It has been shown for both constitutive and IPTG-inducible CDI$^{EC93\text{-}EC869\ o11}$ inhibitor cells, that collision with susceptible target cell colonies induces target cell filamentation at the colony interface. In contrast when CDI$^{EC93\text{-}EC869\ o11}$ inhibitor cells collided with immune target cells, either expressing CdiI$^{EC869\ o11}$ or *ΔyciB* mutants, no filamentation of target cells could be observed. Surprisingly, lysis events of filamentous cells were very rare and probably occur at the same rate as normal cell lysis.

*E.coli* filamentation is generally observed as a stress response to various environmental stimuli such as nutrient limitation, fluid shear stress and protistan predation (Young, 2006). One pathway that activates filamentation of *E.coli* is the so-called SOS response. It is usually activated upon DNA damage and results in cell filamentation and prophage induction (Janion, 2008). Filamentation of cells is caused by expression of the inhibitor of cell division SulA (former SfiA)(Huisman et al., 1984). As CdiA-CT$^{EC869\ o11}$ is a DNase, it is likely that target cells activate SOS response when the toxin is delivered into their cytoplasm, resulting in filamentation of target cells. Morse *et al*. showed that susceptible target cells were filamentous and had lost genomic DNA after 6 h coculture with CDI $^{EC93\text{-}C869\ o11}$ inhibitor cells in liquid media. Immune target cells in contrast showed normal cell morphology and genomic DNA after coculture ((Morse et al., 2012), Figure 6).

Even though filamentation caused by SulA activation is usually reversible, in this case where the DNase CdiA-CT$^{EC93\text{-}Ec869\ o11}$ is delivered to cells, it is unlikely that cells are able to resume normal growth.

Target cell filamentation observed here is often accompanied by an increase of cell diameter, cells seem to be swollen. Furthermore cells seem to be more fluorescent than cells farther away from the colony boundaries. Even if filamentous target cell initially seem to keep growing, they do so at a very low rate. This is especially obvious if filamentation of target cells is compared with filamentation of cells overexpressing CdiI$^{EC869\ o11}$. Cells overexpressing CdiI$^{EC869\ o11}$ seem to maintain a similar diameter as non-filamentous cells elongating at a fast pace, whereas target cells at the CDI$^{EC93\text{-}Ec869\ o11}$ inhibitor interface increase diameter and grow if at all very slowly.

This is a further hint as to that target cell filamentation caused by collision with CDI$^{EC93\text{-}EC869\ o11}$ inhibitors is no transient state, but is probably irreversible.

### 5.3.2 Colony interface of inhibitor/target colonies is smoothened by target cell filamentation

When comparing Figure 23 and Figure 24 the effect of target cell filamentation on colony boundaries becomes clear. Filamentous susceptible target cells align in parallel to the border, constructing a continuous smooth border. Immune target cells that maintain normal cell morphology intercalate with

inhibitor cells at the border, invasions of immune target and inhibitor cells into the other colony are common. The resulting roughness of the border is in sharp contrast to the smoothed border in the case of susceptible target cells. The lined up filamentous cells seem to build a natural barrier between colonies protecting other target cells from the access of inhibitor cells.

### 5.3.3 $CDI^{EC93\text{-}EC869\ o11}$ is far less potent during surface growth than in liquid media

When comparing the data obtained by competing target cells with inhibitor cells in liquid media with that acquired for surface growing *E.coli* by time-lapse microscopy the sharp disparity in killing efficiency is notable. Only 3 h of coculture with $CDI^{EC93\text{-}EC869\ o11}$ inhibitors is able to reduce susceptible target cell viability by about $10^3$ - $10^4$. Movies taken during collision of target and inhibitor during surface growth cells do not offer any obvious explanation of this sharp decrease in target cell viability. Almost no target cell lysis events could be detected, yet collision with inhibitor cells results in target cell filamentation and deformation.

As time-lapse microscopy was performed on supplemented M9 media and competitions in liquid media were performed in LB media, it cannot be ruled out that the different killing efficiency is caused by different media composition. Competition between inhibitor and target strains in liquid culture could be repeated using supplemented M9 media to eliminate media composition as the cause.

One explanation for the observed difference in killing efficiency could be the limited exposure of target cells to inhibitor cells during surface growth. The accessible contact surface between target and inhibitor cells is much lower during surface growth than it is in liquid culture (see Figure 27). In liquid inhibitor cells can access target cells from all angles. Aggregates of target and inhibitor cells might not be stable, so that different inhibitor cells are able to inhibit one target cell. During surface growth, however, access to target cells is limited and the cells constellation is stable. The same target and inhibitor cells will remain in contact unless they lyse or are dragged away during colony growth. Experiments with $CDI^{EC93\text{-}Bp\ 1026b}$ (Ala tRNase) in liquid culture showed that almost all target cell $tRNA_{1B}^{Ala}$ was degraded within the first 10 minutes, but no decrease in cell viability could be determined in CFU assays at this point (Ruhe et al., 2014). This hints that cells once separated from inhibitor cells might be able to recover from exposure to small amounts of toxin. The amount of toxin transferred during contact on a 2D surface might just not be sufficient to kill target cells efficiently.

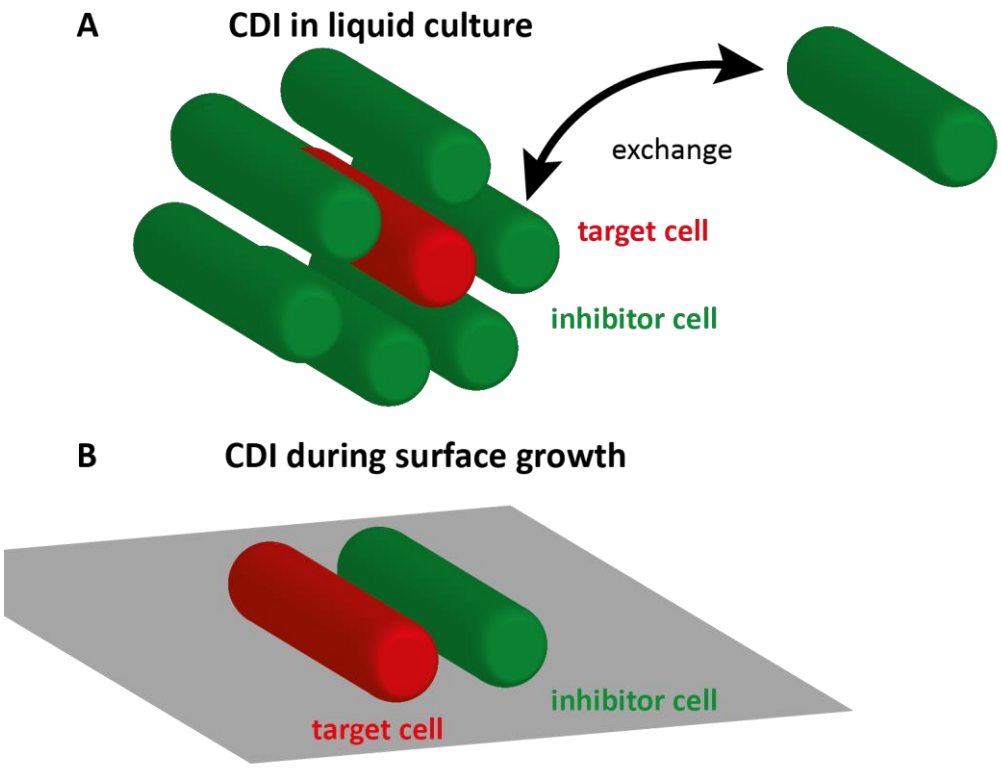


**Figure 27: Accessible contact surface is much higher when CDI occurs in liquid culture (A) as when it occurs during surface growth (B).**

Another possible explanation is that the direct comparison between the competition in liquid culture quantified by CFU assays and the competition on 2D surface observed by time-lapse microscopy is difficult. CFU assays rely on the ability of cells to form visible colonies on plates. Cells that are able to regrow to form a colony are generally termed viable. However, cells inhibited by CDI might be in the state termed viable but non culturable (VBNC) (Xu et al., 1982; Hayes and Low, 2009). Cells that have been assigned to this state showed some metabolic activity and membrane integrity but could not be cultured or only under special circumstances.

Earlier experiments with the first CDI toxin CdiA-CT$^{EC93}$ showed that cells suppressed by the toxin showed metabolic activity and membrane integrity but could only be regrown when carbohydrates as were added as an energy source. Interestingly this toxin also induced target cell filamentation (Aoki et al., 2009). Thus, inhibition of target cells by CDI might not actually kill cells, but rather push them into the viable but non culturable state. Cells filament but stay intact, i.e. do not lyse, and might be able to recover from inhibition under certain circumstances and for certain CDI toxin activity. It is hard to imagine that a target cell can recover from the action of a DNase like CdiA-CT$^{EC869\ o11}$, but it might be possible for other less potent toxins such as the RNase toxins employed in chapter 4.

### 5.3.4 Biological implications of the observed "weak" CDI during surface growth

The effect of CDI during surface growth reported here is not as drastic as in liquid cultures. If inhibitor cells do not seem to "gain ground" by inhibiting target cells, what is the biological role of CDI during surface growth after all?

The observed smoothness of the colony boundaries caused by CDI during surface growth might be a hint that CDI is not used for direct competition, but more for fencing off a colony of isogenic cells from surrounding cells. Invasion of other "non-self" cells into the colony is not possible, as they will be converted into filamentous cells that create an even stronger boundary. Similarly Anderson *et al*. when investigating biofilm formation with CDI in *Burkholderia pseudomallei* strains found that CDI shaped biofilm structures, by excluding "non-self" cells from pillar structures (Anderson et al., 2014).

Cell filamentation, originally seen as sign of cell sickness and death, is more and more seen as an active mechanism to survive potentially lethal stresses (Justice et al., 2008). For example, filamentation has been shown to help pathogens like uropathogenic *E.coli* to evade innate immune response (Justice et al., 2006) and *Burkholderia pseudomallei* to survive antibiotic treatment (Chen et al., 2005). Interestingly, the two CDI toxins CdiA-CT$^{Bp\ 1026b}$ and CdiA-CT$^{UPEC536}$, both tRNases whose effect might be reversible, were isolated from these two strains. As it is still not clear when CDI genes are activated in the natural environment of bacteria, CDI could have a role in inducing morphological changes in a subpopulation of cells to survive stresses.

### 5.3.5 CdiI$^{EC869\ o11}$ overexpression presumably induces the SOS response

The observed filamentation of cells overexpressing the antitoxin CdiI$^{EC869\ o11}$ is apparently different from that found in susceptible target cells subjected to the toxin CdiA-CT $^{EC869\ o11}$. Cells keep growing steadily which results in remarkable buckling and looping of filamentous cells. As described in 5.3.1 filamentation is often caused by induction of the SOS response. Induction of the SOS response could be due to binding of CdiI$^{EC869\ o11}$ to an off-target, potentially a DNA binding enzyme, or due to aggregation of CdiI$^{EC869\ o11}$. The crystal structure of the CdiA-CT/CdiI$^{EC869\ o11}$ complex revealed a stabilization by ß-augmentation that is observed in virus assembly or aggregation of amyloids (Morse et al., 2012). Thus CdiI$^{EC869\ o11}$ when overexpressed might form complex aggregates causing cell filamentation.

Interestingly both known features that confer immunity to target cells from CDI$^{EC93\text{-}EC869\ o11}$ inhibition are connected to cell division. Deletion of *yciB* confers immunity, a protein presumably involved in cell septation and CdiI$^{EC869\ o11}$ when expressed at low levels confers immunity, but results in excessive cell filamentation, thus inhibiting cell division, when overexpressed. This could be a coincidence or a hint that a mechanism or protein involved in cell division is essential for EC869 toxin activity. As purified

CdiI$^{EC869\ o11}$ could not completely suppress DNase “nickase” activity of CdiA-CT$^{EC869\ o11}$ *in vitro* (Morse et al., 2012) a scenario where a third factor is needed to suppress toxin activity *in vivo* might be reasonable.

# 6 A CDI/attenuation based buffer gate

## 6.1 Design of an attenuation-based genetic buffer gate

For a more detailed investigation of CDI during surface growth a reporter for toxin delivery would be desirable. Two of the known CDI toxins CdiA-CT$^{Bp\ 1026b}$ and CdiA-CT$^{EC869\ o5}$ have a specific tRNase activity. This specific activity could be monitored by repurposing a well-studied transcriptional regulation mechanism: the ribosome based transcriptional attenuation of the tryptophan operon (Merino et al., 2008).

The tryptophan operon encoding the genes for tryptophan biosynthesis is regulated by ribosome mediated transcriptional attenuation. When the cell is starved for tryptophan the expression of genes of the tryptophan operon is upregulated leading to increased tryptophan biosynthesis (Kolter and Yanofsky, 1982).

The tryptophan operon consists of a short open reading frame *trpL* followed by the structural genes (*trpE, trpD, trpC, trpB, trpA*) (see Figure 28A). *trpL* contains a tandem repeat of trp codons (UGGUGG). As transcription and translation is coupled in *E.coli* ribosomes translate the mRNA while RNA polymerases are still transcribing the DNA. When the tryptophan level in the cell is high, tRNA$^{Trp}$ is present, the ribosome can read through the *trp* codons uninterrupted. The *trpL* mRNA folds into a secondary structure containing two hairpin structures 1:2 and 3:4. The latter is a so called intrinsic terminator resulting in transcription termination, the downstream structural genes are not transcribed (see Figure 28B). However, during tryptophan starvation tRNA$^{Trp}$ remain largely uncharged causing the ribosome to stall at the *trp* codons occluding the mRNA segment 1 preventing the hairpin structure 1:2 from forming. Instead the alternative secondary structure 2:3 folds, which prevents the intrinsic terminator 3:4. RNA polymerases keep transcribing the operon and the following structural genes are transcribed (see Figure 28C) (Lee and Yanofsky, 1977; Yanofsky, 2000).

The CDI toxin CdiA-CT$^{Bp\ 1026b}$ is a specific tRNA$^{Ala}$ RNase (Nikolakakis et al., 2012) and the toxin CdiA-CT$^{EC869\ O5}$ is a specific tRNA$^{Gln}$ RNase (Ruhe et al., 2014). A modified leader region could be used to report toxin activity. CdiA-CT$^{Bp1026b}$ was chosen as it seems to be weaker than the CdiA-CT$^{EC869\ o5}$ toxin (see chapter 4.2.1). CdiA-CT$^{Bp1026b}$ specifically degrades tRNA$_{1B}^{Ala}$ (recognizes GCA codon) *in vivo* (Nikolakakis et al., 2012).

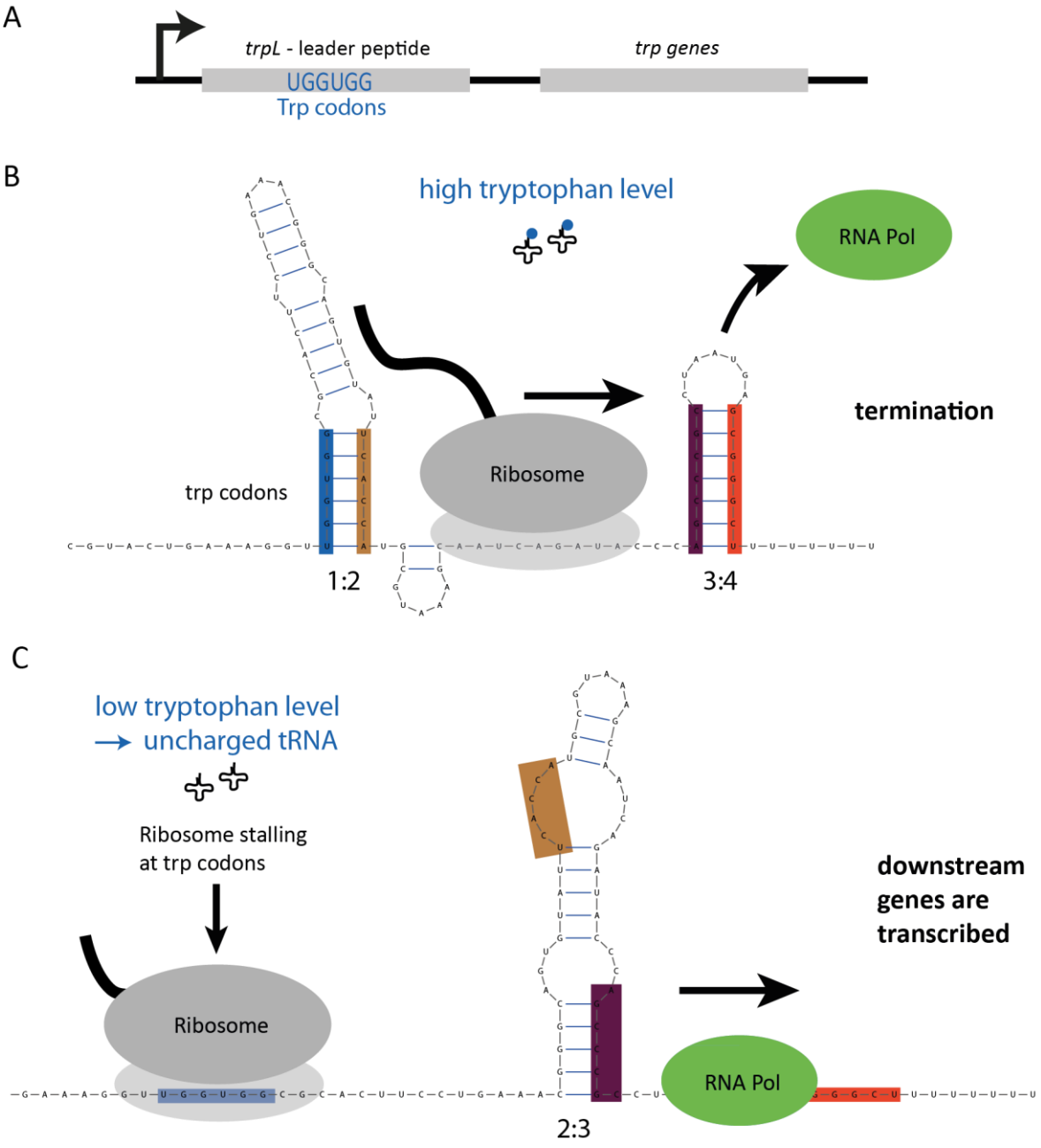


**Figure 28: Regulation of the *trp* operon by ribosome-mediated transcription attenuation. (A) Structure of the *trp* operon. The structural genes are proceeded by the regulatory leader sequence *trpL*. (B) When tryptophan level in the cell is high charged $tRNA^{Trp}$ are present and the ribosome reads unhindered through the *trp* codons. The *trpL* mRNA folds into a secondary structure involving two hairpins 1:2 and 3:4. 3:4 is an intrinsic terminator causing transcription termination. (C) Tryptophan starvation results in mainly uncharged $tRNA^{Trp}$. The ribosome translating the transcript pauses at the trp codons masking sequence 1 resulting in an alternative secondary structure involving the secondary structure 2:3. The terminator (3:4) cannot form and transcription continues, the downstream structural genes are transcribed.**

The devised switch constructs consists of a constitutive promoter driving the transcription of the modified *trpL* regulatory sequence and a reporter gene, e.g. *gfp* (see Figure 29A). The modified leader peptide contains tandem *ala* codons (GCA) instead of tandem *trp* codons. These codons are recognized by $tRNA_{1B}^{Ala}$. When the toxin CdiA-$CT^{Bp1026b}$ is absent from the cell the level of the charged $tRNA_{1B}^{Ala}$ is regular. Ribosomes translating the modified *trpL* mRNA sequence run through the transcript without

pausing. The regular *trpL* leader hairpin structures 1:2 and 3:4 form, where 3:4 is an intrinsic terminator causing transcription termination. In this case the reporter gene is not transcribed (see Figure 29B). Yet when the toxin CdiA-CT$^{Bp1026b}$ is present within the cell and degrades tRNA$_{1B}^{Ala}$ the ribosome stalls at the *ala* codons leading to the alternative secondary structure of the mRNA (hairpin 2:3). No terminator (3:4) forms and transcription continues to the reporter gene (see Figure 29C).

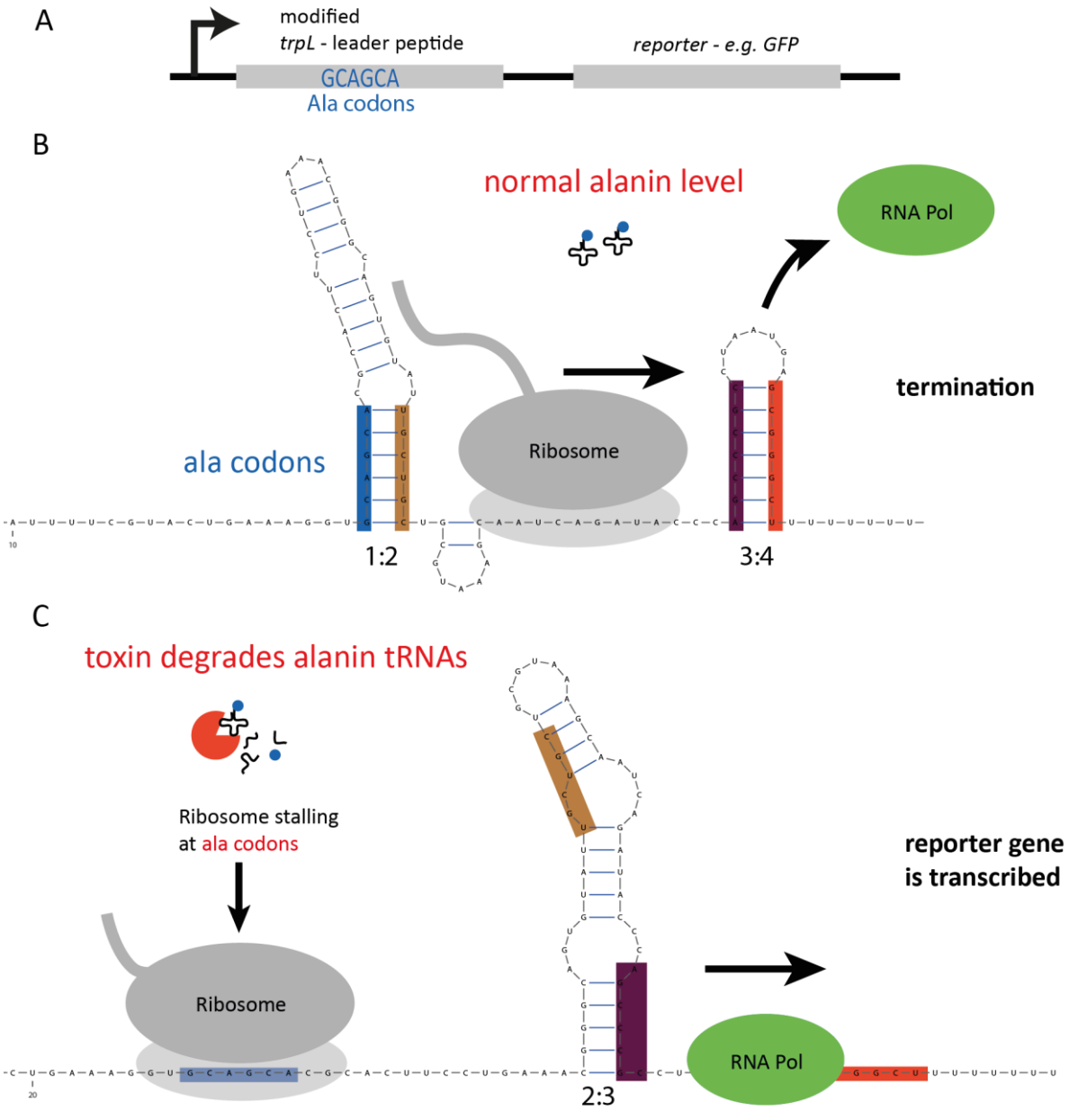


**Figure 29: Molecular mechanism of the attenuation based buffer gate. (A) Coding sequence of the proposed attenuation based switch. The modified regulatory leader sequence *trpL* is followed by a reporter gene. (B) When the toxin is absent charged tRNA$_{1B}^{Ala}$ is present and the ribosome reads undisturbed through the *ala* codons. The *trpL* mRNA folds into a secondary structure (1:2, 3:4) which contains an intrinsic terminator (3:4) causing transcription termination. (C) If present the toxin CdiA-CT$^{Bp1026b}$ degrades tRNA$_{1B}^{Ala}$. Hence the ribosome translating the transcript pauses at the ala codons masking sequence 1. The mRNA folds into the alternative secondary structure (2:3). The terminator (3:4) cannot form and transcription continues to the reporter gene.**

As this attenuation based switch regulates the transcriptional current of RNA polymerase along the DNA it can be seen as a genetic logic gate. Input and output of the attenuation based switch are transcription rates, the control signal is CdiA-CT$^{Bp1026b}$ (Figure 30A). When the control signal is low the output of the gate is low, whereas a high control signal leads to a high output (see Figure 30B). Such behaviour is consistent with a logic buffer gate.

What makes this attenuation based switch special is the nature of the control signal. As the control signal is CdiA-CT$^{Bp1026b}$ it can either be individually expressed within the cell or it can be delivered into the cell in a contact-dependent manner by expression of *cdiBAI*$^{EC93\text{-}Bp\ 1026b}$ by a neighboring cell. Upon transfer of the toxin domain into the target cell tRNA$_{1B}^{Ala}$ would be degraded and the downstream genes would be transcribed.

In case the downstream gene is a fluorescent protein like GFP, the attenuation based switch could be used as a reporter for toxin delivery in inhibition experiments (see Figure 31A).

By adding *cdiBAI*$^{EC93\text{-}Bp\ 1026b}$ to the transcribed downstream genes one could obtain a mechanism for contact-dependent signalling in *E.coli*. Upon delivery of the toxin from a neighboring cell a fluorescent protein and *cdiBAI*$^{EC93\text{-}Bp\ 1026b}$ are expressed. The signal receiving cell would therefore turn into a rebroadcasting cell transferring the control signal into other neighboring cells (see Figure 31B).

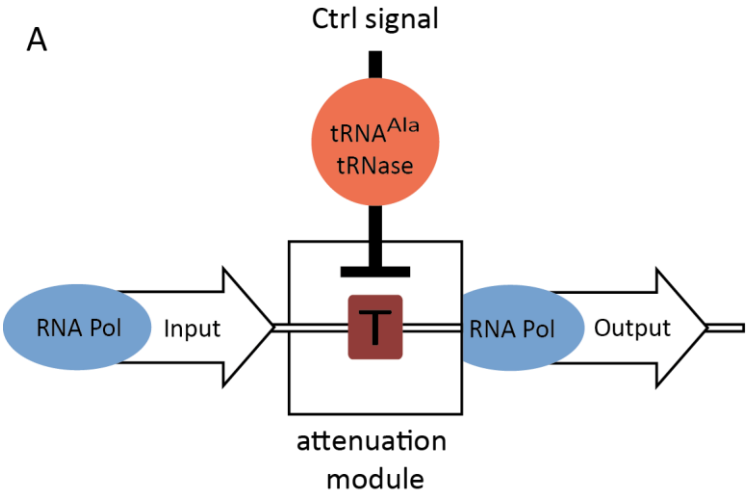


B

| Truth table | |
|---|---|
| Ctrl | Out |
| 0 | 0 |
| 1 | 1 |

**Figure 30: An attenuation-based logic buffer gate. (A) Input and ouput of the gate are transcriptional rates. The control signal is the tRNA$_{1B}^{Ala}$ tRNase CdiA-CT$^{Bp1026b}$. (B) Truth table of the buffer gate.**

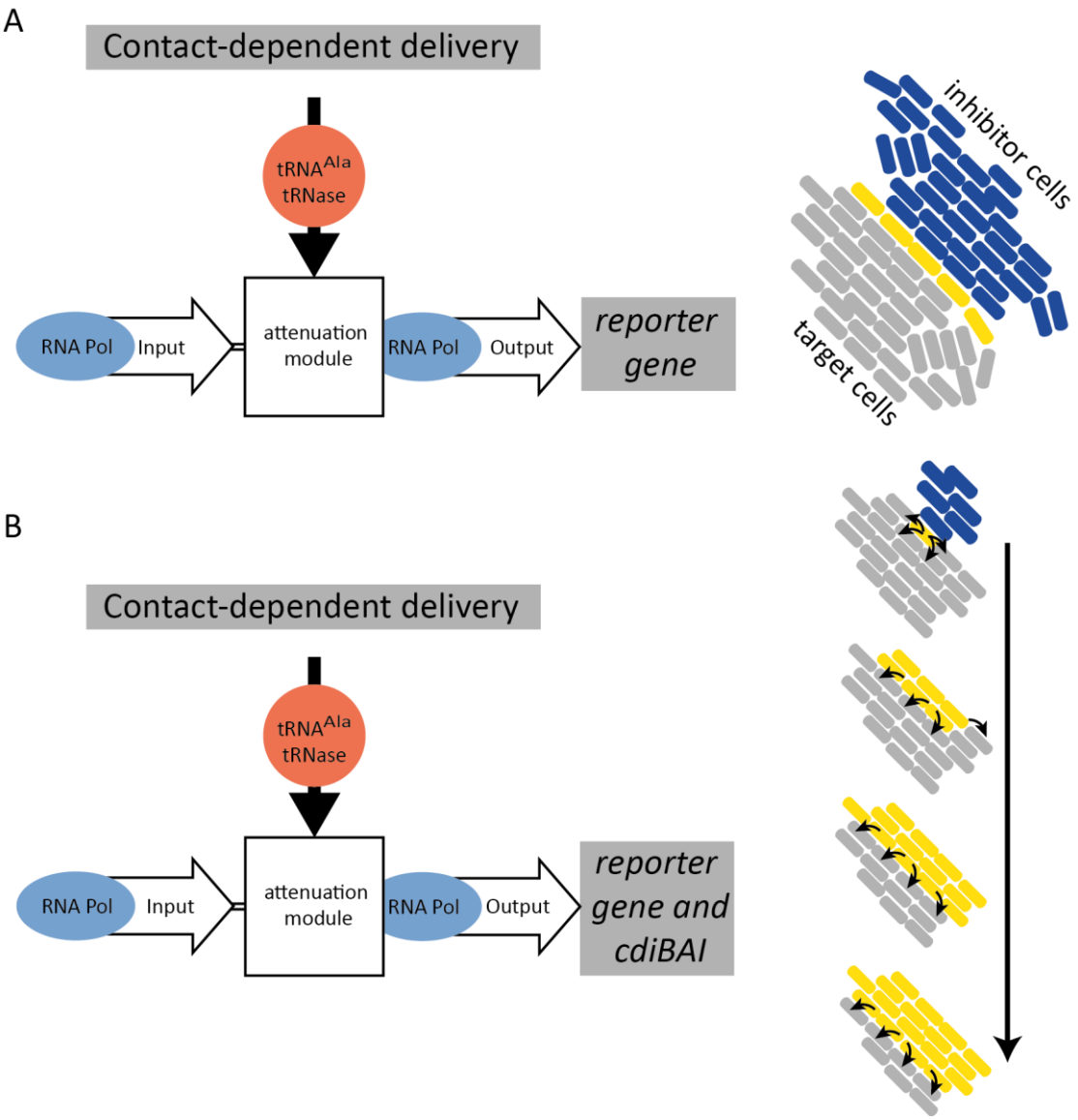


**Figure 31: Possible applications of the attenuation based switch. (A) At the interface of a colony expressing *cdiBAI*$^{Bp1026b}$ the toxin is delivered to target cells containing the attenuation-based switch. These cells will upregulate expression of a fluorescent protein. (B) The attenuation-based switch could be employed for contact-dependent signaling between *E.coli* cells. The output of the buffer gate would be the expression of *cdiBAI*$^{Bp1026b}$ which would transfer the control signal Bp1026b into the next cell.**

## 6.2 Results

### 6.2.1 RNA secondary structure guided design of the CdiA-CT$^{Bp1026b}$ attenuation-based buffer gate

Design of the modified leader sequence was guided by RNA secondary structure prediction to ensure correct folding of the mRNA.

Recently Liu et al. designed a similar attenuation based switch (Liu et al., 2011). The group placed the *trpL* leader sequence under control of a constitutive promoter on a low copy plasmid and introduced

an amber codon at the position of the second *trp* codon resulting in continuous transcription of GFP as a reporter gene. By introducing an amber tRNA and the corresponding aminoacyl tRNA synthetase into the cell the codon could be decoded and transcription was terminated before reaching the downstream genes (Liu et al., 2011). With this design the group was able to achieve a 6-fold attenuation.

For sequence design of the modified *trpL* leader sequence the complete genomic sequence ($trpL_{gen}$), the genomic sequence with the both *trp* codons changed to *ala* codons (GCA) ($trpL_{2ala}$) and the sequence of the amber-codon switch from Liu et al. ($trpL_{amber}$) were used to predict RNA secondary structure with RNAstructure. To predict the secondary structure that forms in the case of transcription termination (see Figure 28A/Figure 29A) (hairpins 1:2 and 3:4) RNA sequence starting 1 bp upstream the *trp* codons until the poly-U sequence was used (see Table 15). To predict the structure in the case of the stalled ribosome (see Figure 29B/Figure 30B) (hairpin 3:4) a shortened sequence version was employed (see Table 15).

For transcription termination the predicted secondary structure of $trpL_{2ala}$ looks significantly different as the structures of $trpL_{gen}$ and $trpL_{amber}$ (compare Figure 32A/B/C). Moreover the folding free energy change of $trpL_{2ala}$ (-24.8 kcal/mol) is considerably lower than those of $trpL_{gen}$ (-33.1 kcal/mol) and $trpL_{amber}$ (-29.9 kcal/mol) (see Table 15). An additional mutation was introduced into $trpL_{2ala}$ to restore base-pairing in the 1:2 hairpin structure ($trpL_{Bp\ 1026b}$). The predicted structure of $trpL_{Bp\ 1026b}$ is congruent to that of $trpL_{gen}$ (compare Table 15D with A).

In the case of a stalled ribosome (continuing transcription) the predicted structures of $trpL_{gen}$, $trpL_{amber}$ and $trpL_{2ala}$ are all equal as the sequence input is the same, too (see Figure 32E/F/G). $trpL_{Bp\ 1026b}$ predicted secondary structure slightly deviates from this structure (compare Figure 32H to E/F/G). As the predicted folding free energy change of $trpL_{Bp\ 1026b}$ is higher (-17.5 kcal/mol) than of $trpL_{gen}$ (-15.1 kcal/mol) it was assumed that this secondary structure will still be able to suppress terminator formation (3:4).

The genomic *trpL* contains an alanine codon (GCA) at the third position. This codon was changed to code for valine to avoid premature stalling of ribosome.

**Table 15: RNA sequences used to predict secondary structure of the *trpL* leader sequences. The *trp* codons in the genomic sequence are highlighted in cyan, deviations from the genomic sequence are highlighted in red.**

| Sequence name | Sequence used for prediction<br>Dot-Bracket Notation of Secondary Structure | E [kcal/ mol] |
|---|---|---|
| $trpL_{gen}$ | UUGGUGGCGCACUUCCUGAAACGGGCAGUGUAUUCACCAUGCGUAAAGCAAUCA<br>GAUACCCAGCCCGCCUAAUGAGCGGGCUUUUUUUU<br>.((((((.(((((.((((...)))).)))))..)))))).((.....)).....(((((((.....))))))).... | -33.1 |
| $trpL_{2ala}$ | UGCAGCACGCACUUCCUGAAACGGGCAGUGUAUUCACCAUGCGUAAAGCAAUCA<br>GAUACCCAGCCCGCCUAAUGAGCGGGCUUUUUUUU<br>.....(((((.((((...)))).)))))........(((.....))).....(((((((.....))))))).... | -24.8 |
| $trpL_{amber}$ | UUGGUAGGGCACUUCCUGAAACGGGCAGUGUAUUCACCAUGCGUAAAGCAAUC<br>AGAUACCCAGCCCGCCUAAUGAGCGGGCUUUUUUUU<br>.((((...(((((.((((...)))).)))))....)))).((.....)).....(((((((.....))))))).... | -29.9 |
| $trpL_{Bp\ 1026b}$ | UGCAGCACGCACUUCCUGAAACGGGCAGUGUAUUGCUGCUGCGUAAAGCAAUCA<br>GAUACCCAGCCCGCCUAAUGAGCGGGCUUUUUUUU<br>.((((((.(((((.((((...)))).)))))..)))))).((.....)).....(((((((.....))))))).... | -35.5 |
| $trpL_{gen}$ | AACGGGCAGUGUAUUCACCAUGCGUAAAGCAAUCAGAUACCCAGCCCGCCUAAU<br>GA<br>..(((((...(((((.....(((.....)))....)))))...))))).... | -15.1 |
| $trpL_{2ala}$ | AACGGGCAGUGUAUUCACCAUGCGUAAAGCAAUCAGAUACCCAGCCCGCCUAAU<br>GA<br>..(((((...(((((.....(((.....)))....)))))...))))).... | -15.1 |
| $trpL_{amber}$ | AACGGGCAGUGUAUUCACCAUGCGUAAAGCAAUCAGAUACCCAGCCCGCCUAAU<br>GA<br>..(((((...(((((.....(((.....)))....)))))...))))).... | -15.1 |
| $trpL_{Bp\ 1026b}$ | AACGGGCAGUGUAUUGCUGCUGCGUAAAGCAAUCAGAUACCCAGCCCGCCUAAU<br>GA<br>..(((((...(((((..((((......))))....)))))...))))).... | -17.5 |

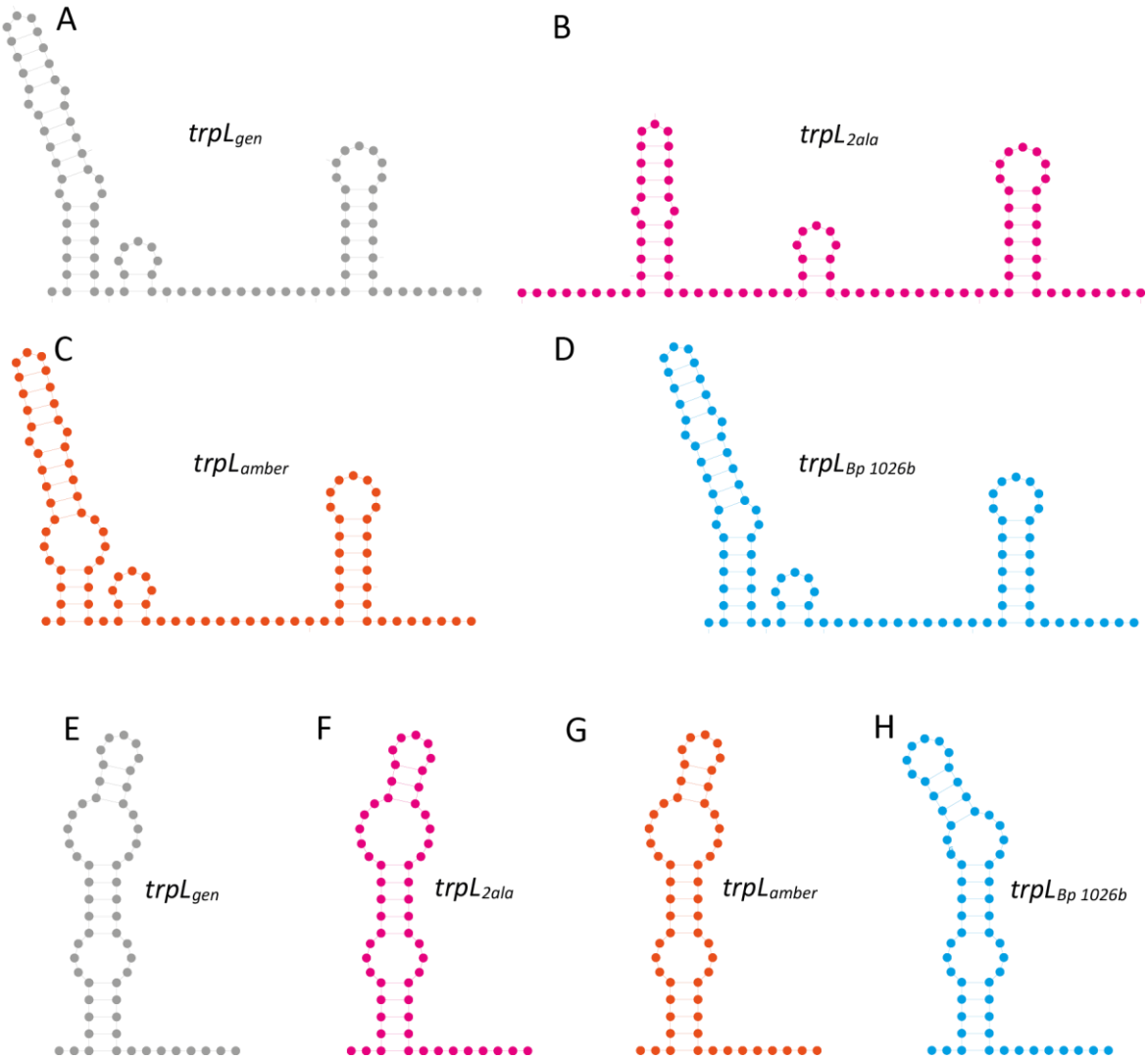


**Figure 32: Predicted secondary structures of *trpL*$_{Bp\ 1026b}$ are similar to those of *trpL*$_{gen}$. (A) - (D) Predicted RNA secondary structure for transcription termination (hairpins 1:2 and 3:4). (E) - (H) Predicted RNA secondary structure for stalled ribosome/continuous transcription.**

For construction of the CdiA-CT$^{Bp1026b}$ attenuation based buffer gate a geneblock containing the strong constitutive promoter J23119 followed by the modified DNA sequence of *trpL*, a fragment of *trpE* and a strong RBS was ordered. This geneblock was subcloned into the biobrick vectors pSB4C5 and pSB4A5 with a transcriptionally fused YFP/GFP (see Figure 33).

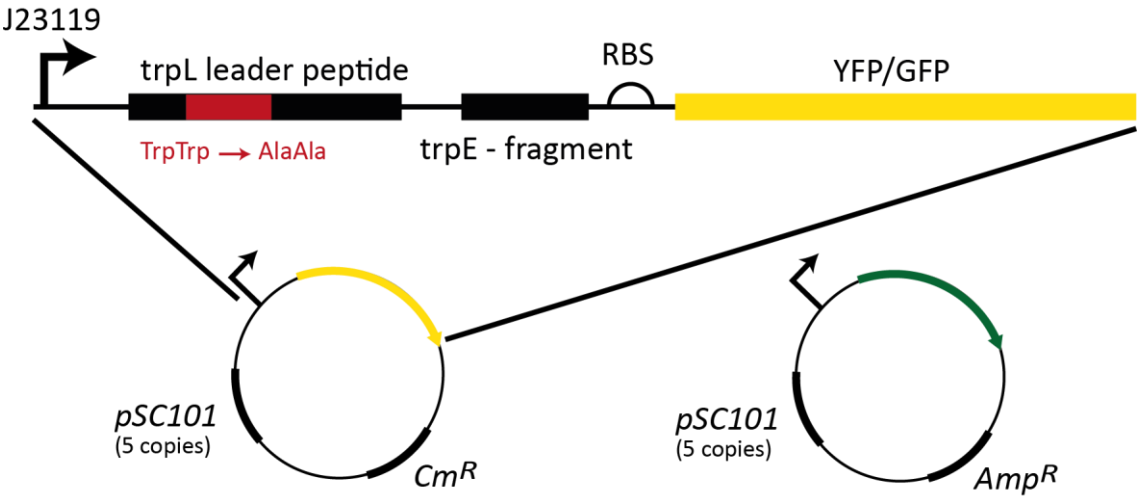


**Figure 33: Schematic of the two constructs BR29 and BR44.**

Initial tests of the attenuation based switch showed no fluorescence increase when cells carrying the switch plasmids (pBR29 or pBR44) were mixed with CDI$^{EC93\text{-}Bp\ 1026b}$ inhibitor cells in solution or during collision in time-lapse imaging.

## 6.3 Discussion

Initial tests did not show the desired function of the devised attenuation based switch. Several different causes could be responsible for this behavior.

The changes made to the *trpL* leader sequence might have changed secondary structure of the mRNA transcript such that efficient attenuation cannot take place. However, there are two examples of successful changes to the *trpL* leader sequence: the above-mentioned (chapter 6.2.1) transcriptional switch where an amber codon was introduced instead of the second *trp* codon (Liu et al., 2011) and an fluorescent reporter for screening of translational inhibitors (Osterman et al., 2012). Osterman et al. made more substantial changes to *trpL* similar as has been done here.

As the CDI$^{Bp1026b}$ inhibitor strain used for the preliminary experiments was not tested for functionality in liquid competition assays, the possibility that this strain is not able to transfer CdiA-CT$^{Bp1026b}$ into cells carrying the buffer gate plasmids cannot be ruled out.

CdiA-CT$^{Bp1026b}$ effects are quite strong as has been shown in chapter 4.2.1. Hence toxin delivery to cells carrying the buffer gate plasmid might rapidly effect the ability of the cell to produce proteins. In this case even if the terminator sequence is suppressed and downstream genes are transcribed, cells might not be able to translate the mRNA producing the fluorescent protein. In order to mitigate toxin activity the antitoxin CdiI$^{Bp\ 1026b}$ could be transcriptionally fused to the fluorescent protein. The basal level of CdiI$^{Bp\ 1026b}$ would help to avoid the complete shut down of protein synthesis upon toxin delivery. A short transcriptional burst from the modified *trpL* gene could take place. The accumulated antitoxin

would then neutralize toxin activity. Cells could be able to recover from the toxin effect and the increase in fluorescent protein should still be visible if a stable version is used.

Another explanation for the failing of the logic buffer gate to be activated could be that the control signal, CdiA-CT$^{Bp1026b}$, is not specific enough. It has been shown that CdiA-CT$^{Bp1026b}$ specifically cleaves tRNA$_{1B}^{Ala}$ *in vivo* in *E.coli*, but also other *E.coli* tRNA species were degraded *in vitro* (Nikolakakis et al., 2012). If CdiA-CT$^{Bp1026b}$ also cleaves other tRNA species *in vivo*, the ribsome might stall prematurely on the *trpL* leader mRNA, preventing the formation of correct secondary structure.

# 7 A novel CDI based selection marker

## 7.1 Current selection marker systems

Antibiotics in combination with antibiotic resistance genes on plasmids are widely used as a selection marker system in laboratory and industry alike. However, during fermentation processes or on plasmids for gene therapy or DNA vaccines this system is problematic.

ß-lactam antibiotics such as ampicillin can cause hypersensitivity reactions in humans and thus are undesirable in any fermentation product or on therapeutic vectors (Solensky, 2003). Removal and quantification of residual antibiotic are expensive and time-consuming procedures.

Horizontal gene transfer of antibiotic resistance genes might contribute to the rise of antibiotic resistance strains. Recently it has been shown that the ampicillin resistance gene *bla* sourced from synthetic vectors can be found in environmental samples of Chinese rivers (Chen et al., 2012).

Integration of genes into the genome of *E.coli* often includes antibiotic selection markers that in turn cannot be used for plasmid retention, decreasing the choice of antibiotic markers.

Other disadvantages of antibiotic selection system are the high cost of antibiotics and the potential toxicity of the resistance gene products upon expression in mammalian hosts (Mairhofer et al., 2010; Vandermeulen et al., 2011; Oliveira and Mairhofer, 2013).

Therefore much effort has been put into developing antibiotic free selection markers. The developed methods fall into the four categories: essential gene complementation, RNA based systems, operator-repressor titration and toxin-antitoxin systems.

In the essential gene complementation system a deletion or amber codon is introduced into the essential gene on the chromosome of the strain. The plasmid complements this deletion by either providing a functional copy of the essential gene or an amber-codon suppressor tRNA. Examples of these are the complementation of a glycine auxotrophic strain (Vidal et al., 2008), or the so-called pCOR plasmids coding for amber suppressor tRNAs (Soubrier et al., 1999, 2005).

RNA-based selection systems rely on the silencing of the expression of toxic proteins by the transcription of an antisense RNA from the plasmid (Luke et al., 2009).

For implementing the operator-repressor titration selection system the lac operator and promoter sequence were placed in front of the essential gene *dapD*. In the absence of the high copy plasmid also encoding the lac operator sequence, the lac repressor solely binds to the operator site on the chromosome repressing the expression of the essential gene (Cranenburgh et al., 2001).

The toxin-antitoxin system CcdB/CcdA when employed as selection marker relies on the so called postsegregational killing. The toxin CcdB inhibits the gyrase of E.coli which is neutralized by the CcdA antitoxin by binding. The antitoxin has a shorter half-life time as the toxin, thus cells that loose the plasmid are killed by the toxin when all antitoxin is degraded (Peubez et al., 2010).

All these systems represent an “intrinsic” selection pressure as opposed to the “extrinsic” pressure of antibiotics. The nature of the “toxic” effect relies within the cell, i.e. is produced within the cell, whereas antibiotics are an external agent. Point mutations in the respective “toxic” gene sequences might already be able to remove selection pressure. Moreover contaminations with other *E.coli* strains that do not carry the selection marker cannot be removed. In contrast antibiotics will reliably suppress contaminations.

A selection system that could replace antibiotics should be easy to implement, exert external pressure, have a small metabolic load and offer a variety of different selection markers (compare to kanamycin, ampicillin, chloramphenicol ...).

## 7.2 Results

### 7.2.1 Design of a novel selection system based on CDI

Contact-dependent growth inhibition with its variety of different toxin activity and the orthogonality of toxin/antitoxin provides the opportunity to build a selection system with several markers.

Selection for plasmid containing cells could be achieved by placing the toxin on the genome and the corresponding antitoxin on the plasmid to be selected. The toxin expression should be inducible to allow for enumeration of cells in absence of the plasmid (see Figure 34A). Either the gene for the C-terminal toxin domain CdiA-CT, or the full-length toxin gene *cdiBA* could be placed under control of the inducible promoter. Upon induction of the toxin with inducer cells containing the antitoxin-encoding plasmid could proliferate, whereas the growth of cells without plasmid would be inhibited (see Figure 34B).

When only CdiA-CT is used for selection the system would only exert “internal” pressure, i.e. only cells carrying the functional toxin on the genome are influenced by its induction. In this system mutations in the toxin could easily lead to plasmid loss and contaminations cannot be suppressed. In contrast the use of the full-length gene *cdiBA* secures a unique “internal and external” selection pressure. Cells expressing the full-length toxin will transfer the toxin into all neighboring cells, exerting selection pressure on them. Cells with a mutation in their own toxin or contaminants can no longer escape selection pressure but are inhibited in their growth by other cells (see Figure 34C).

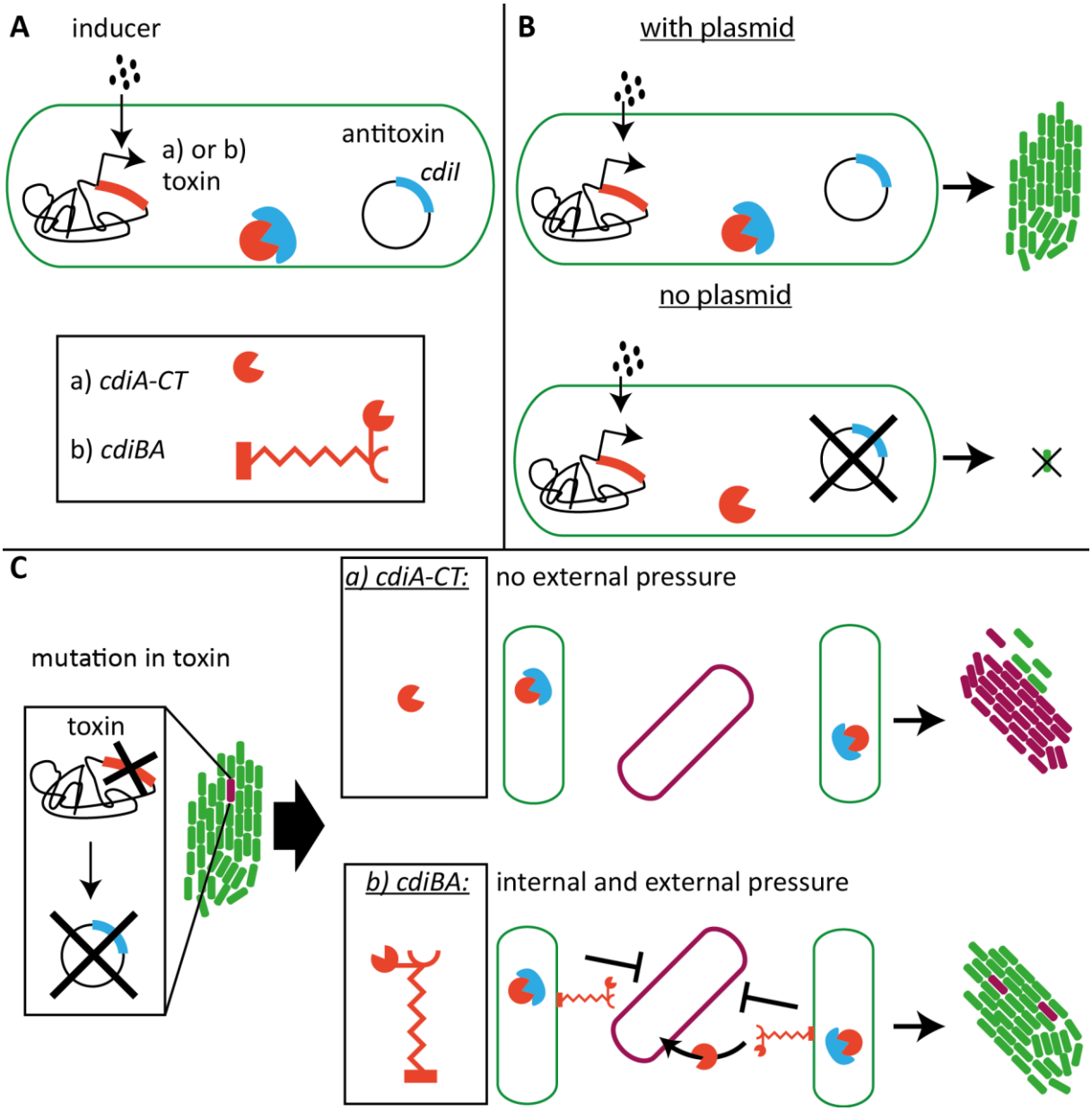


**Figure 34: Schematic depiction of a selection system based on CDI. (A) The toxin, either only *cdiA-CT* (a) or the full-length module *cdiBA* (b), is incorporated on the genome under the control of an inducible promoter. The corresponding antitoxin CdiI is constitutively expressed from the plasmid to be selected. (B) Upon toxin expression cells containing the antitoxin plasmid can proliferate, whereas growth of cells without the plasmid is inhibited. (C) Mutation in the genomic toxin abolishes selection pressure when only *cdiA-CT* is used (a), allowing cells without plasmids to proliferate. Using the full-length toxin *cdiBA* (b) cells with mutations in the toxin or contaminants will still be inhibited by surrounding cells transferring their toxin.**

To test the general suitability of CDI as a novel selection system a simple testing setup for one CDI variant was devised. As shown in chapter 4.2.1, the 16S rRNase ECL performs best as a switch, i.e. high-level expression of ECL suppresses growth, whereas cells grow normally in the absence of toxin induction or when the antitoxin is expressed. This toxin was therefore chosen as the first candidate for the selection system.

Three strains were designed, one expressing CdiA-CT$^{ECL}$ (ara_cdiA-CT), one CdiBA$^{EC93\text{-}ECL}$ (ara_cdiBA) and the control strain expressing GFP (ara_ctrl) under the control of the pBAD promoter.

In order to be able to quickly and easily distinguish between positive cells (containing the plasmid) and negative cells (no plasmid), the selection plasmids contain a constitutively expressed mRFP1 cassette. Both selection plasmids pAT and pCtrl contain the ColE1 origin. The plasmid pAT constitutively expresses the ECL antitoxin under the control of the strong promoter J23100 (Registry of Standard Biological Parts; http://partsregistry.org/Main_Page).

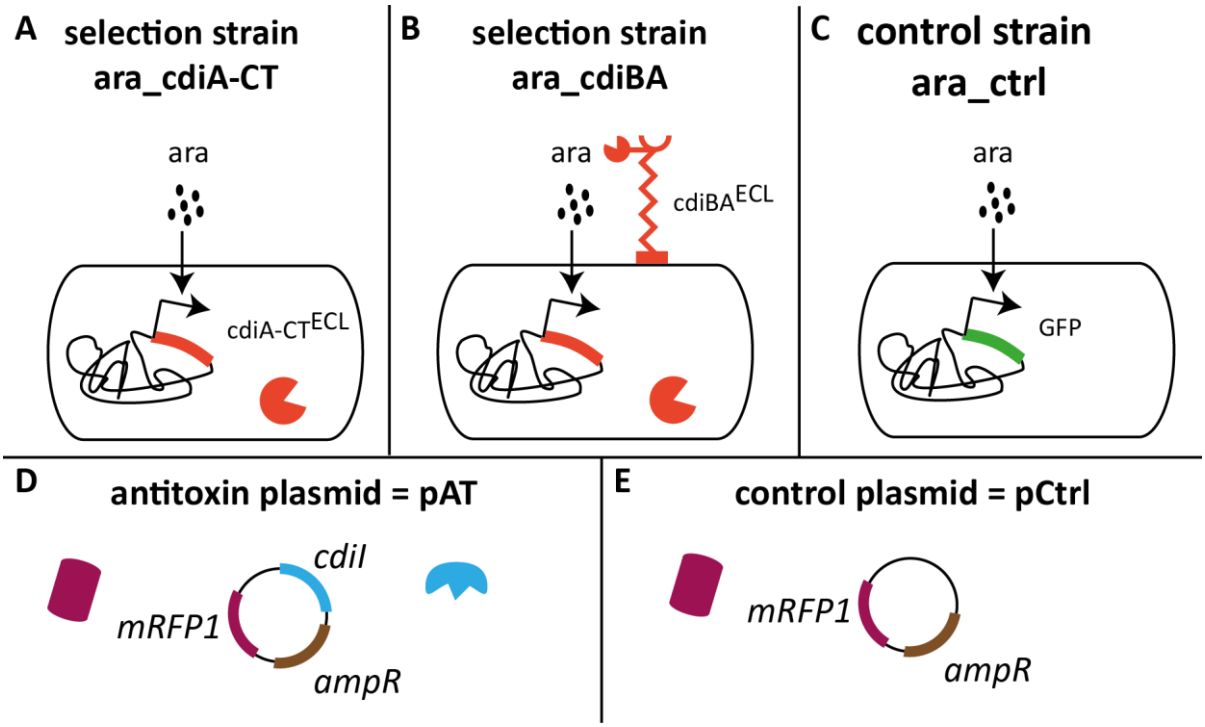


**Figure 35: Components of the devised selection system test. The selection strains are either expressing CdiA-CT (A) or CdiBA (B) under the control of pBAD. The control strain expresses GFP under pBAD (C). The antitoxin plasmid constitutively expressed the antitoxin and mRFP1 (D), whereas the control plasmid pCtrl (E) only constitutively expresses mRFP1 as a visual marker.**

### 7.2.2 Selection based on cdiA-CT/cdiI

The strain ara_cdiA-CT (pBR33 integrant) and ara_Ctrl (pBR33Ctrl integrant) were successfully constructed. However, it was impossible to construct the integration vector pBR33 first, subsequently transforming it into the target strain. Instead integration vectors carrying the expression modules were directly assembled within the target strains carrying the helper vector (see 3.2.10). Figure 36 shows the results of the analytical PCR verifying integration. The observed band pattern is consistent with successful integration of the assembled integration vectors. To date the strain ara_cdiBA could not be constructed. Even if the pBAD promoter was suppressed by addition of 0.4% glucose to the media, no successful and functional integrant could be identified.

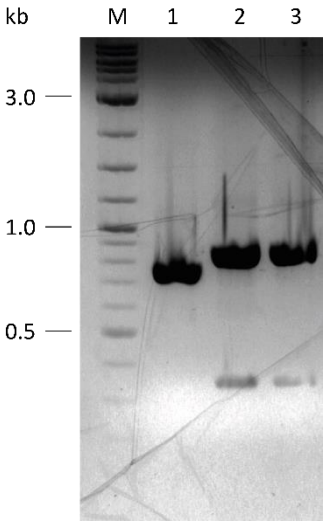


**Figure 36: Successful integration of pBR33 and pBR33Ctrl into the chromosome of DH5αZ1. M: Marker, 1: DH5αZ1, 2: pBR33 integrated into DH5αZ1, 3: pBR33Ctrl integrated into DH5αZ1. The band pattern is consistent with no integration for DH5αZ1 (740 bp) and successful integration for 2 and 3 (343 bp and 824 bp).**

Competent cells of both strains ara_cdiA-CT and ara_Ctrl were generated and transformed with pAT. A solution based growth assay was performed to test toxin activity. The strain ara_cdiA-CT grew slightly slower than the control strain ara_Ctrl in the absence of the inducer arabinose (see Figure 37A, compare black and yellow line). Upon induction with arabinose growth of ara_cdiA-CT can be slowed (0.001 % arabinose) or completely suppressed (0.01 % and 0.1 % arabinose). When the strain ara_cdiA-CT carried the antitoxin expressing plasmid pAT growth is similar to the control strain ara_Ctrl at all inducer concentrations (see Figure 37B). The control strain ara_Ctrl showed the same growth rate for all conditions, different inducer concentrations and with or without the plasmid pAT (Figure 37C/D).

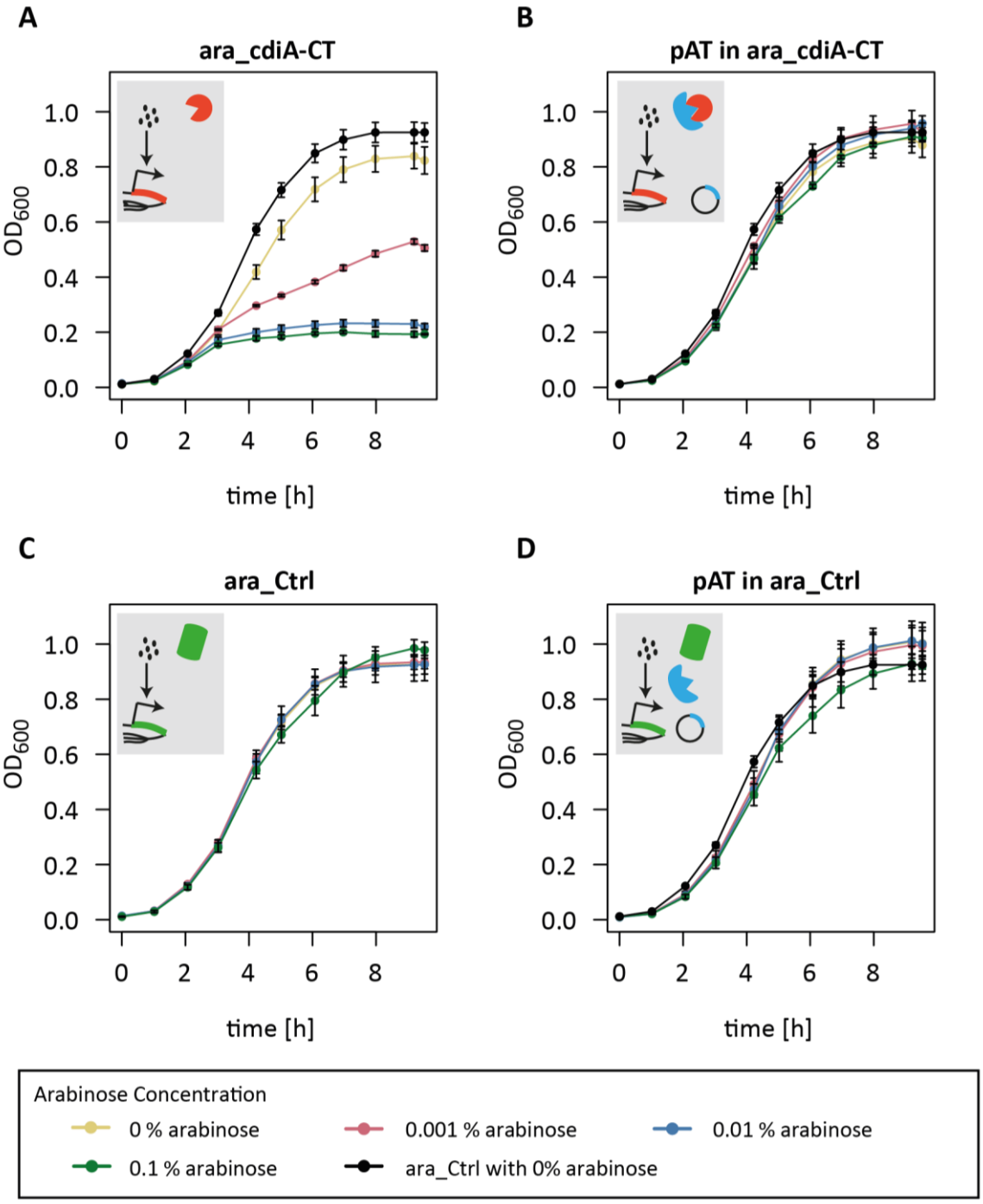


**Figure 37: Growth of the strain ara_cdiA-CT can be suppressed with arabinose and rescued by transformation with pAT. Growth of the strain ara_cdiA-CT is suppressed upon induction with arabinose inducing toxin expression (A). This phenotype can be rescued by the plasmid pAT constitutively expressing the antitoxin (B). The control strain ara_Ctrl grows at similar rates independent of arabinose concentration and with or without the plasmid pAT. Values are mean ± SD of three independent samples.**

For plate-based selection assays the arabinose concentration of 0.1 % arabinose (w/v) was chosen to avoid mixed populations of induced and uninduced cells (Siegele and Hu, 1997) (for a more detailed discussion see chapter 4.2.3) which would interfere with proper selection of plasmid carrying cells.

First selection tests showed positively selected red colonies growing on a thin lawn of white, negative cells. To reduce this background, the transformation procedure was slightly modified. After heat-shock LB media supplemented with 0.1 % arabinose (w/v) was added to the cells to induce toxin expression (see 3.5 for details).

A time-course experiment was conducted to determine optimal recovery time in LB with 0.1 % arabinose (w/v) (see Figure 38). Ara_cdiACT and ara_Ctrl were transformed with pAT. After heat shock 1 ml of LB with 0.1 % arabinose (w/v) was added to the cells. After 1 h 100 µl of cells were plated on both LB agar plates with carbenicillin and on LB agar plates with 0.1 % arabinose. After 2 h and 3 h incubation time 100 µl of the mixture was plated on LB agar plates with 0.1 % arabinose. As expected both strains show only positively selected red colonies when selected on carbenicillin plates. When pAT was selected on 0.1 % arabinose plates in the control strain ara_Ctrl a white bacterial lawn formed for all incubation times (1 h, 2 h, 3 h). This observation is in agreement that arabinose has no selection power in this strain, cells quickly loose the plasmid pAT. The ara_cdiA-CT strain transformed with pAT selected on 0.1 % arabinose plates displayed big red and white colonies at 1 h incubation time which grew on top of a slight bacterial lawn. This bacterial lawn decreased at 2 h incubation time and completely vanished at 3 h incubation time. Thus proper selection of pAT in the strain ara_cdiA-CT on arabinose plates is possible when recovery time in LB with 0.1 % arabinose is increased to 3 h. Even if the bacterial lawn can be removed by this incubation extension the plate still shows big white colonies (see inset Figure 38).

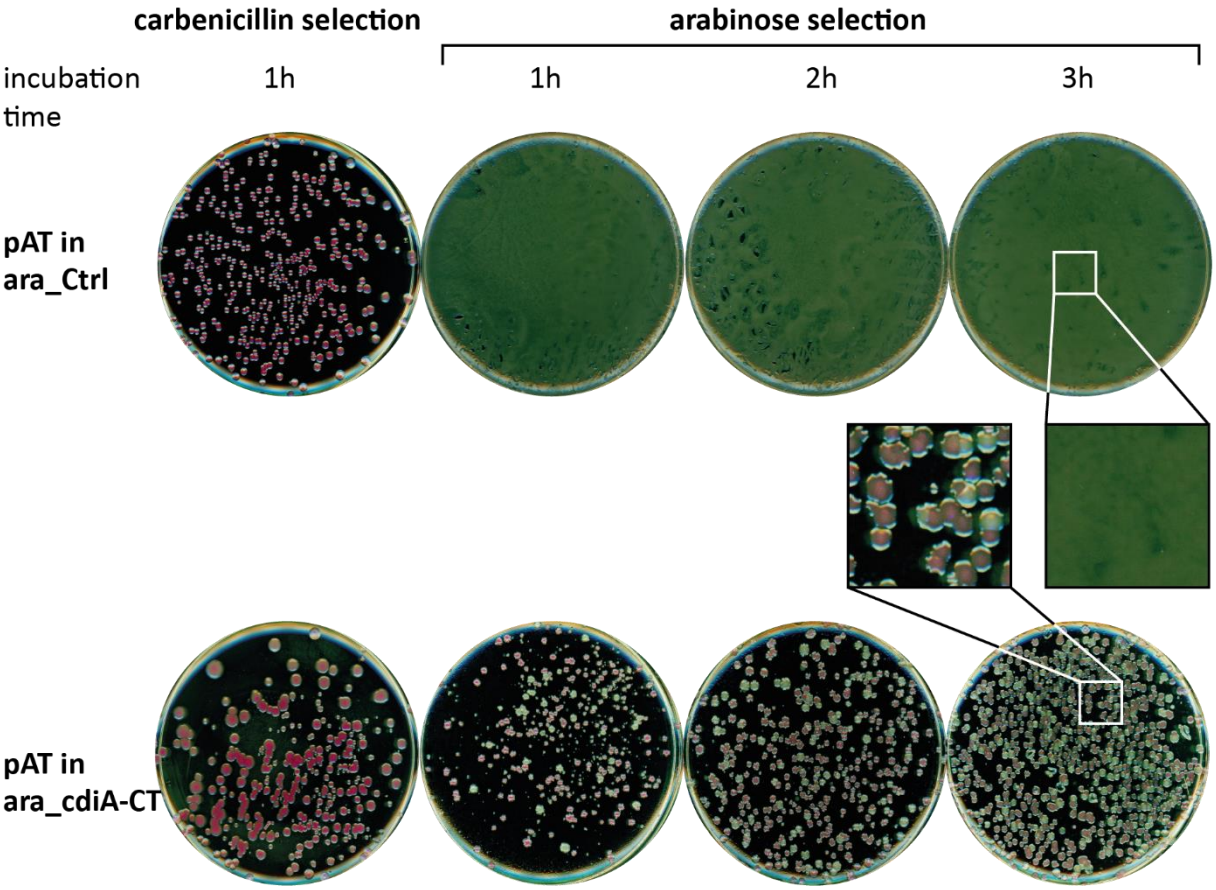


**Figure 38: Selection for pAT with arabinose is successful for ara_cdiA-CT but not for ara_Ctrl. When pAT is selected for on carbenicillin plates both strains show red colonies (far left plates). Selection on arabinose plates results in a white bacterial lawn for the control strain (upper 3 right plates). Selection for pAT on arabinose plates in the strain ara_cdiA-CT results in a mixed population of big red and white colonies (lower 3 right plates). Increasing incubation time in LB with 0.1 % arabinose (from left to right) decreases the bacterial lawn which is present after 1 h of incubation (2$^{nd}$ lower plate) until it has disappeared after 3 h incubation time (4$^{th}$ lower plate).**

Big, white colonies were streaked on carbenicillin plates to determine if they contain pAT and on kanamycin plates to determine if they contain an integration cassette. Cells did not grow on carbenicillin plates indicating that pAT expressing the antitoxin is absent, but grew on kanamycin plates. To confirm that the white colonies do contain an integration cassette analytical PCR was performed. As expected from their ability to grow on kanamycin plates, white colonies showed the band pattern that is consistent with an integration cassette (see Figure 43), indicating that the colonies represent escape mutants.

To further quantify the selection performance three separate aliquots of competent cells of each strain (ara_cdiA-CT/ara_Ctrl) were transformed with 1 ng of pAT and pCtrl. Every replicate was incubated for 3 h in LB with 0.1 % arabinose after heat shock and subsequently 75 µl were plated on carbenicillin plates and on 0.1 % arabinose plates. When selection is performed on carbenicillin plates the amount

of red/positive colonies is similar for the transformation of ara_cdiA-CT with pAT and for the transformation of ara_Ctrl with pAT and pCtrl. However, for the transformation of ara_cdiA-CT with pCtrl only isolated colonies (<10) could be detected (see Figure 39A). All ara_cdiA-CT cells are presumably killed during the recovery phase where toxin is expressed. When selection is performed on arabinose plate transformation of ara_Ctrl results in a white bacterial lawn showing that arabinose itself does not exert any selection pressure on normal *E.coli* strains. When ara_cdiA-Ct is transformed with pAT a mix of red/positive and white/negative colonies appears on the plate. Transformation of ara_cdiA-CT with pCtrl and subsequent selection on arabinose results in a number of white colonies (see Figure 39B). The amount of white colonies on these plates corresponds to the amount of white colonies detected on the plates for transformation with pAT (compare first two white columns Figure 39B). The experiment was repeated and strains were transformed with a lower amount of DNA (0.25 ng) (see Figure 42). The overall result for the different transformation is similar as described above. The amount of red colonies decreased on both carbenicillin plates and arabinose plates which is consistent with lower plasmid availability. However, the amount of white colonies appearing on the arabinose plates for the transformation of ara_cdiA-CT with pAT and pCtrl seems to be the same as in the earlier experiment (compare Figure 39 and Figure 42). Thus the amount of white/negative colonies is invariant for the given set of competent cells and does not scale with plasmid availability. The amount of white colonies appearing on arabinose plates when ara_cdiA-CT is transformed with either pAT or pCtrl is 112 ± 33.

Estimating the total amount of cells plated to about $1 \cdot 10^7$, the frequency of a white/negative colony is about $1 \cdot 10^{-5}$ or less (for details see chapter 3.5.2).

The strain ara_cdiA-CT was restreaked on LB plates twice and isolated colonies were picked. However, newly generated competent cells showed a similar amount of big, white colonies when selection was performed on arabinose plates.

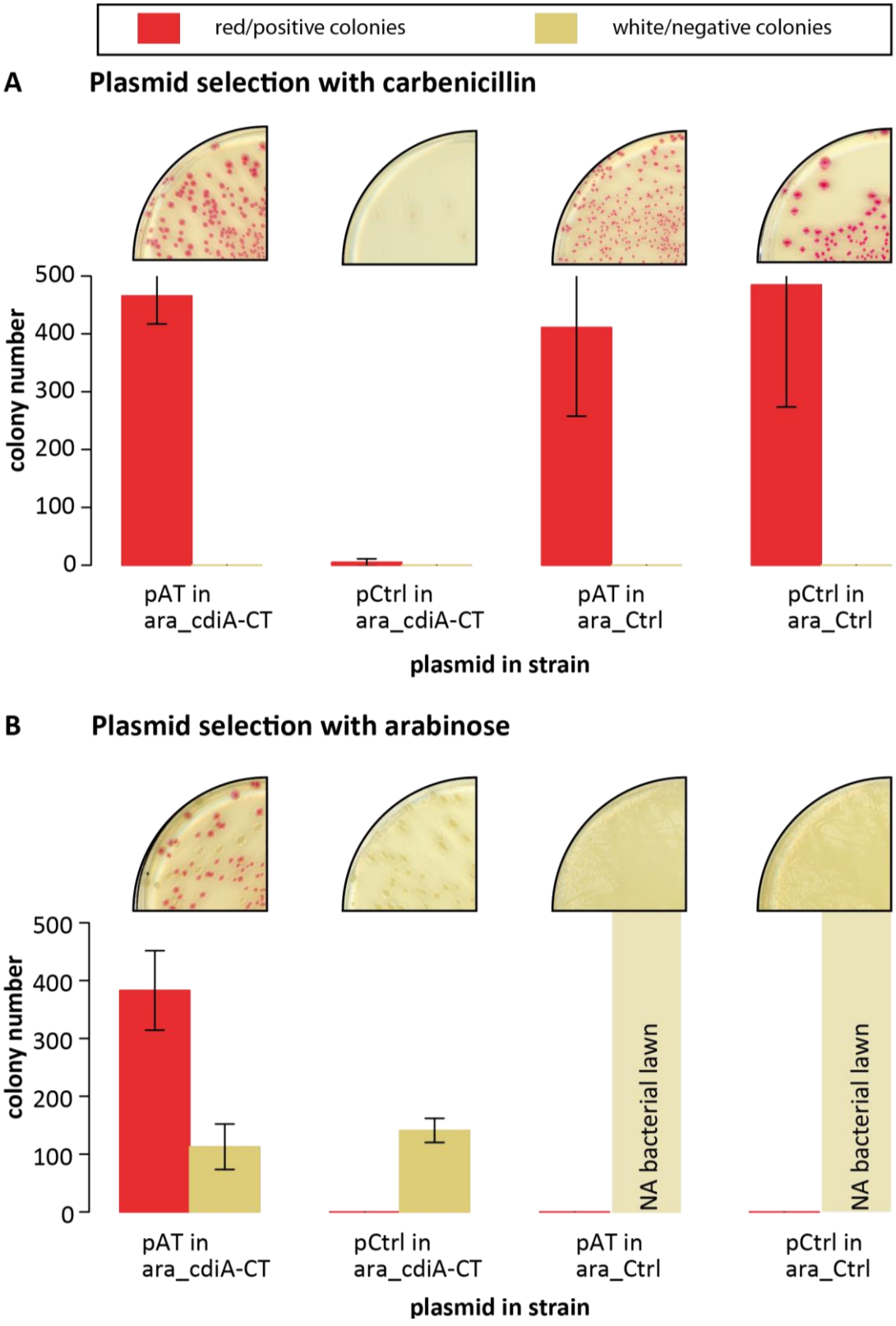


**Figure 39: pAT can successfully be selected with arabinose in the strain ara_cdiA-CT. (A) Selection on carbenicillin plasmid yields equal amounts of positive/red transformants when ara_cdiA-CT is transformed with pAT or ara_Ctrl is transformed with pAT or pCtrl. Transformation of ara_cdiA-CT with pCtrl yields no colonies on carbenicillin plates. (B) Arabinose selection of the transformation of ara_cdiA-CT with pAT results in positively selected red colonies, but also in a number of negative/white colonies. Transformation of ara_cdiA-Ct with pCtrl results in a similar amount of white colonies when selected on arabinose. Selection on arabinose leads to the formation of a white bacterial lawn for transformation of ara_Ctrl with pAT or pCtrl.**

In order to test if pAT can be maintained in ara_cdiA-CT only by arabinose selection pressure in liquid culture overnight cultures were inoculated. Three red colonies were picked from the transformation of pAT in ara_cdiA-CT selected on arabinose plates and on carbenicillin plates. The three colonies originating from arabinose plates were inoculated into LB media with 0.1 % arabinose, the three colonies from carbenicillin plates in LB media with carbenicillin. After centrifugation the pellets of all 6 clones showed a deep red color corresponding to the mRFP1 expression from the pAT plasmid (see.Figure 40A). Plasmid DNA yield of pAT in ara_cdiA-CT under arabinose selection pressure is similar or even higher than under carbenicillin selection pressure (see Figure 40B).

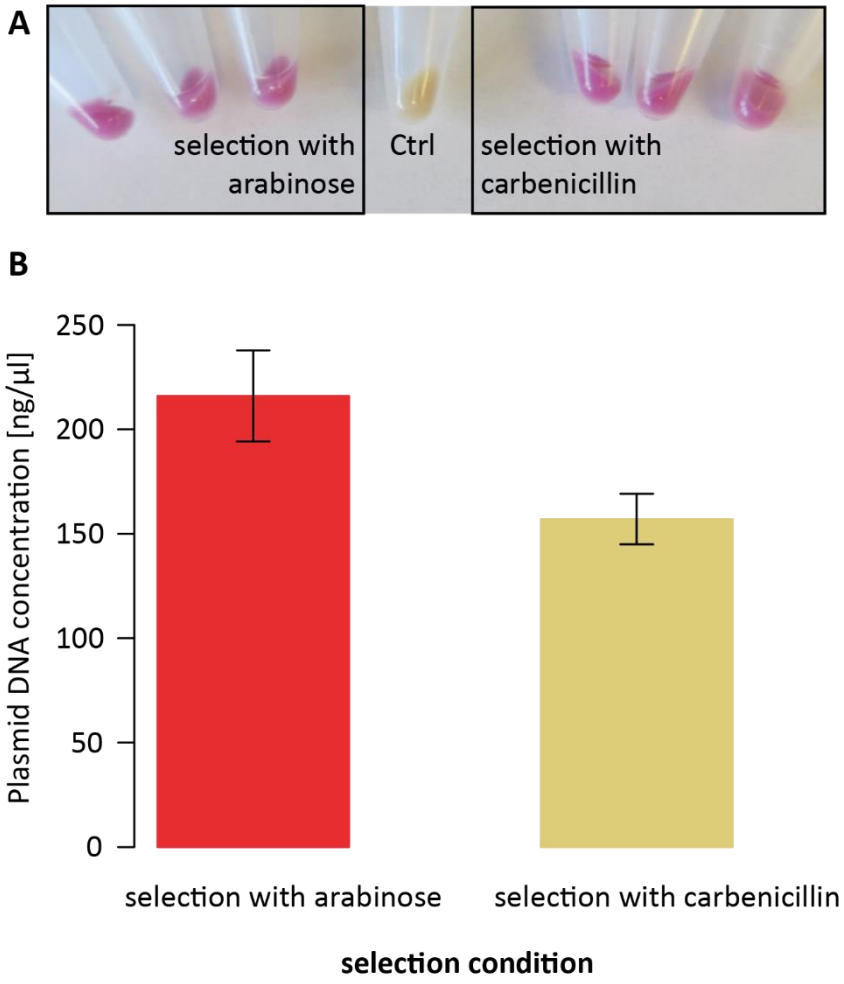


**Figure 40: Selection of pAT in ara_cdiA-CT by arabinose is efficient in liquid culture. (A) Dell pellets of overnight cultures from cultures with arabinose selection pressure (left) and carbenicillin selection pressure (right) show similar red color caused by RFP expression. (B) Plasmid DNA yield of cells grown in presence of arabinose or carbenicillin.**

## 7.3 Discussion

In general the selection strain ara_cdiA-CT seems to be functional. Toxin induction by arabinose suppresses growth of almost all cells when the antitoxin expressing plasmid (pAT) is absent. Cells containing the antitoxin plasmid (pAT) can be selected on arabinose plates and in liquid culture. The efficiency of the pAT selection by arabinose in the strain ara_cdiA-CT is even clearer when compared to the strain ara_Ctrl. Selection for pAT with arabinose in this strains results in a dense white bacterial lawn.

Even if selection in the ara_cdiA-CT is comparably efficient when seen in context of the amount of cells originally present, the escape frequency, reflected by white colonies appearing on the arabinose plates, is still too high. As transformation efficiency seems to be on a similar magnitude as the escape frequency selection using the strain ara_cdiA-CT is not reasonable. Depending on the amount of plasmid DNA used for transformation and transformation efficiency of the competent cells, white colonies might constitute a significant portion of all colonies.

For optimization it is crucial to know the origin of these white colonies. They could either represent a contamination or a small fraction of cells that contain an inactivating mutation in the toxin.

As the strain ara_cdiA-CT and ara_ctrl were handled simultaneously it is feasible that a contamination occurred. Both strains contain their integration cassette at the same site in the genome thus would not be distinguishable by colony PCR. However, even after restreaking newly generated competent cells showed a big white colonies when selection was performed with arabinose. In this light it is highly unlikely, that the white colonies represent a contamination. To completely rule out this possibility, the integration cassette of white colonies could be sequenced.

The escape frequency, i.e. the frequency at which white/negative colonies appear, is estimated to be less than $1 \cdot 10^{-5}$. Recently two groups reported the escape frequency of auxotroph strains generated by incorporation of the stop codon TAG into essential genes, to be between $10^{-3}$ to $10^{-7}$ (Mandell et al., 2015; Rovner et al., 2015). In this case analyzed escape mutants contained a single point mutation reverting the stop codon TAG into the Tyr codon TGG. Thus the observed white colonies could represent a fraction of cells containing mutations in the toxin coding region or the driving promoter pBAD.

Use of the full-length toxin for selection would lower this escape frequency and eliminate potential contaminants. Unfortunately, the full-length toxin could not be integrated into the chromosome. Integration of the full-length toxin into the chromosome under the control of the same promoter and RBS strength as the cdiA-CT domain might not be possible. Even if toxin activity of full-length toxin and CdiA-CT domain should be the same, cells containing the full-length toxin might be impacted much

stronger. The full-length toxin is a huge protein (3727 amino acids). Leaky, basal expression of this huge protein combined with the protein synthesis supressing toxin activity (16S rRNase) might be too detrimental for cells.

# 8 Conclusion and Outlook

Out of four CDI toxin/antitoxin pairs tested herein CdiA-CT$^{ECL}$/CdiI$^{ECL}$ was able to tune growth rate of cells over a wide range. Growth regulation could be achieved on a population level and presumably also on a single cell level. The 16S rRNase activity of CdiA-CT$^{ECL}$ mimics natural growth control of *E.coli* and could replace previously employed modes for growth control like media composition and antibiotic treatment. For further fine-tuning of growth rate using the CdiA-CT$^{ECL}$/CdiI$^{ECL}$ expression module different antitoxin expression levels could be varied over different toxin expression levels, presumably allowing an even finer adjustment of *E.coli* growth rate. For use of the growth control by the CdiA-CT$^{ECL}$/CdiI$^{ECL}$ pair in pattern formation, optimization of the cell-lineage marking system is needed.

Time-lapse microscopy of colliding microcolonies was employed to determine the role of CDI during surface growth. The CDI$^{EC93\text{-}EC869\ o11}$ system encoding a DNase was used. Collision of inhibitor colonies with target colonies induced target cell filamentation and smoothed the colony interface. Filamentation of target cells might be caused by the SOS response in target cell, a system usually induced by DNA damage transiently halting cell division. In order to investigate if the triggered SOS response is the cause of target cell filamentation SulA-promoter activity could by monitored by reporter gene expression (Justice et al., 2006).

Filamentation by activation of SulA is usually transient. When the cause for the SOS response, e.g. a chemical compound is removed, filamentous cells divide and resume normal growth. However, in the case presented here, where the DNase CdiA-CT$^{EC93\text{-}Ec869\ o11}$ is delivered to cells, cells are unlikely to recover when genomic DNA is destroyed. Further investigations are needed to examine if cdiA-CT$^{EC93\text{-}EC869\ o11}$ delivery at the interface between target inhibitor cell colonies results in full loss of genomic DNA in target cells. To answer this question time-lapse microscopy of colliding target and inhibitor colonies using the DNA stain SYTOX green or a DNA associated fluorescent protein like HupA-mCherry could be performed (Fisher et al., 2013; Bakshi et al., 2014).

Filamentation of target cells causes smoothing of the colony interface that could be quantified using fractal analysis. Fractal analysis developed by Mandelbrot (Mandelbrot, 1982) has been used over the years to quantify the roughness in several biological systems, for example the branching of blood vessels or cellular morphology (Smith et al., 1989; Cross, 1997; Kam et al., 2009). Recently fractal dimensions of colony boundaries of growing *E.coli* colonies were measured to quantify the effect of cell morphology on boundary roughness (Rudge et al., 2013).

Competition of inhibitor cells with target cells in liquid media decreased target cell viability substantially. The obtained time-lapse movies of CDI during surface growth show a much weaker

inhibition of target cells. This difference in killing efficiency could be caused by differences in media composition. To completely rule out this possibility competitions in liquid culture could be repeated using the supplemented M9 media used for time-lapse microscopy. Decreased killing efficiency during surface growth could as well be due to lower accessibility of target cells during surface growth limiting the amount of toxin transferred. Furthermore direct comparison between competition in liquid media and during surface growth may not be possible as target cell properties are measured differently. The CFU assay performed for competitions in liquid culture relies on the ability of cells to regrow to form a visible colony, whereas the time-lapse microscopy performed here was able to assess morphology of cells but only provided very little information about target cell viability.

A buffer gate based on transcription attenuation mechanism responding to the Ala tRNase CdiA-CT$^{Bp\ 1026b}$ as a control signal was devised. This buffer gate could be used as a reporter for toxin delivery during time-lapse microscopy. The leader sequence of the tryptophan operon trpL was modified using RNA secondary structure guided design. Initial tests of the two constructs built showed no functionality. In order to properly test the function of the attenuation based buffer gate further experiments with an assured working CDI$^{Bp1026b}$ inhibitor strain have to be conducted. If the switch proves non-functional, a similar switch where the *trp* codons in the *trpL* are exchanged for *gln* codons could be designed. This switch would respond to CdiA-CT$^{EC869\ o5}$ as a control signal. Alternatively a reporter responding to the toxin CdiA-CT$^{EC869\ o11}$ could be designed based on SOS response induction upon DNA damage caused by CdiA-CT$^{EC869\ o11}$ DNase activity.

The CdiA-CT$^{ECL}$/CdiI$^{ECL}$ pair was chosen to test the suitability of CDI for a novel selection marker system. A simple test system with two selection strains, one encoding the C-terminal toxin domain CdiA-CT, one encoding the full-length toxin under control of the arabinose inducible promoter pBAD on the chromosome, was devised. A selection plasmid constitutively expressing the antitoxin with a translationally fused mRFP1 was built. Selection experiments with the strain encoding only the C-terminal toxin domain showed proper selection of the antitoxin-encoding plasmid both on plates and in liquid media. However, colonies not harbouring the plasmid appeared at about the same rate as positive cells. These colonies could either represent a contamination or toxin resistant mutants. The escape frequency, i.e. the amount of cells able to grow under selection pressure without carrying the plasmid, was estimated to be about $10^{-5}$. This frequency is in good agreement with escape mutants found for auxotroph strains, hence, it is likely that the colonies represent resistant mutants rather than contaminations. To completely rule out this possibility, the integration cassette of white colonies could be sequenced. The second selection strain encoding the full-length toxin under control of the same promoter and RBS strength could not be generated. It might be possible to achieve the integration of the full-length toxin module by lowering the RBS strength of the construct. Considering the huge

metabolic load that cells are subjected to when the full-length toxin would be induced for selection and the potency of the CDI in liquid culture, a very low level of full-length toxin expression might be desirable in any event.

# 9 List of abbreviations

| | |
|---|---|
| CDI | Contact-dependent growth inhibition |
| CdiA-NT | N-terminal domain of CdiA |
| CdiA-CT | C-terminal domain of CdiA, domain with actual toxin activity |
| ara | arabinose |
| atc | anhydrotetracycline |
| TLM | Time-lapse microscopy |

# 10 Bibliography


Anderson, M.S., Garcia, E.C., and Cotter, P.A. (2014) Kind Discrimination and Competitive Exclusion Mediated by Contact-Dependent Growth Inhibition Systems Shape Biofilm Community Structure. **10.**:

Aoki, S.K., Diner, E.J., de Roodenbeke, C.T., Burgess, B.R., Poole, S.J., Braaten, B. a, et al. (2010) A widespread family of polymorphic contact-dependent toxin delivery systems in bacteria. *Nature* **468**: 439–42.

Aoki, S.K., Malinverni, J.C., Jacoby, K., Thomas, B., Pamma, R., Trinh, B.N., et al. (2008) Contact-dependent growth inhibition requires the essential outer membrane protein BamA (YaeT) as the receptor and the inner membrane transport protein AcrB. *Mol. Microbiol.* **70**: 323–40.

Aoki, S.K., Pamma, R., Hernday, A.D., Bickham, J.E., Braaten, B. a, and Low, D. a (2005) Contact-dependent inhibition of growth in Escherichia coli. *Science* **309**: 1245–8.

Aoki, S.K., Poole, S.J., Hayes, C.S., and Low, D. a. (2011) Toxin on a stick: Modular CDI toxin delivery systems play roles in bacterial competition. *Virulence* **2**: 356–359.

Aoki, S.K., Webb, J.S., Braaten, B. a, and Low, D. a (2009) Contact-dependent growth inhibition causes reversible metabolic downregulation in Escherichia coli. *J. Bacteriol.* **191**: 1777–86.

Azam, T.A., Iwata, A., Nishimura, A., Ueda, S., and Ishihama, A. (1999) Growth phase-dependent variation in protein composition of the Escherichia coli nucleoid. *J. Bacteriol.* **181**: 6361–6370.

Bakshi, S., Choi, H., Rangarajan, N., Barns, K.J., Bratton, B.P., and Weisshaar, J.C. (2014) Nonperturbative imaging of nucleoid morphology in live bacterial cells during an antimicrobial peptide attack. *Appl. Environ. Microbiol.* **80**: 4977–4986.

Bassler, B.L. and Losick, R. (2006) Bacterially speaking. *Cell* **125**: 237–46.

Beck, C.M., Morse, R.P., Cunningham, D. a, Iniguez, A., Low, D. a, Goulding, C.W., and Hayes, C.S. (2014) CdiA from Enterobacter cloacae delivers a toxic ribosomal RNase into target bacteria. *Structure* **22**: 707–18.

Blin, G., Denise, A., Dulucq, S., Herrbach, C., and Touzet, H. (2009) VARNA: Interactive drawing and editing of the RNA secondary structure. *IEEE/ACM Trans. Comput. Biol. Bioinform.* **7**: 309–22.

Chang, D.-E., Smalley, D.J., and Conway, T. (2002) Gene expression profiling of Escherichia coli growth transitions: an expanded stringent response model. *Mol. Microbiol.* **45**: 289–306.

Chen, J., Jin, M., Qiu, Z.G., Guo, C., Chen, Z.L., Shen, Z.Q., et al. (2012) A survey of drug resistance bla genes originating from synthetic plasmid vectors in six Chinese rivers. *Environ. Sci. Technol.* **46**: 13448–13454.

Chen, K., Sun, G.W., Chua, K.L., and Gan, Y. (2005) Modified virulence of antibiotic-induced *Burkholderia pseudomallei* filaments. *Antimicrob. Agents Chemother.* **49**: 1002–9.

Cranenburgh, R.M., Hanak, J. a, Williams, S.G., and Sherratt, D.J. (2001) Escherichia coli strains that allow antibiotic-free plasmid selection and maintenance by repressor titration. *Nucleic Acids Res.* **29**: E26.

Cross, S.S. (1997) Fractals in Pathology. *J. Pathol.* **182**: 1–8.

Diner, E.J., Beck, C.M., Webb, J.S., Low, D. a, and Hayes, C.S. (2012) Identification of a target cell permissive factor required for contact-dependent growth inhibition (CDI). *Genes Dev.* **26**: 515–25.

Edelstein, A., Amodaj, N., Hoover, K., Vale, R., and Stuurman, N. (2010) Computer control of microscopes using μManager. *Curr. Protoc. Mol. Biol.* **Chapter 14**: Unit14.20.

Ehrenberg, M., Bremer, H., and Dennis, P.P. (2013) Medium-dependent control of the bacterial growth rate. *Biochimie* **95**: 643–58.

Engler, C., Gruetzner, R., Kandzia, R., and Marillonnet, S. (2009) Golden gate shuffling: a one-pot DNA shuffling method based on type IIs restriction enzymes. *PLoS One* **4**: e5553.

Engler, C., Kandzia, R., and Marillonnet, S. (2008) A one pot, one step, precision cloning method with high throughput capability. *PLoS One* **3**: e3647.

Fisher, J.K., Bourniquel, A., Witz, G., Weiner, B., Prentiss, M., and Kleckner, N. (2013) Four-dimensional imaging of E. coli nucleoid organization and dynamics in living cells. *Cell* **153**: 882–895.

Garcia, E.C., Anderson, M.S., Hagar, J. a., and Cotter, P. a. (2013) BurkholderiaBcpA mediates biofilm formation independently of interbacterial contact-dependent growth inhibition. *Mol. Microbiol.* **89**: 1213–1225.

Gibson, D.G., Young, L., Chuang, R.-Y., Venter, J.C., Hutchison, C. a, and Smith, H.O. (2009) Enzymatic assembly of DNA molecules up to several hundred kilobases. *Nat. Methods* **6**: 343–5.

Gourse, R.L., Gaal, T., Bartlett, M.S., Appleman, J. a, and Ross, W. (1996) rRNA transcription and growth rate-dependent regulation of ribosome synthesis in Escherichia coli. *Annu. Rev. Microbiol.* **50**: 645–677.

Haldimann, a and Wanner, B.L. (2001) Conditional-replication, integration, excision, and retrieval plasmid-host systems for gene structure-function studies of bacteria. *J. Bacteriol.* **183**: 6384–93.

Hayes, C.S., Koskiniemi, S., Ruhe, Z.C., Poole, S.J., and Low, D. a (2014) Mechanisms and biological roles of contact-dependent growth inhibition systems. *Cold Spring Harb. Perspect. Med.* **4.**:

Hayes, C.S. and Low, D. a (2009) Signals of growth regulation in bacteria. *Curr. Opin. Microbiol.* **12**: 667–73.

Huisman, O., D'Ari, R., and Gottesman, S. (1984) Cell-division control in Escherichia coli: specific induction of the SOS function SfiA protein is sufficient to block septation. *Proc. Natl. Acad. Sci. U. S. A.* **81**: 4490–4494.

Janion, C. (2008) Inducible SOS response system of DNA repair and mutagenesis in Escherichia coli. *Int. J. Biol. Sci.* **4**: 338–344.

Justice, S.S., Hunstad, D. a, Cegelski, L., and Hultgren, S.J. (2008) Morphological plasticity as a bacterial survival strategy. *Nat. Rev. Microbiol.* **6**: 162–168.

Justice, S.S., Hunstad, D. a, Seed, P.C., and Hultgren, S.J. (2006) Filamentation by Escherichia coli subverts innate defenses during urinary tract infection. *Proc. Natl. Acad. Sci. U. S. A.* **103**: 19884–19889.

Kam, Y., Karperien, A., Weidow, B., Estrada, L., Anderson, A.R., and Quaranta, V. (2009) Nest expansion assay: a cancer systems biology approach to in vitro invasion measurements. *BMC Res. Notes* **2**: 130.

Khlebnikov, a, Datsenko, K. a, Skaug, T., Wanner, B.L., and Keasling, J.D. (2001) Homogeneous expression of the P(BAD) promoter in Escherichia coli by constitutive expression of the low-affinity high-capacity AraE transporter. *Microbiology* **147**: 3241–7.

Kolter, R. and Yanofsky, C. (1982) Attenuation in amino acid biosynthetic operons. *Annu. Rev. Genet.*

Koskiniemi, S., Lamoureux, J.G., Nikolakakis, K.C., t'Kint de Roodenbeke, C., Kaplan, M.D., Low, D. a, and Hayes, C.S. (2013) Rhs proteins from diverse bacteria mediate intercellular competition. *Proc. Natl. Acad. Sci. U. S. A.* **110**: 7032–7.

Lander, A.D. (2011) Pattern, growth, and control. *Cell* **144**: 955–69.

LaSarre, B. and Federle, M.J. (2013) Exploiting quorum sensing to confuse bacterial pathogens. *Microbiol. Mol. Biol. Rev.* **77**: 73–111.

Lasswell, H.D. (1948) The structure and function of communication in society. *Commun. Ideas* 37–52.

Lawley, T.D., Gordon, G.S., Wright, A., and Taylor, D.E. (2002) Bacterial conjugative transfer: visualization of successful mating pairs and plasmid establishment in live Escherichia coli. *Mol. Microbiol.* **44**: 947–56.

Lee, F. and Yanofsky, C. (1977) Transcription termination at the trp operon attenuators of Escherichia coli and Salmonella typhimurium: RNA secondary structure and regulation of termination. *Proc. Natl. Acad. Sci. U. S. A.* **74**: 4365–4369.

LeRoux, M., De Leon, J. a, Kuwanda, N.J., Russell, A.B., Pinto-Santini, D., Hood, R.D., et al. (2012) Quantitative single-cell characterization of bacterial interactions. *Proc. Natl. Acad. Sci. U. S. A.* **109**: 19804–19809.

Liu, C.C., Qi, L., Yanofsky, C., and Arkin, A.P. (2011) Regulation of transcription by unnatural amino acids. *Nat. Biotechnol.* **29**: 164–8.

Lobedanz, S. and Søgaard-Andersen, L. (2003) Identification of the C-signal, a contact-dependent morphogen coordinating multiple developmental responses in Myxococcus xanthus. *Genes Dev.* **17**: 2151–2161.

Locke, J.C.W. and Elowitz, M.B. (2009) Using movies to analyse gene circuit dynamics in single cells. *Nat. Rev. Microbiol.* **7**: 383–92.

Lou, C., Stanton, B., Chen, Y.-J., Munsky, B., and Voigt, C. a (2012) Ribozyme-based insulator parts buffer synthetic circuits from genetic context. *Nat. Biotechnol.* **30**: 1137–42.

Luke, J., Carnes, A.E., Hodgson, C.P., and Williams, J. a. (2009) Improved antibiotic-free DNA vaccine vectors utilizing a novel RNA based plasmid selection system. *Vaccine* **27**: 6454–6459.

Mairhofer, J., Cserjan-Puschmann, M., Striedner, G., Nöbauer, K., Razzazi-Fazeli, E., and Grabherr, R. (2010) Marker-free plasmids for gene therapeutic applications-Lack of antibiotic resistance gene substantially improves the manufacturing process. *J. Biotechnol.* **146**: 130–137.

Mandelbrot, B.B. (1982) The Fractal Geometry of Nature W. H. Freeman and Company.

Mandell, D.J., Lajoie, M.J., Mee, M.T., Takeuchi, R., Kuznetsov, G., Norville, J.E., et al. (2015) Biocontainment of genetically modified organisms by synthetic protein design. *Nature* **518**: 55–60.

Meinhardt, H. (2008) Models of biological pattern formation: from elementary steps to the organization of embryonic axes. *Curr. Top. Dev. Biol.* **81**: 1–63.

Merino, E., Jensen, R. a, and Yanofsky, C. (2008) Evolution of bacterial trp operons and their regulation. *Curr. Opin. Microbiol.* **11**: 78–86.

Morse, R.P., Nikolakakis, K.C., Willett, J.L.E., Gerrick, E., Low, D. a, Hayes, C.S., and Goulding, C.W. (2012) Structural basis of toxicity and immunity in contact-dependent growth inhibition (CDI) systems. *Proc. Natl. Acad. Sci. U. S. A.* **109**: 21480–5.

Mutalik, V.K., Guimaraes, J.C., Cambray, G., Lam, C., Christoffersen, M.J., Mai, Q.-A., et al. (2013) Precise and reliable gene expression via standard transcription and translation initiation elements. *Nat. Methods* **10**: 354–60.

Ng, W.-L. and Bassler, B.L. (2009) Bacterial quorum-sensing network architectures. *Annu. Rev. Genet.* **43**: 197–222.

Niba, E.T.E., Naka, Y., Nagase, M., Mori, H., and Kitakawa, M. (2007) A genome-wide approach to identify the genes involved in biofilm formation in E. coli. *DNA Res.* **14**: 237–246.

Nikolakakis, K., Amber, S., Wilbur, J.S., Diner, E.J., Aoki, S.K., Poole, S.J., et al. (2012) The toxin/immunity network of Burkholderia pseudomallei contact-dependent growth inhibition (CDI) systems. *Mol. Microbiol.* **84**: 516–29.

Oliveira, P.H. and Mairhofer, J. (2013) Marker-free plasmids for biotechnological applications - implications and perspectives. *Trends Biotechnol.* **31**: 539–547.

Oster, G.F. and Murray, J.D. (1989) Pattern formation models and developmental constraints. *J. Exp. Zool.* **251**: 186–202.

Osterman, I. a, Prokhorova, I. V, Sysoev, V.O., Boykova, Y. V, Efremenkova, O. V, Svetlov, M.S., et al. (2012) Attenuation-based dual-fluorescent-protein reporter for screening translation inhibitors. *Antimicrob. Agents Chemother.* **56**: 1774–83.

Peubez, I., Chaudet, N., Mignon, C., Hild, G., Husson, S., Courtois, V., et al. (2010) Antibiotic-free selection in E. coli: new considerations for optimal design and improved production. *Microb. Cell Fact.* **9**: 65.

R Core Team (2014) R: A Language and Environment for Statistical Computing.

Reuter, J.S. and Mathews, D.H. (2010) RNAstructure: software for RNA secondary structure prediction and analysis. *BMC Bioinformatics* **11**: 129.

Rovner, A.J., Haimovich, A.D., Katz, S.R., Li, Z., Grome, M.W., Gassaway, B.M., et al. (2015) Recoded organisms engineered to depend on synthetic amino acids. *Nature* **518**: 89–93.

Rudge, T.J., Federici, F., Steiner, P.J., Kan, A., and Haseloff, J. (2013) Cell Polarity-Driven Instability Generates Self-Organized, Fractal Patterning of Cell Layers. *ACS Synth. Biol.*

Ruhe, Z.C., Low, D. a, and Hayes, C.S. (2013) Bacterial contact-dependent growth inhibition. *Trends Microbiol.* **21**: 230–7.

Ruhe, Z.C., Nguyen, J.Y., Beck, C.M., Low, D. a, and Hayes, C.S. (2014) The proton-motive force is required for translocation of CDI toxins across the inner membrane of target bacteria. *Mol. Microbiol.* **94**: 466–81.

Ruhe, Z.C., Wallace, A.B., and Low, D.A. (2013) Receptor Polymorphism Restricts Contact-Dependent Growth Inhibition to Members of the Same Spectoies.

Sezonov, G., Joseleau-Petit, D., and D'Ari, R. (2007) Escherichia coli physiology in Luria-Bertani broth. *J. Bacteriol.* **189**: 8746–9.

Siegele, D. a and Hu, J.C. (1997) Gene expression from plasmids containing the araBAD promoter at subsaturating inducer concentrations represents mixed populations. *Proc. Natl. Acad. Sci. U. S. A.* **94**: 8168–72.

Smith, T.G., Marks, W.B., Lange, G.D., Sheriff, W.H., and Neale, E. a (1989) A fractal analysis of cell images. *J. Neurosci. Methods* **27**: 173–180.

Solensky, R. (2003) Hypersensitivity reactions to beta-lactam antibiotics. *Clin. Rev. Allergy Immunol.* **24**: 201–219.

Soubrier, F., Cameron, B., Manse, B., Somarriba, S., Dubertret, C., Jaslin, G., et al. (1999) pCOR: a new design of plasmid vectors for nonviral gene therapy. *Gene Ther.* **6**: 1482–1488.

Soubrier, F., Laborderie, B., and Cameron, B. (2005) Improvement of pCOR plasmid copy number for pharmaceutical applications. *Appl. Microbiol. Biotechnol.* **66**: 683–688.

Strassmann, J.E., Gilbert, O.M., and Queller, D.C. (2011) Kin Discrimination and Cooperation in Microbes. *Annu. Rev. Microbiol.* **65**: 349–367.

Vandermeulen, G., Marie, C., Scherman, D., and Préat, V. (2011) New Generation of Plasmid Backbones Devoid of Antibiotic Resistance Marker for Gene Therapy Trials. *Mol. Ther.* **19**: 1942–1949.

Vidal, L., Pinsach, J., Striedner, G., Caminal, G., and Ferrer, P. (2008) Development of an antibiotic-free plasmid selection system based on glycine auxotrophy for recombinant protein overproduction in Escherichia coli. *J. Biotechnol.* **134**: 127–136.

Volkmer, B. and Heinemann, M. (2011) Condition-Dependent cell volume and concentration of Escherichia coli to facilitate data conversion for systems biology modeling. *PLoS One* **6**: 1–6.

Webb, J.S., Nikolakakis, K.C., Willett, J.L.E., Aoki, S.K., Hayes, C.S., and Low, D. a (2013) Delivery of CdiA nuclease toxins into target cells during contact-dependent growth inhibition. *PLoS One* **8**: e57609.

West, S. a and Gardner, A. (2010) Altruism, spite, and greenbeards. *Science* **327**: 1341–1344.

Xu, H.-S., Roberts, N., Singleton, F.L., Attwell, R.W., Grimes, D.J., and Colwell, R.R. (1982) Survival and Viability of Nonculturable Escherichia coli and Vibrio cholerae in the Estuarine and Marine Environment. *Microb. Ecol.* **8**: 313–323.

Yanofsky, C. (2000) Transcription attenuation: Once viewed as a novel regulatory strategy. *J. Bacteriol.* **182**: 1–8.

Young, J.W., Locke, J.C.W., Altinok, A., Rosenfeld, N., Bacarian, T., Swain, P.S., et al. (2012) Measuring single-cell gene expression dynamics in bacteria using fluorescence time-lapse microscopy. *Nat. Protoc.* **7**: 80–8.

Young, K.D. (2006) The selective value of bacterial shape. *Microbiol. Mol. Biol. Rev.* **70**: 660–703.

# 11 Appendix

## 11.1 Additional Figures

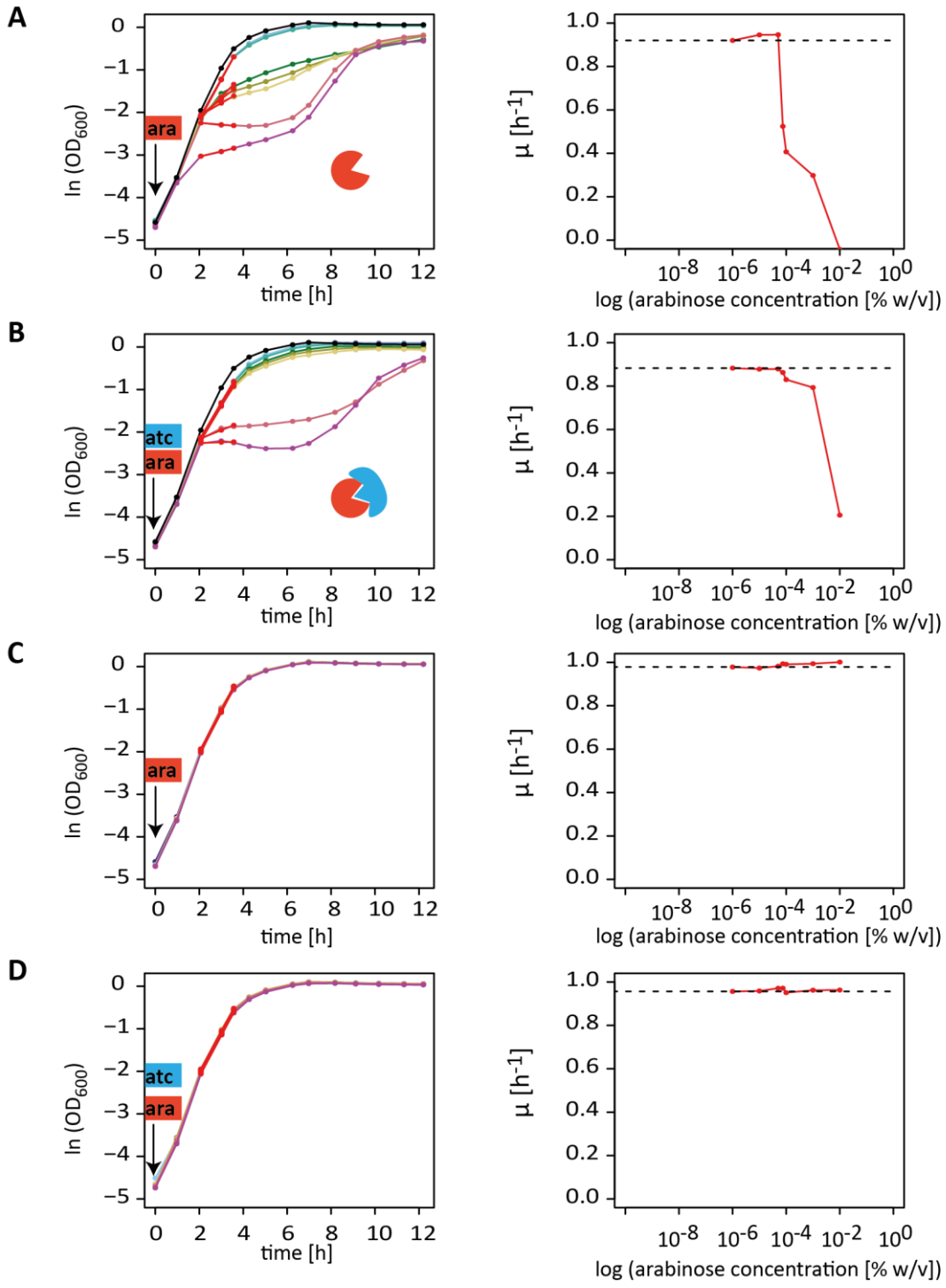


**Figure 41: Determination of the growth rate μ. Log ($OD_{600}$) plotted versus growth time (left plots). Data points between 2 and 4 h were linearly fit (red lines) and the obtained growth rate (μ) plotted against the employed arabinose concentration (right plots). Dashed lines represent growth rate when no arabinose is present. Plots correspond to (A) BW27786 carrying ECL expression plasmid subjected to varying arabinose concentrations (B) BW27786 with ECL expression plasmid at varying arabinose concentrations and atc addition. (C) and (D) BW27786 carrying the control plasmid at varying arabinose concentrations without and with atc addition.**

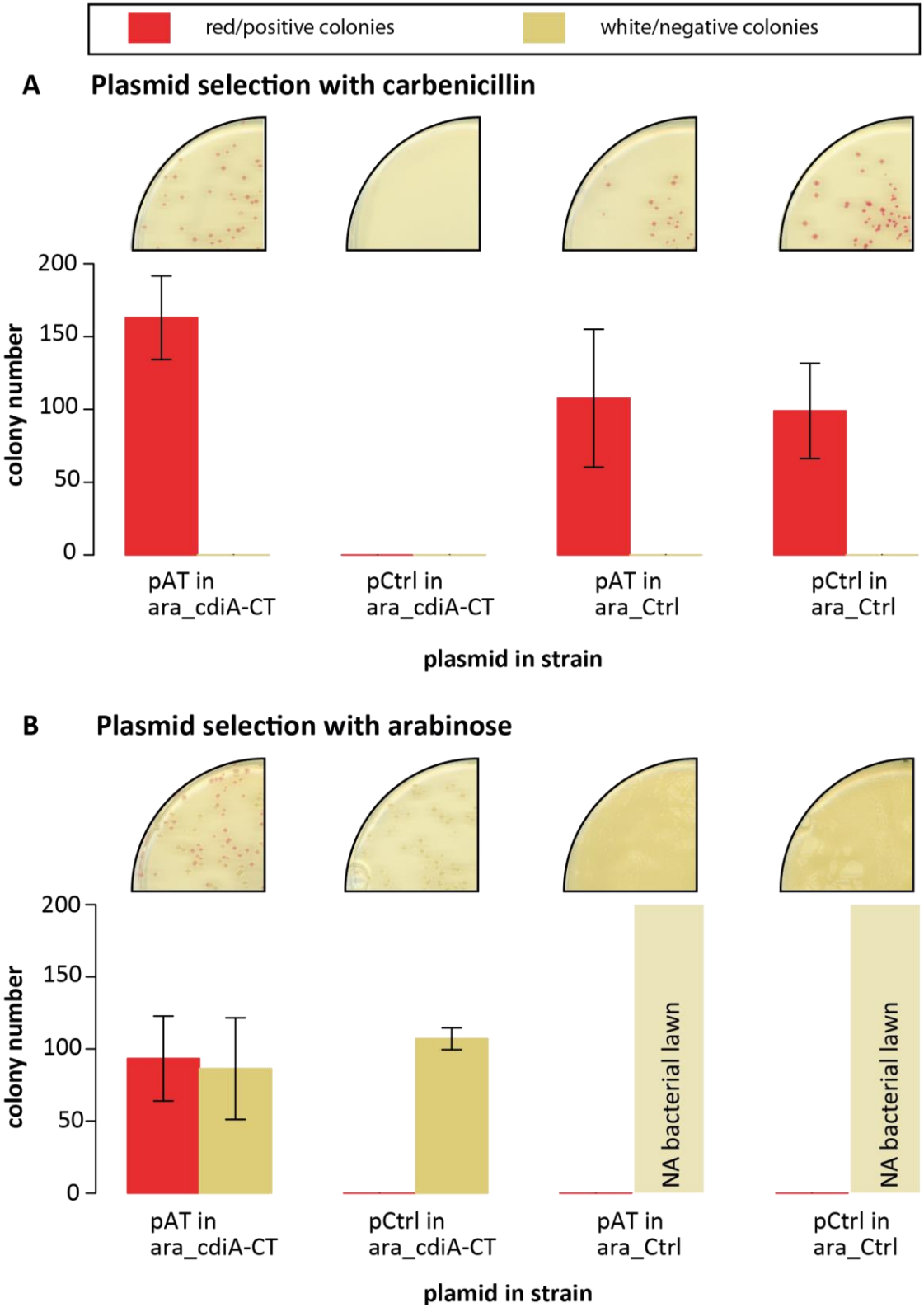


**Figure 42: White/negative colonies for transformation of pAT/pCtrl in ara_CdiA-CT do not depend on plasmid amount. pAT can successfully be selected with arabinose in the strain ara_cdiA-CT. (A) Selection on carbenicillin plasmid yields equal amounts of positive/red transformants when ara_cdiA-CT is transformed with pAT or ara_Ctrl is transformed with pAT or pCtrl. Transformation of ara_cdiA-CT with pCtrl yields no colonies on carbenicillin plates. (B)Arabinose selection of the transformation of ara_cdiA-CT with pAT results in positively selected red colonies, but also a number of negative/white colonies. Transformation of ara_cdiA-Ct with pCtrl results in a similar amount of white colonies when selected on arabinose. Selection on arabinose leads to the formation of a white bacterial lawn for transformation of ara_Ctrl with pAT or pCtrl.**

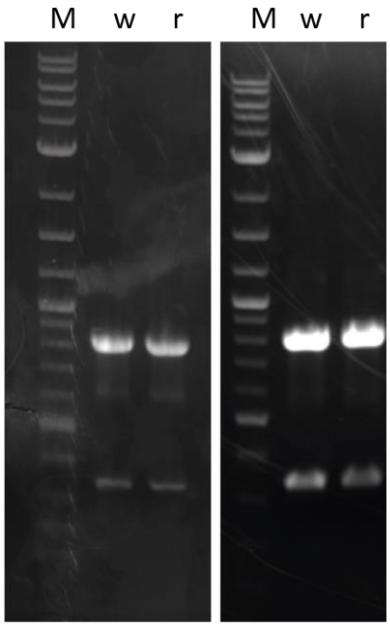


**Figure 43: White colonies growing on arabinose plates that were plated with ara_CdiA-CT strain transformed with pAT contain an integration cassette. Colony PCR was performed using the integration verification primers P1, P2, P3 and P4. M: marker; white: white colony (contains no pAT); red: red colony (contains pAT).The band pattern is consistent with an integration of a pIT4KH vector (343 bp and 824 bp).**

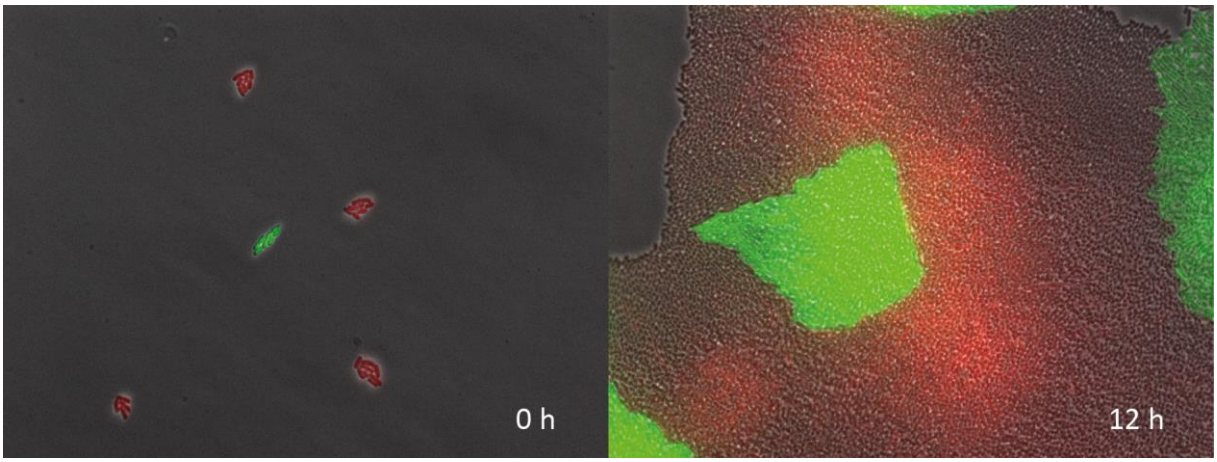


**Figure 44: Growth of susceptible target cells (red) and CDI$^{EC93\text{-}Ec869\ o11}$ inhibitor cells (green) results in sharp geometric forms. Filamentation of target cells smoothes the interface of the colonies. The five starting colonies (left image) grow to form an inhibitor colony (green) in a squared form (right image).**

## 11.2 Schematic construct diagrams

In the following construct diagrams part names with construct backbone, antibiotic resistance and origin of replication are listed. Part names as listed in the Registry of Standard Biological Parts (http://parts.igem.org/Main_Page) were added when available. Use of ribozyme-based insulator parts SccJ and RiboJ (Lou et al., 2012) and the bicistronic junctions BCD2 and Gene10_LeuL (Mutalik et al., 2013) is indicated where applicable.

pBR1, pBR6, pBR7, pBR8

J64100 backbone, $Cm^R$, ColE1 origin

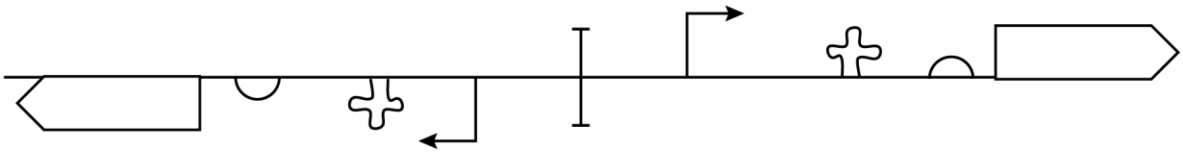

antitoxin *cdiI* | Gene10_LeuL | SccJ | R0040 pTet | B0014 double terminator | I0500 araC/pBAD | RiboJ | BCD2 | toxin *cdiA-CT*

pBR24

J61002 backbone, $Amp^R$, ColE1 origin

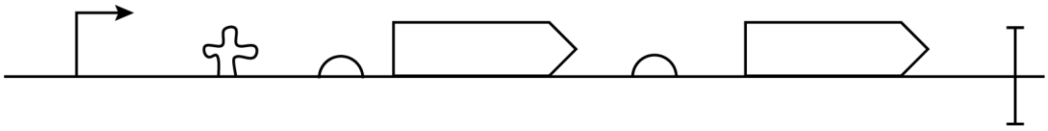

J23100 strong constitutive promoter | SccJ | Gene10_LeuL | antitoxin *cdiI*$^{ECL}$ | B0034 double terminator | mRFP1 | B0015 double terminator

pBR29 (pBR44)

pSB4C5 (pSB4A5) backbone, $Cm^R$ ($Amp^R$), pSC101 origin

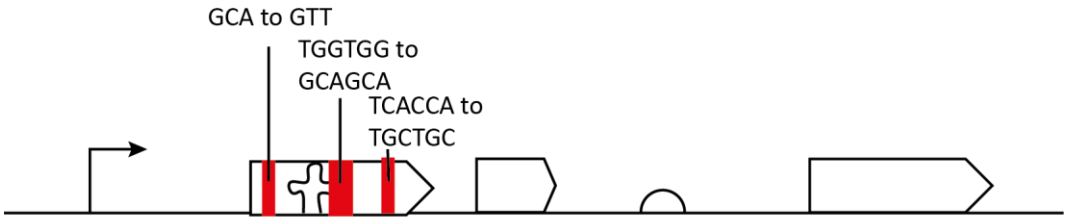


J23119 strong constitutive promoter | *trpL* | *trpE* fragment | strong RBS | Z0301 venus YFP (superfolderGFP

pBR33 (pBR33GFP)

pIT4KH, $Kan^R$, oriR pir dependent

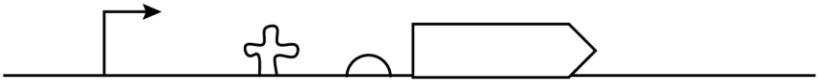

I0500 araC/pBAD | RiboJ | BCD2 | toxin *cdiA-CT*

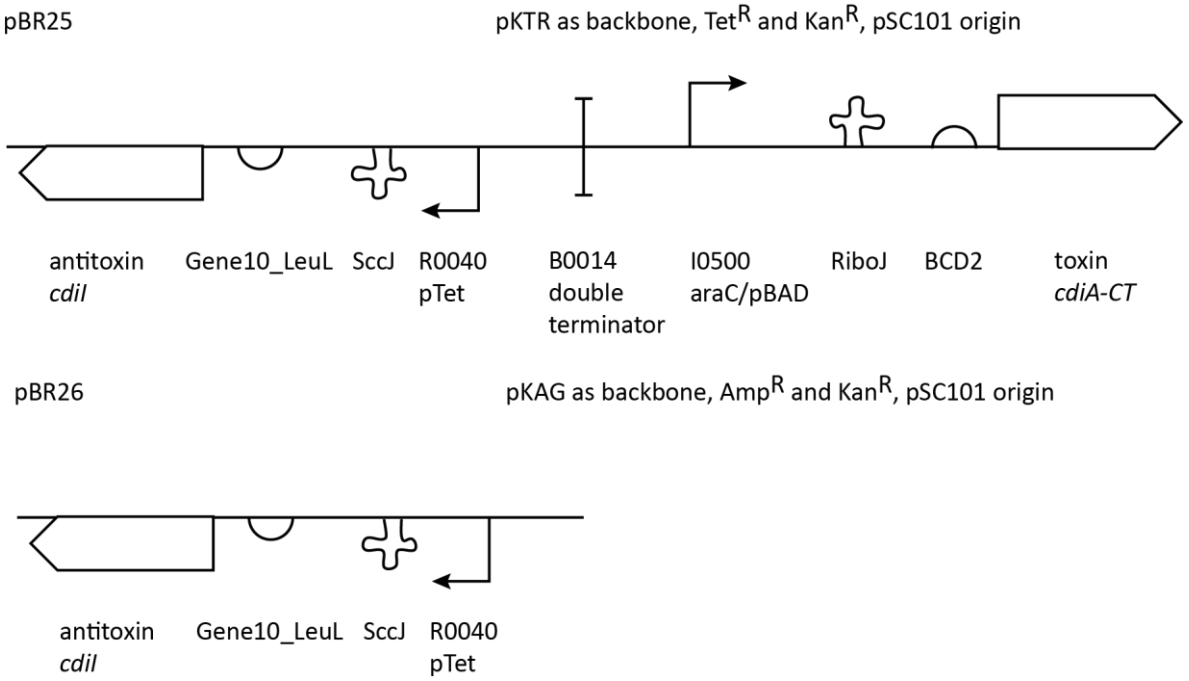


## 11.3 Additional tables

**Table 16: List of used primers and synthesized genes**

| Name | Sequence |
|---|---|
| BR1_UPEC536_cdiI_fw | CCTGAAGGTCTCAGTTATCATCAGTGGTGGTGGTGGTGG |
| BR2_UPEC536_cdiI_rev | ATATATGGTCTCACGCATTCATCTGGAGCTGATTTAATGATTACCTTACGTAAATTGATTGGAAACATCAATATGAC |
| BR3_UPEC536_cdiACT_fw | CGTTAAGGTCTCGATGCTAAGGAGGTTTTCTAATGGTTGAGAATAATGCGCTGAGTCTGG |
| BR4_UPEC536_cdiACT_rev | ATTAACGGTCTCGCTAGTACTCTAGTATCATATTCCATATCCTTTCAAGGCTGATTCTATTT |
| TS329_revBsaIGen10LeuL | GCTGAGGGTCTCATGCGATAATGTTTAGTCATGCTAGCCATG |
| TS433_rBsaIpref | TACAAAGGTCTCTTAACTCTAGAAGCGGCCGCGAATTC |
| TS455_bsaIfSuff | AATTAGGTCTCACTAGTAGCGGCCGCTGCAG |
| TS460_bsaIrBCD2 | TACAAAGGTCTCAGCATGATTAAGATGTTTCAGTACGAAAATTGC |
| BR5_sequencing pCH10540_fw | CACCATTGCTTCAGGTATTGCAG |
| BR6_sequencing pCH10540_rev | TCAACTCTCCCTCCAGGTACT |
| BR7_gfp in rha_bb_fw | AATACGGGTCTCCGAAATTCTTTTACTTGAGGATAAATTATGCGTAAAGGCGAAGAGCTG |
| BR8_gfp in rha_bb_rev | CTGACTGGTCTCCTGAGGGGTCATTTGTACAGTTCATCCATACCATGC |
| BR9_rha_backbone_fw | CGATGAGGTCTCGCTCATCCGAAAGGGCGTATTCATATGC |
| BR10_rha_backbone_rev | ATAGTCGGTCTCGTTTCATTACGACCAGTCTAAAAAGCGCCT |
| VF3 | TATCACGAGGCCCTTTCGT |
| VR3 | CTCACTGACTCGCTGCG |
| JEXP-F | AAAACGTCGATTTTTCAAGATA |

| | |
|---|---|
| **JEXP-R** | **TGATTCTGTGGATAACCGTAT** |
| **P1 (integration verification)** | **GGAATCAATGCCTGAGTG** |
| **P2 (integration verification)** | **ACTTAACGGCTGA CATGG** |
| **P3 (integration verification)** | **ACGAGTATCGAGA TGGCA** |
| **P4 (integration verification)** | **GGCATCAACAGCACATTC** |
| **BR15_ECL_cdiI_fw** | **AGCGATGGTCTCAGTTATCAGTTGTTAAGACTATGATAAAAATCTAAAACACTATTT** |
| **BR16_ECL_cdiI_rev** | **CATTTCGGTCTCTCGCATTCATCTGGAGCTGATTTAATGTTTGGAATATTCTCTAAAGGTGAACCAGT** |
| **BR17_ECL_cdiACT_fw** | **CACTCCGGTCTCCATGCTAAGGAGGTTTTCTAATGTCGCTGGCACTGGTTGC** |
| **BR18_ECL_cdiACT_rev** | **TCGCAAGGTCTCACTAGTACTCTAGTACTAGTCCTTAATCCTGTTTAGTCCGC** |
| **BR19_EC869_cdiI_fw** | **TAGCTCGGTCTCCGTTATCACTAACCTACTGCCTCAAAAAAACTTTCC** |
| **BR20_EC869_cdiI_rev** | **GGAGCTGGTCTCACGCATTCATCTGGAGCTGATTTAATGAAATTAACTGTAGATAGCGTTATTAATGAACC** |
| **BR21_EC869_cdiACT_fw** | **CCTTGCGGTCTCTATGCTAAGGAGGTTTTCTAATGTATCTGAGTAAAGCCCAGAAAGCTC** |
| **BR22_EC869_cdiACT_rev** | **TACTGCGGTCTCACTAGTACTCTAGTATTATTTATACAACGCATGCTTTAATACTGGATA** |
| **BR23_1026b_cdiI_fw** | **GGATGAGGTCTCCGTTATCATCACCTCCGGTATTCGTTATCTTG** |
| **BR24_1026b_cdiI_rev** | **CTGAAAGGTCTCACGCATTCATCTGGAGCTGATTTAATGGCAATTGACTTGTTTTGCTATCTCTCA** |
| **BR25_1026b_cdiACT_fw** | **TGCTCAGGTCTCGATGCTAAGGAGGTTTTCTAATGGGCTCTTTATCAGGCAAGCC** |
| **BR26_1026b_cdiACT_rev** | **ACCTGGGGTCTCGCTAGTACTCTAGTATTAATTCCCCTTTGGCTTTATGATGGT** |
| **BR27_pTRC99A fw** | **TCCGGCTCGTATAATGTGTGG** |
| **BR30_67_bb+RFP_fw** | **CCACCACCACCACCACTGATGTACTAGTGAAAGAGGAGAAATACTAGATGGC** |
| **BR31_67_bb+RFP_rev** | **TGACATTTTCTCCTCTTTAGTCAGACGCTAGCACTGTACCTAGGACTGA** |
| **BR32_cdiIUpec536 in 67_fw** | **GTCTGACTAAAGAGGAGAAAATGTCAATGATTACCTTACGTAAATTGATTGGAAACA** |
| **BR33_cdiIUpec536 in 67_rev** | **ACTAGTACATCAGTGGTGGTGGTGGTG** |
| **BR34_rha for tet_bb_fw** | **TTAGCTCGGTCTCCTAGTAGAGTCACACTGGCTCACCTT** |
| **BR35_rha for tet_bb_rev** | **TCACTGGGGTCTCGATGCTGTAGTGGGATGTGTGTCTCAC** |
| **BR36_rha for tet_prom_fw** | **ATCCAGGGTCTCAGCATCTTTTCATTACGACCAGTCTAAAAAGCGC** |
| **BR37_rha for tet_prom_rev** | **TTCAGGAGGTCTCGACTAGAGGCCCATTTTCCTGTCAGTAACGA** |
| **BR38_SccJ_Gtta_remove_cdiI** | **GTACTCGGTCTCGGTTATACTAGAGTTATGACAACTTGACGGC** |
| **BR39_fw** | **CAGTGCGGTCTCAGTTATACTAGAGTTATGACAACTTGACGGCT** |
| **BR40_rev** | **CGATTCGGTCTCTCTAGCTGCAGCGGCCGCTACTAG** |
| **BR41_at in 67_fw** | **TTGACGGCTAGCTCAGTCCTAGGTACAGTGCTAGCAGATGCTGTAGTGGGATGTGTGT** |
| **BR42_at in 67_rev** | **CGTTTTATTTGATGCCTGGCTCTAGTAGAATTCGCGGCCGCTTCTA** |
| **BR43_67_bb_fw** | **TACTAGAGCCAGGCATCAAATAAAACG** |
| **BR44_67_bb_rev** | **TACCTAGGACTGAGCTAGCCGTCAA** |
| **BR45_seq_pIT3_CH_fw** | **TGAACGTTGCGAAGCAACGG** |
| **BR46_seq_pIT3_CH_rev** | **TAGGCGCCATGCATCTCGAG** |
| **BR47_pIT4_OH_Gi_fw** | **TAACCCGTAGAAAAGATCAAAAGATCTTCTTG** |
| **BR48_pIT4_OH_Gi_rev** | **AGCATACCTCTTTTTGACATACTTCGG** |
| **BR49_ara_ECL in pIT4_KO_Gi_fw** | **GAAGTATGTCAAAAAGAGGTATGCTTTATGACAACTTGACGGCTACATCATT** |
| **BR50_ECL in pIT4_KO_Gi_rev** | **ATCTTTTGATCTTTTCTACGGGTTACTGCAGCGGCCGCTACTAG** |

| | |
|---|---|
| BR51_rha_ECL in pIT4_KO_Gi_fw | GCCCATTTTCCTGTCAGTAACGAGAAGGTCGCGAATTCAGGCGCTTTTTAGACTGGT CGTAATGAAAAGCTGTCACCGGATGTGCT |
| BR52_rha_pIT4_KO_Gi_rev | CTTCTCGTTACTGACAGGAAAATGGGCAGCATACCTCTTTTTGACATACTTCGG |
| BR54_ECL_in 67rfp_bb_fw | TTTTTATCATAGTCTTAACAACTGATACTAGTGAAAGAGGAGAAATACTAGATGGC |
| BR55_ECL_in 67rfp_rev | TCAGTTGTTAAGACTATGATAAAAATCTAAAACACTAT |
| BR56_segr_pl_bb_fw | TTATTAGAAAAACTCATCGAGCATCAAATGAA |
| BR57_segr_pl_bb_rev | TACTAGCAGAAATCATCCTTAGCGAAAGC |
| BR58_ECL_cdiCT_fw | TCGCTAAGGATGATTTCTGCTAGTACTGCAGCGGCCGCTACT |
| BR59_ECL_cdiCT_rev | GATGCTCGATGAGTTTTTCTAATAAGAATTCGCGGCCGCTTCTAG |
| BR60_ECL_cdiI_fw | TCGCTAAGGATGATTTCTGCTAGTATCCCTATCAGTGATAGAGATTGACATCC |
| BR61_seq_segr_pla_fw | TTGGGGCTCACTCAAAGGC |
| BR62_seq_segr_pla_rev | CCGTTACCAGGACCTTGCCA |
| BR63_seq_FS541_186int | GCACCAACGCCTGACTGCCCCATCCCC |
| BR64_FL_bb_fw | GCAGGTAGGAACTCGGTTGAGAATAATTCGCTGGCACTGGTTGCC |
| BR65_FL_bb_rev | AGTTATCCTGCCGGTGCCGCATTAGAAAACCTCCTTAGCATGATTAAGATGTTT |
| BR66_FL_cdiB_Ainsert_fw | CTAATGCGGCACCGGCAGGATAACT |
| BR67_FL_cdiB_Ainsert_rev | ATTATTCTCAACCGAGTTCCTACCTGC |
| BR68_segr_pl_GG_fw | TACAAAGGTCTCATAACTTATTAGAAAAACTCATCGAGCATCAAATGAAAC |
| BR69_segr_pl_GG_rev | CACTTAGGTCTCTCTAGTACTAGCAGAAATCATCCTTAGCGAAAG |
| BR70_seq_pIT4KO insert | TGCAAGTAGCAGATTACGCGC |
| BR71_pSB4C5_bb_fw | TACTAGTAGCGGCCGCTGC |
| BR72_pSB4C5_bb_rev | CTCTAGAAGCGGCCGCGAA |
| BR73_Genebl1_4c5_fw | CTCGAATTCGCGGCCGCTTCTAGAGTTGACAGCTAGCTCAGTCCTAGG |
| BR74_Genebl1_YFP_rev | ATAATTCCTCTCCTTTGCTTACCATAGATCCTTCCTCCTGGATCCTTAC |
| BR75_YFP_fw | ATGGTAAGCAAAGGAGAGGAATTATTTACAG |
| BR76_YFP_4C5_rev | ACTCCTGCAGCGGCCGCTACTAGTATTATTTGTACAGTTCGTCCATACCCAG |
| BR77_BR30_GG_fw | ACACGCGGTCTCAATGCTGCGGAGGGTTTCTAATGGGCTCTTTATCAGGCAAGCCG |
| BR78_BR31_GG_fw | ACACGCGGTCTCAATGCGACGGAGCGTTTCTAATGGGCTCTTTATCAGGCAAGCCG |
| BR79_BR32_GG_fw | ACACGCGGTCTCAATGCGAAGGACAGTTTCTAATGGGCTCTTTATCAGGCAAGCCG |
| BR80_pIT4KH_fw | AGGCATGCCTCGAGATGCA |
| BR81_pIT4KH_rev | CTCTAGAGGATCCCCGGGTAC |
| BR82_i0500_fw | CTCGGTACCCGGGGATCCTCTAGAGTTATGACAACTTGACGGCTACATCATT |
| BR83_suff_rev | TGCATCTCGAGGCATGCCTCTGCAGCGGCCGCTACT |
| BR84_i0500_seq_fw | CTCTCTACTGTTTCTCCATACCCGT |
| BR85_pIT4KH_rev | TGTCAGTTTAGGTTAGGCGCCA |
| VF2 | TGCCACCTGACGTCTAAGAA |
| TS77_YFPrevnearRBs | CAACCAGGATCGGAACAACTCCTG |
| BR86_Prom_reg_fw | ATTATCGGTCTCACTAGCCCAAAAAAACGGGTATGGA |
| BR87_Prom_reg_rev | TATTGAGGTCTCAGTGCTCAGTATCTCTATCACTGATAGGGA |
| BR88_RiboJ_fw | ACATATGGTCTCAGCACAGCTGTCACCGGATGTGCTT |
| BR89_SccJ_rev | GTGAATGGTCTCTCTAGCAGATGCTGTAGTGGGATGTGTGT |
| BR90_ara_cdiI_fw_segrpla | TCGCTAAGGATGATTTCTGCTAGTATTATGACAACTTGACGGCTACATCATTCA |
| BR91_gebl1_GFP_rev | TGAACAGCTCTTCGCCTTTACGCATAGATCCTTCCTCCTGGATCCTTAC |
| BR92_gfp_fw | ATGCGTAAAGGCGAAGAGCTG |

| | |
|---|---|
| **BR93_gfp_rev** | **ACTCCTGCAGCGGCCGCTACTAGTATCATTTGTACAGTTCATCCATACCATGC** |
| **BR94_gebl_FL_fw** | **GGTTTTCCCAGTCACGACGGATCCCTTGACAGCTAGCTCAGTCCTAGG** |
| **BR95_FL1026b_fw** | **TACTAGTGAAAGAGGAGAAATACTAGATGCGGCACCGGCAG** |
| **BR96_FL1026b_rev** | **GGGATCCGTCGTGACTGGG** |
| **BR98_seq_FL tox** | **GAATTCGCGGCCGCCA** |
| **BR99_seq_FLtox_Rev** | **GGGCAACAATGTTCTGTTTGCC** |
| **BR100** | **GCT AGC CCA AAA AAA CGG GTA TGG** |
| **BR101** | **CTA TCA CTG ATA GGG ATG TCA ATC TCT ATC AC** |
| **BR102** | **AGA TTG ACA TCC CTA TCA GTG ATA GAG ATA CTG AGC ACA GCT GTC ACC GGA TGT GCT** |
| **BR103** | **TCC ATA CCC GTT TTT TTG GGC TAG CAG ATG CTG TAG TGG GAT GTG TGT** |
| **BR104_FL_fw** | **GGTTTTCTAATGCGGCACCGGCAG** |
| **BR105_FL_rev** | **GTTAGGCGCCATGCATCTCGAGGCATGCCTCTAGTCCTTAATCCTGTTTAGTCCGCT** |
| **BR106_GFP_seq_rev** | **ACCATTAGTTGCGTCACCTTCAC** |
| **Geneblock1** | **TTGACAGCTAGCTCAGTCCTAGGTATAATACTAGCGGCGCACTCCCGTTCTGGAT AATGTTTTTTGCGCCGACATCATAACGGTTCTGGCAAATATTCTGAAATGAGCTGT TGACAATTAATCATCGAACTAGTTAACTAGTACGCAAGTTCACGTAAAAAGGGTA TCGACAATGAAAGTGATTTTCGTACTGAAAGGTGCAGCACGCACTTCCTGAAACG GGCAGTGTATTGCTGCTGCGTAAAGCAATCAGATACCCAGCCCGCCTAATGAGCG GGCTTTTTTTTGAACAAAATTAGAGAATAACAATGCAAACACAAAAACCGACTCT CGAACTGCTAACCTGCGAAGGCGCTTATCGCGACAATCCCACCGCGCTTTTTCACC AGTTGTGTGGGTAAGGATCCAGGAGGAAGGATCT** |